DAMPING SUBSYNCHRONOUS RESONANCE USING SUPPLEMENTARY CONTROLS AROUND THE STATIC SYNCHRONOUS SERIES COMPENSATOR

By

Mahlomola Joseph Masenkane

BScEng

Submitted in the fulfillment of the academic requirement for the degree of Master of Science in Electrical Engineering, in the School of Engineering, College of Agriculture, Engineering and Science, University of KwaZulu-Natal, Durban, South Africa

July 2018

As the candidate's supervisor, I agree/do not agree to the submission of this thesis

Dr. Rudiren Pillay Carpanen…….

Date……

DECLARATION 1 – PLAGIARISM

I **Mahlomola Joseph Masenkane**, declare that

1. The research reported in this thesis, except where otherwise indicated, is my original research.
2. This thesis has not been submitted for any degree or examination at any other university.
3. This thesis does not contain other persons' data, pictures, graphs or other information, unless specifically acknowledged as being sourced from other persons.
4. This thesis does not contain other persons' writing unless specifically acknowledged as being from other researchers. Where other resources have been quoted, then:
    a. Their words have been re-written but the general information attributed to them has been referenced
    b. Where their exact words have been used, then their writing has been placed in italics and inside quotation marks, and referenced.
5. This thesis does not contain text, graphics or tables copied and pasted from the internet, unless specifically acknowledged, and the source being detailed in the thesis and in the References section.

Mahlomola Joseph Masenkane ……..……. ……

(BScEng) Signature Date

Supervisor: R. Pillay Carpanen ……..……. ……

(BScEng, MScEng, PhD, MIEEE) Signature Date

DECLARATION 2 - PUBLICATIONS

DETAILS OF CONTRIBUTION TO PUBLICATIONS:

Some of the findings in this thesis have been presented and published in an internationally refereed conference paper [85].

Some studies conducted will be published in an international journal [90].

Signed …….

Dedicated to my family

ACKNOWLEDGEMENTS

Firstly, I would like to express my gratitude to my supervisor Dr Rudiren Pillay Carpanen for his professional guidance, constructive critics and recommendations in the course of this research work and during the writing and correction of this document. I acknowledge Dr Rudiren Pillay Carpanen for arranging the much needed funding for this research project.

My special thanks also go to Mr Clarence Leoaneka who is with the Durban University of Technology for his constant advices and guidance regarding post-graduate studies. My colleagues in the Descipline of Electrical, Electronic and Computer Engineering are also acknowledged for their encouragement and these are Thabelang, Mathew, Patrick and Ayanda who is also an electrical engineer at Eskom.

I would like to sincerely thank my family for their support and best wishes. Particularly my wife Mrs ‘Mabohlokoa and my sister ‘Neheng and two wonderful brothers Thabo and Paulus.

Lastly, I thank my friend Keabetsoe for his courage throughout my research work.

ABSTRACT

The demand for electric power increases rapidly with the growth in human population whereas expansion of existing power transmission infrastructure is restrained by difficulties in obtaining rights of way, resource scarcity and environmental policies inter alia. This has called for better utilization of existing transmission facilities which, for many years has been achieved through series compensation of transmission lines using conventional series capacitor banks. However, during major system disturbances, these conventional series capacitors weaken the damping of torsional oscillations in the neighboring turbine-generator shafts, which may lead to the failure and damage of the shafts concerned; a phenomenon known as subsynchronous resonance (SSR).

Alternative means of series compensation using high-speed semiconductor switches has been realized following introduction of Flexible AC Transmission Systems (FACTS) in power systems. This research work focuses on damping of SSR using damping controls around the second-generation series device of the FACTS family namely the static synchronous series compensator (SSSC). The SSSC is designed to inject voltage in series with the transmission line and in quadrature with line current to emulate capacitive reactance in series with the transmission line. In this research work, a model of the SSSC is developed in Power System Computer Aided Design (PSCAD) and the IEEE First Benchmark Model (FBM) is used for SSR analysis. Initially, the resonant characteristics of the SSSC compensated transmission line is studied to determine whether this device has a potential to excite SSR on its own. The results confirm earlier work by other researchers using a detailed model of the SSSC, showing that introduction of a SSSC can indeed excite SSR, although not to the same extent as conventional series capacitors.

The research work then considers the addition of supplementary damping controllers to the SSSC to add positive damping to subsynchronous oscillations caused by the SSSC itself as well as by a combination of conventional series capacitors and a SSSC in the IEEE FBM. Finally, the research work considers a more complex transmission system with an additional transmission line that incorporates conventional series capacitors. Time-domain simulation results and Fast Fourier Transform analyses show that a damping controller around the SSSC can be used to mitigate SSR either due to the SSSC itself, or due to conventional series capacitors in the same line as the SSSC or due to conventional series capacitors in an adjacent line of an interconnected transmission network.

TABLE OF CONTENTS

LIST OF SYMBOLS

Acronyms

AC	Alternating Current
DC	Direct Current
FACTS	Flexible AC Transmission Systems
FBM	First Benchmark Model
FFT	Fast Fourier Transform
HVDC	High Voltage Direct Current
IEEE	Institute of Electrical and Electronic Engineers
IGBT	Insulated-Gate Bipolar Transistor
PSCAD	Power System Computer Aided Design
SSDC	Subsynchronous Damping Controller
SSR	Subsynchronous resonance
SSSC	Static Synchronous Series Compensator
SPWM	Sinusoidal Pulse Width Modulation
VSI	Voltage Source Inverter

Symbols

D_E, D_G, D_B, D_A, D_I, D_H	Damping coefficients of the respective shaft inertia
K_{AB}, K_{BG}, K_{AB}, K_{IA}, K_{HI}	Stiffness coefficients in the sections of the turbine-generator shaft
R_L	Resistance of the transmission line
X_L	Inductive reactance of the transmission line
X_t	Leakage reactance of the transmission transformer
X_C	Compensating reactance provided by fixed series capacitors
X_{Comp}	Total compensating reactance in the line
X_{SSSC}	Compensating reactance provided by the SSSC
X_{C1}	Compensating reactance provided by fixed series capacitors in Line 1
X_{C2}	Compensating reactance provided by fixed series capacitors in Line 2
X_{sys}	Downstream reactance of the system
T_B, T_A, T_I, T_H	Torques developed in different sections of the turbine
T_e	Generator electromagnetic torque
K_{ssr}	Subsynchronous damping controller gain
X_{SSSC_min}	Lower limit to the compensating reactance provided by the SSSC
X_{SSSC_max}	Upper limit to the compensating reactance provided by the SSSC

LIST OF FIGURES

LIST OF TABLES

CHAPTER ONE

INTRODUCTION

1.1. General

With the human population estimated to rise to 11.2 billion by the year 2100 [1], rapid increase in electric power demand will continue to prevail for domestic, industrial and transportation purposes to sustain and improve the human lives. Projections on the global electricity consumption indicate an astounding 75% increase from 15 000 TWh in the year 2000 to 27 000 TWh in 2020, corresponding to the population increase from 6.1 billion to 7.5 billion [2]. On the other hand, more environmentally friendly and sustainable energy sources such as solar and wind farms are being integrated into existing electric grids, raising a need for bulk transmission of electric power over long distances from generating units to load centers. However, construction of new generation plants and installation of new transmission lines to meet these demands are hindered by high costs, difficulties in obtaining rights of way and severe environmental restrictions [3] among other factors.

More efficient ways of transmitting power are explored while efforts are being made to enhance the power transfer capability of existing transmission lines. Wireless power transmission is an alternative way of power transmission without the use of transmission lines. However, industrial utilization of this concept has not been fully realized [4] owing to the technical challenges that remain unsolved, particularly in high power, long-range applications, although there are promising technologies implemented in power lasers, microwave and vacuum transmission [5]. In light of the above challenges, transmission planners are left with no option but to better utilize existing transmission facilities by increasing their loadability, i.e. enabling them to be operated closer to their stability margins without compromising the security of the power system.

1.2. Series Compensation of Transmission Lines

Conventional series capacitor banks have been widely used as an economic way of improving the power transfer capability of transmission lines. These capacitors cancel portion of the transmission line's inductive reactance, reduce the transmission losses, increase the load sharing among parallel lines and improve the transient as well as the steady state stability of the power system [6]. The concept of series capacitor compensation is explained in details using a single line diagram of a power system in figure 1.1. The power P, transmitted over an uncompensated transmission line is given by equation 1.1, where V_s and V_r are the sending end and receiving end voltages respectively, X_L is the inductive reactance of the line and δ_s and δ_r are the phase angles of the sending end and receiving end voltages respectively. For a transmission line compensated with series capacitor of capacitive reactance X_C, the power transferred over the line is given by equation 1.2.

(a) without series compensation (b) with series compensation

***Figure 1.1**: Single machine infinite bus system with and without series capacitive compensation*

$$P = \frac{V_s V_r}{X_L} \sin(\delta_s - \delta_r) \tag{1.1}$$

$$P = \frac{V_s V_r}{X_L - X_C} \sin(\delta_s - \delta_r) \tag{1.2}$$

In principle, series capacitor compensated transmission line appears electrically shorter than an uncompensated transmission line of the same length and parameters [7]. Comparison of equations 1.1 and 1.2 shows that the maximum power that can be transmitted is higher for series compensated transmission lines than for uncompensated lines.

Although Charles Concordia warned about possible detrimental interactions between series capacitors and multi-mass turbine-generators back in 1937 [8-9], it was only in 1970, and again in 1971 that the actual turbine-generator shaft failures due to these interactions were experienced at the Mohave power station in Nevada, USA. This interaction, now known as subsynchronous resonance (SSR), has since attracted the attention of many researchers worldwide.

1.3. Background to SSR Phenomenon in Series Compensated Networks

Majority of the generated electricity comes from large turbine-generators with long rotors typically consisting of several rotating sections [8]. Due to these long multi-inertia shaft structures, these turbine-generators are normally characterized by several torsional vibration-modes, the number of which depends on the sections on the turbine-generator shaft. The mechanical damping of the torsional vibrations in the turbine-generator shaft is small and it is positive due to friction and windage losses as well as the flow of steam or gas around the rotor. When such a turbine-generator is radially connected to a series capacitor compensated line as in figure 1.2, the resonant frequency of the electrical network, f_{er} is given by equation 1.3.

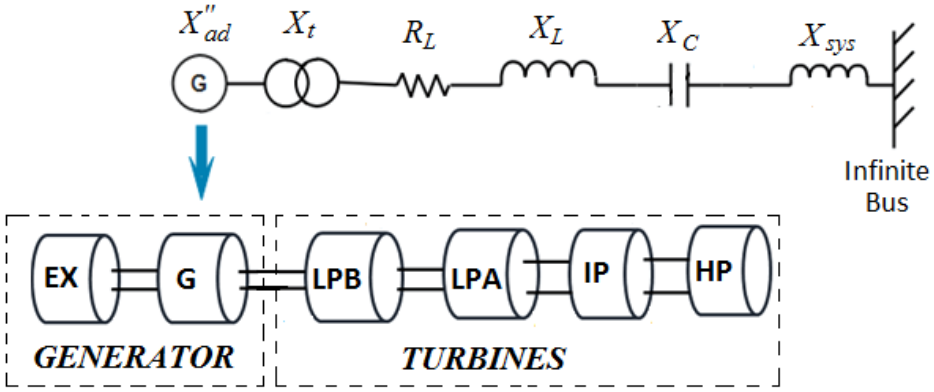

***Figure 1.2**: Multi-inertia turbine generator connected to series compensated transmission line*

$$f_{er} = f_0 \sqrt{\frac{X_C}{X_{Ltot}}} \tag{1.3}$$

Where:

f_0 = synchronous frequency of the power system

X_C = capacitive compensating reactance

X_{Ltot} = total inductive reactance of the electrical system (i.e. $X''_{ad} + X_t + X_L + X_{sys}$)

X_t = leakage reactance of the step-up transformer

X_L = inductive reactance of the transmission line

X''_{ad} = sub-transient reactance of the generator

When a disturbance occurs in such a system, oscillations in generator rotor at subsynchronous frequencies f_n induce armature voltages with frequencies ($f_0 \pm f_n$) [10]. These voltages set up currents in the armature which in turn develop electromagnetic torque at the same frequency f_n. The damping of the torsional oscillations in the turbine-generator shaft is weakened if the resonant frequency of the system's electrical network f_{er} is close to the subsynchronous frequency (f_0 - f_n). When currents at frequencies included in these oscillations enter the machine windings, the machine and the electric network should ideally combine to damp out these oscillations. If not, these oscillations may grow in amplitudes (unstable) or may be stable but poorly damped (sustained). Occurrence of these subsynchronous oscillations, which are typically in the range of 10 - 50 Hz [11] on the generator shaft increases stress and fatigue, developing cracks which will lead to shaft failure due to damage.

The IEEE Subsynchronous resonance task force [12] defines SSR as follows:

'SSR is an electric power condition where energy is exchanged between the electric network and mechanical system of the turbine-generator shaft at one or more of the natural frequencies of the combined system below the synchronous frequency of the power system.'

1.3.1. Forms of SSR

The SSR phenomenon typically manifests itself in three different forms namely; induction generator effect (IGE), torsional interaction (TI) and transient torque or torque amplification (TA).

1.3.1.1. Induction Generator Effect

This form of SSR results from self-excitation of the generator and involves the electrical system only. IGE occurs if an electrical resonance exists at a subsynchronous frequency and a negative resistance (due to negative slip) from the rotor side exceeds the positive resistance in the lines [13]. Turbine-generators near heavily series compensated networks are more likely to experience this form of SSR.

1.3.1.2. Torsional Interaction

Torsional interaction SSR involves the electrical system as well as the mechanical system of the shaft. Large subsynchronous currents which produce oscillatory torque result if the frequency of the subsynchronous component of armature voltage mentioned above, ($f_0 - f_n$), is close to the electrical resonant frequency, f_{er}. SSR due to torsional interaction occurs if the phase of the produced torque is such that it enhances the excited torsional oscillations. *TI* is reported to be more significant and is believed to be responsible for the catastrophic shaft failures at the Mohave power station [14].

1.3.1.3. Transient Torque or Torque Amplification

Disturbances in a system with capacitor compensated transmission line(s) give rise to transient rotor electromagnetic torques at the frequencies $(f_0 \pm f_{er})$. Post-disturbance shaft torques of large amplitudes result if the subsynchronous component of the transient torque $(f_0 - f_{er})$ gets close to one of the natural torsional frequencies of the mechanical system. SSR due to *TA* involves both the electrical and mechanical systems but is initiated by severe disturbances such as faults**.**

1.3.2. SSR Analytical Tools

Different techniques have been proposed to assess the potential risk of SSR in power systems and the famous ones include; eigenvalue analysis, frequency scanning as well as non-linear electromagnetic transient analysis.

1.3.2.1. Eigenvalue Analysis

With this method, all components of the power system are modelled mathematically with non-linear equations which are later linearized about an operating point of interest. The

eigenvalues of the linearized matrix representing the whole system are obtained and used to determine the stability of the system. The method is normally computationally intensive.

1.3.2.2. Frequency Scanning

Frequency scanning technique determines the network impedance as seen from behind the stator winding of the generator under study as a function of frequency. This method provides preliminary analysis of SSR problem and only indicates the risk of SSR [15], therefore needs to be verified by means of time domain simulations

1.3.2.3. Non-linear Electromagnetic Transient Analysis

Also known as time domain simulations, this method of SSR analysis utilizes the non-linear differential equations to represent various components of the power system which are solved by iterative step-by-step numerical integration [3] using a simulation program. This method is accurate and saves time in investigations.

In this dissertation, the SSR analysis will focus on frequency scanning as the study system has been modelled on PSCAD which uses continuous-time models.

1.4. Flexible AC Transmission Systems (FACTS)

With more advances in high power semiconductor devices, the state-of-the-art voltage source converter-based FACTS controllers were developed [15]. FACTS controllers are capable of rapidly controlling the power flow in transmission lines and to safely allow the power system to be operated closer to its stability limits. This is achieved through simultaneous or selective control of the parameters affecting the power flow in a transmission line (i.e. bus voltages, impedance and phase angle). Depending on their connection to the power system, FACTS controllers can be categorized into series controllers, shunt controllers, series-shunt controllers or series-series controllers. Shunt FACTS controllers regulate the bus voltages to control the reactive power while series FACTS controllers control the line reactance to modify the power flow in the line. Series-shunt FACTS controllers can be designed to control both the bus voltages and phase angles or all of the factors affecting the power flow in the line.

According to IEEE [11], the term FACTS refers to:

> *"A power electronic based system and other static equipment that provide control of one or more ac transmission system parameters to enhance controllability and increase power transfer capability."*

Application of FACTS in power systems has enabled not only the fast and flexible control of power flow in transmission lines, but also mitigation of SSR caused by series capacitors. Examples of the

FACTS controllers include the Static Compensator (STATCOM), Thyristor Controlled Series Capacitor (TCSC), SSSC and Unified Power Flow Controller (UPFC).

1.5. Research Objectives and Related Key Questions

FACTS controllers involve the incorporation of power-electronic controlled devices into AC power transmission systems in order to safely extend the power-transfer capability of these systems closer to their stability limits. The key question has been whether it is possible to utilize the FACTS devices already installed for other purposes to mitigate the SSR problem in a power system. Previous research has shown that one member of the family of FACTS series compensators which is the Static Synchronous Series Compensator (SSSC), can effectively damp torsional oscillations caused by the SSSC itself or due to the presence of conventional series capacitors in the transmission line [9, 17-19]. However, the research work in [9, 17-19] has considered a single transmission line in the power system. In a practical transmission system, however, it is likely to be the case that an additional transmission line that incorporates a conventional series capacitor might be present in the system.

The aim of this research study is to investigate whether supplementary controls can be added to the SSSC to damp torsional oscillations caused by a conventional series capacitor in an adjacent line of the transmission system. Different critical operating points of the transmission system will be considered to investigate whether the supplementary controls are effective for a range of values of series compensation.

1.6. Thesis Organisation

The work in this thesis comprises of six chapters. Chapter One introduces the concept of series compensation of transmission lines and subsynchronous resonance. The first chapter also discusses the root cause of subsynchronous resonance in the turbine-generators that are radially connected to series compensated transmission lines as well as the various forms SSR and the analytical tools used to assess the potential risk of SSR in the power system. Chapter Two presents the reported incidents of SSR and reviews the work in the literature regarding the SSR remedial measures undertaken by utilities or proposed including the use of FACTS controllers. In Chapter Three, mathematical modelling of the power system under study is presented and the ability of the SSSC scheme used in the thesis to provide the required amount of series compensation. Susceptibility of the SSSC's internal controls to the sources of disturbance in the transmission system is also evaluated in Chapter Three. Chapter Four investigates the effects of the SSSC's internal controls on the dynamics of the transmission line and establishes the SSR characteristics of the SSSC in the IEEE first benchmark model. The design of the supplementary damping controller around the SSSC is presented in Chapter Five and to damp SSR in the IEEE FBM with single transmission line and in the modified IEEE FBM

with parallel transmission lines. The conclusions from the research work findings and suggestions for future work are in Chapter Six.

1.7. Research Publication

Some of the findings of this dissertation have been presented at an international conference [85] and will appear in an international journal [90].

CHAPTER TWO

REVIEW ON SUBSYNCHRONOUS RESONANCE AND ITS COUNTERMEASURES

2.1. Introduction

The previous chapter has considered series capacitor compensation of transmission lines and its benefits in power transmission. The challenges and hazards associated with this technique are also discussed, in particular with regard to subsynchronous resonance, which presents a major threat to the nearby turbine-generator units. Chapter One has also highlighted on how FACTS devices can alleviate transmission bottlenecks and safely allow optimum utilization of transmission facilities.

This chapter reviews the work available in the literature regarding SSR, its causes and some practical cases where it occurred or it was detected. Finally, the chapter reviews the protective and mitigating measures against SSR that are available in the literature, including the use of different FACTS devices.

2.2. Causes of Subsynchronous Oscillations

There are a few power system configurations that are susceptible to subsynchronous oscillations. Those include radial connection of turbine-generators with series capacitor compensated transmission lines, adverse control interactions with the FACTS devices, wind turbine-generators (especially the doubly-fed induction generator type) [20-22] or HVDC systems [23-25], speed governors or generator-exciter controls.

If these oscillations are not sufficiently damped, they result in the flow of subsynchronous currents in the stator windings of the generator. Thus, damping or weakening of SSR oscillations requires elimination or suppression of these currents.

2.3. Reported Cases of SSR occurrence or detection

The first two reported incidents of shaft failure due to subsynchronous resonance were from the Mohave Power plant, one in 1970 and the other in 1971. It was only after the latter case that the cause of the failure was identified as SSR, where an electrical resonance at 30.5 Hz excited a mechanical resonance at 30.1 Hz.

Also, in 1977 the field tests performed in [26] detected adverse subsynchronous control interactions between a ±250 kV, 500 MW HVDC link and a 438 MW turbine-generator in the Square Butte power station, USA. However, no shaft failure occurred in this particular case due to proactive testing

measures and subsequent modification of the HVDC link controls to suppress the torsional interactions.

Another subsynchronous control interaction was reported in South-East of Texas at the Electric Reliability Council of Texas (ERCOT) power system, in 2009. In this particular event, a doubly fed asynchronous wind turbine-generator was radially connected to the 50% series compensated 345 kV line following loss of another line due to a fault. The control system of the wind turbine presented into the grid a negative resistance under subsynchronous conditions [21] resulting in subsynchronous oscillations damaging the wind generators and series capacitors.

2.4. SSR Protection and Mitigation

One way of avoiding SSR is to choose the values of series capacitors such that f_{er} is not anywhere near $f_0 - f_n$ [27]. However, this method does not allow full utilization of transmission lines. In addition, it does not guarantee stability, especially during loss of some lines due to faults as this may shift the electric resonant point. Different methods are proposed in the literature for protection and mitigation of SSR in series compensated networks. While most protective schemes have been successfully implemented in practice, they only protect the equipment and do not damp or mitigate the subsynchronous oscillations. One protective technique is installation of passive SSR filters, either at the generator or at the series capacitor banks to block flow of currents at subsynchronous frequencies. Redundant torsional relays can also be used to monitor torsional oscillations in the generator shaft and send a trip output to either bypass the series capacitor, trip a line or trip the affected generator if the shaft fatigue equals a specified value [8].

On the other hand, SSR mitigation techniques can restore the system stability while allowing the equipment (i.e. generators and transmission lines) to continue operating. The work of this thesis is based on the mitigative remedial approach that aims at damping out SSR and minimizing the loss of generation or transmission lines due to SSR. The ability of the FACTS controllers to provide fast and flexible control of power flow has been utilized by many researchers to add positive damping to subsynchronous oscillations in power systems. This can be achieved by modifying the control systems of the FACTS devices already installed in the power system for other purposes.

2.5. Use of FACTS Controllers to damp SSR

The use of various FACTS controllers in SSR mitigation is reviewed below.

2.5.1. Damping SSR using a Static Compensator (STATCOM)

A STATCOM is a shunt FACTS device which regulates voltage through injection or absorption of reactive power from the power system. The work in [28] presents an auxiliary subsynchronous

damping controller to damp SSR through modulation of the reactive current reference to the STATCOM. Damping of SSR using the subsynchronous current injector (SSCI) is presented in [29], where subsynchronous component of line current is filtered and injected into the system by the STATCOM. This technique reportedly prevents the flow of subsynchronous current in the generator and increases damping of the critical torsional frequencies of the system. Further studies regarding the use of STATCOM controller to damp SSR can be found in [30-41].

2.5.2. Damping SSR using Thyristor Controlled Series Capacitor (TCSC)

A TCSC can rapidly control power flow over a transmission line by modifying the line reactance. This device consists of a series capacitor shunted by a Thyristor-controlled reactor and is classified as a series FACTS device. The work in [42] employs the closed loop current control of the TCSC to damp SSR due to torsional interaction and induction generator effect in a wind farm connected to a series compensated network. A subsynchronous damping controller (SSDC) is designed for the TCSC in [43] to damp SSR in the presence of fixed series capacitors. In [44], a phase imbalance scheme is implemented to damp SSR using a TCSC damping controller. The authors in the latter study use a combination of a single phase TCSC and fixed capacitor in one phase of the transmission while the other two phases are compensated with fixed capacitors only. At subsynchronous frequencies, the damping controller modulates the TCSC reactance and creates the phase imbalance in a manner that increases the damping of SSR. The use of a fuzzy logic damping controller for a TCSC to damp SSR in a power system consisting of a wind and steam turbine generators was studied in [45]. The authors in [46] present an SSDC for TCSC, which, upon detecting the subsynchronous current in the system, injects a subsynchronous current that is out of phase with the original subsynchronous current so that both currents cancel out. Damping of SSR in series compensated networks through suitable control of a TCSC is also considered in [47-49].

2.5.3. Damping SSR using a VSC-based HVDC link

HVDC transmission systems have been used for bulk transmission of electric power over long distances or in cases where AC transmission is not feasible. In recent years, HVDC systems are gaining more interest from transmission utilities and are finding increased application in conjunction with AC lines. Fast controllability of the VSC-HVDC link allows rapid modulation or control of dc power [50], a feature that can be used for damping power system oscillations. Addition of supplementary damping controls around the HVDC link to damp SSR has been investigated in [51-53]. The work in [54] has considered damping of SSR using a subsynchronous current injector around a VSC-HVDC link that originates from the same substation with a series compensated AC transmission line. The authors extract subsynchronous components of line current and inject them into the system using an HVDC link to suppress the subsynchronous currents flowing through the generator.

2.5.4. Damping SSR using DFIG-based wind generator

The desire to decarbonize the energy systems in recent years has led to proliferation of wind farms worldwide. One popular type of a wind generator is a Doubly-Fed Induction Generator (DFIG) system that incorporates power electronic converters. The impact of wind farms on SSR has been of great interest to various researchers recently as well as SSR mitigation using various FACTS devices. However, damping of SSR using wind turbine converters has rarely been investigated [55]. The authors in [55-57] have utilized the controllability of the converters in a DFIG-based wind turbine and introduced the supplementary damping control loop for SSR mitigation. The work in [58] focuses on two control techniques namely Fuzzy logic and Particle Swarm Optimization for a DFIG-based damping controller design to mitigate SSR.

2.5.5. Damping SSR using the Static Synchronous Series Compensator (SSSC)

The SSSC controls power flow though modulation of the transmission line's reactance and is classified under series FACTS controllers. Damping of SSR can be achieved by either equipping the SSSC with an external damping controller [8, 59-63], by using a highly frequency selective Kalman Filter or current suppressor [64-65], or through suitable control of the SSSC's internal controls [66-70]. Application of a phase imbalance scheme to damp SSR with a SSSC is investigated in [71-73]. It is reported that the phase imbalance scheme weakens the coupling between mechanical and electrical sides of the turbine-generator, suppresses the energy exchange between the two sides [71] and as a result enhances damping of torsional oscillations.

2.5.6. Damping SSR using Unified Power Flow Controller (UPFC)

The UPFC employs both series and shunt converters and is therefore categorized under series-shunt FACTS controllers. This device is reportedly the most versatile FACTS controller developed so far [74] since it incorporates all capabilities of series compensation, namely voltage regulation and phase shifting. The work of [75-77] presents a subsynchronous damping controller around the UPFC to damp SSR.

Majority of the aforementioned studies employ either the IEEE first benchmark model or the IEEE second benchmark model to evaluate the effectiveness of the SSR damping scheme in each case. Nonetheless, the authors only considered a case where the FACTS devices and conventional series capacitor banks are installed in the same transmission line. This research work now considers a more complex SSR prone power system configuration, with an SSSC and a conventional series capacitor in one transmission line and an additional conventional series capacitor in an adjacent transmission line in parallel. The ability of a SSSC-based supplementary damping controller to damp SSR in a more complex transmission system with multiple sources of SSR is investigated in this thesis.

2.6. Conclusion

This chapter has given an overview regarding subsynchronous oscillations in power systems and established the root cause of SSR, which is the flow of subsynchronous currents in the stator windings of the generator. Mitigation of SSR through rapid control of power flow in transmission lines using various power electronic controlled FACTS devices has also been highlighted. The following chapter presents the mathematical modelling of the IEEE first benchmark model with a single transmission line.

CHAPTER THREE

MATHEMATICAL MODELLING OF THE STUDY SYSTEM WITH A SINGLE TRANSMISSION LINE

3.1. Introduction

In order for the utility operator to gain a clearer perception regarding the vulnerability of a power system to adverse interactions due to SSR, studies need to be undertaken as part of the planning process. In addition, these studies should be done using the benchmark study systems that are specifically developed for analyzing SSR [17] such as the IEEE first benchmark model (FBM) or the IEEE second benchmark model (SBM) for SSR analysis [11]. This chapter presents the detailed mathematical modelling of the study system used to analyze SSR in the initial scenario with a single transmission line, i.e. the IEEE FBM.

3.2. The Study System Description

The power system used for SSR analysis is the IEEE FBM adopted from [12]. As was mentioned earlier, initial studies in this thesis focus on the power system with a single transmission line as shown in figure 3.1. The system consists of the single 26 kV, 892.4 MVA turbine-generator that feeds an infinite bus through a 500 kV series compensated transmission line. Coupling between the electrical system and the mechanical system occurs in the turbine-generator. The mechanical system consists of the generator rotor (G) and its rotating exciter (Ex), the low-pressure turbine sections (LPA and LPB), an intermediate pressure turbine section (IP) and the high pressure turbine section (HP).

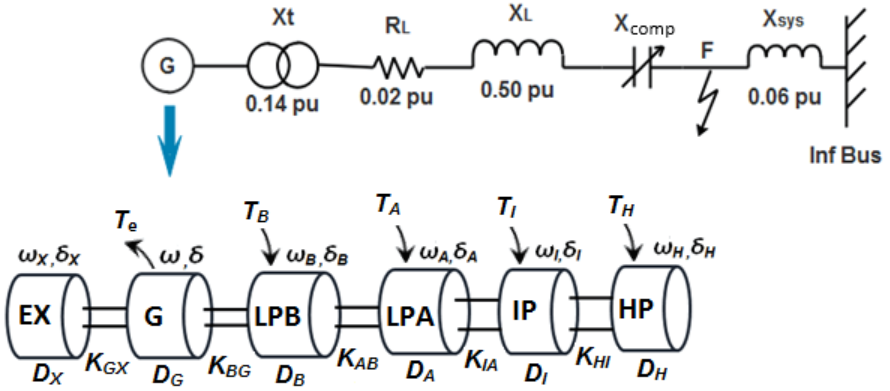

Figure 3.1: *The IEEE FBM SMIB showing the multi-inertia turbine generator connected to series compensated transmission line*

3.3. Modelling of the Study System

Detailed mathematical modelling of the study system forms an integral part of any SSR analytical study. The set of non-linear differential equations is derived through modelling of individual components of the study system. The final differential equations for the combined system (IEEE FBM) are then obtained using the knowledge of mutual interaction among individual models.

3.3.1. The Synchronous Machine Electrical Model

The synchronous machine modelling is based on the direct-quadrature (d-q) axis theory [78]. The electrical damping of the machine is represented by one equivalent damper circuit on the d-axis and two equivalent damper circuits on the q-axis, the convention that is used in [2, 79-80].

The stator voltage equations are as follows, where t is expressed in seconds, w is expressed in rad/s (w_0 = 376.9912 rad/s) and other quantities in per unit [80]:

$$\begin{aligned} e_d &= \frac{1}{w_0}\frac{d\psi_d}{dt} - \frac{w}{w_0}\psi_q - R_a i_d \\ e_q &= \frac{1}{w_0}\frac{d\psi_q}{dt} + \frac{w}{w_0}\psi_d - R_a i_q \end{aligned} \tag{3.1}$$

The rotor voltage equations are as follows:

$$\begin{aligned} e_{fd} &= \frac{1}{w_0}\frac{d\psi_{fd}}{dt} + R_{fd} i_{fd} \\ 0 &= \frac{1}{w_0}\frac{d\psi_{1d}}{dt} + R_{1d} i_{1d} \\ 0 &= \frac{1}{w_0}\frac{d\psi_{1q}}{dt} + R_{1q} i_{1q} \\ 0 &= \frac{1}{w_0}\frac{d\psi_{2q}}{dt} + R_{2q} i_{2q} \end{aligned} \tag{3.2}$$

The stator flux linkage equations are as follows:

$$\begin{aligned} \psi_d &= -L_d i_d + L_{ad} i_{fd} + L_{ad} i_{1d} \\ \psi_q &= -L_q i_q + L_{aq} i_{1d} + L_{aq} i_{2q} \end{aligned} \tag{3.3}$$

The rotor flux linkage equations are as follows:

$$
\begin{aligned}
\psi_{fd} &= L_{ffd} i_{fd} + L_{ad} i_{1d} - L_{ad} i_d \\
\psi_{1d} &= L_{ad} i_{fd} + L_{11d} i_{fd} - L_{ad} i_d \\
\psi_{1q} &= L_{11q} i_{1q} + L_{aq} i_{2d} - L_{aq} i_q \\
\psi_{2q} &= L_{aq} i_{1q} + L_{22q} i_{2q} - L_{aq} i_q
\end{aligned}
\tag{3.4}
$$

The equation for the electromagnetic torque in the air-gap is as follows:

$$
T_e = \psi_d \, i_q - \psi_q i_d \tag{3.5}
$$

Under transient conditions, the overall differential equations describing the performance of the synchronous generator are given by:

$$
\left[\frac{dX_{syn}}{dt} \right] = [At_{syn}] X_{syn} + \left[Bt_{syn} \right] \begin{bmatrix} V_{td} \\ V_{tq} \\ e_{fd} \end{bmatrix} \tag{3.6}
$$

where

$$
\left[X_{syn} \right] = \begin{bmatrix} i_d & i_q & i_{fd} & i_{1q} & i_{1d} & i_{2q} \end{bmatrix}^T
$$

$$
\left[At_{syn} \right] = \left[L \right]^{-1} \left[Qt \right]
$$

$$
\left[Bt_{syn} \right] = \left[L \right]^{-1} \left[Rt \right]
$$

$$
\left[L \right] = \begin{bmatrix}
-L_d & 0 & L_{ad} & 0 & L_{ad} & 0 \\
0 & -L_q & 0 & L_{aq} & 0 & L_{aq} \\
-L_{ad} & 0 & L_{ffd} & 0 & L_{ad} & 0 \\
0 & -L_{aq} & 0 & L_{11q} & 0 & L_{aq} \\
-L_{aq} & 0 & L_{ad} & 0 & L_{11d} & 0 \\
0 & -L_{aq} & 0 & L_{aq} & 0 & L_{22q}
\end{bmatrix}
$$

$$
\left[Q_t \right] = \begin{bmatrix}
w_0 R_a & -wL_q & 0 & wL_{aq} & 0 & wL_{aq} \\
wL_d & w_0 R_a & -wL_{ad} & 0 & -wL_{ad} & 0 \\
0 & 0 & -w_0 R_{fd} & 0 & 0 & 0 \\
0 & 0 & 0 & -w_0 R_{1q} & 0 & 0 \\
0 & 0 & 0 & 0 & -w_0 R_{1d} & 0 \\
0 & 0 & 0 & 0 & 0 & -w_0 R_{2q}
\end{bmatrix}
$$

$$[Rt]=\begin{bmatrix} w_0 & 0 & 0 \\ 0 & w_0 & 0 \\ 0 & 0 & w_0 \\ 0 & 0 & 0 \\ 0 & 0 & 0 \\ 0 & 0 & 0 \end{bmatrix}$$

and the superscript ^{T} denotes the transpose of the matrix while the superscript $^{-1}$ denotes the inverse of the matrix.

After linearization and rearrangement, equation 3.6 becomes:

$$\left[\frac{d\Delta X_{syn}}{dt}\right]=[A_{syn}]\left[\Delta X_{syn}\right]+\left[B_{syn}\right]\left[\Delta U_{syn}\right] \tag{3.7}$$

where

$$\left[\Delta X_{syn}\right]=\left[\Delta i_d \quad \Delta i_q \quad \Delta i_{fd} \quad \Delta i_{1q} \quad \Delta i_{1d} \quad \Delta i_{2q}\right]^T$$

$$\left[\Delta U_{syn}\right]=\left[\Delta V_{td} \quad \Delta V_{tq} \quad \Delta e_{fd} \quad \Delta w\right]^T$$

$$\left[A_{syn}\right]=\left[L\right]^{-1}\left[Q\right]$$

$$\left[B_{syn}\right]=\left[L\right]^{-1}\left[R\right]$$

$$[Q]=w_0\begin{bmatrix} R_a & -L_q & 0 & L_{aq} & 0 & L_{aq} \\ L_d & R_a & -L_{ad} & 0 & -L_{ad} & 0 \\ 0 & 0 & -R_{fd} & 0 & 0 & 0 \\ 0 & 0 & 0 & -R_{1q} & 0 & 0 \\ 0 & 0 & 0 & 0 & -R_{1d} & 0 \\ 0 & 0 & 0 & 0 & 0 & -R_{2q} \end{bmatrix}$$

$$[R]=\begin{bmatrix} w_0 & 0 & 0 & \psi_{q0} \\ 0 & w_0 & 0 & -\psi_{d0} \\ 0 & 0 & w_0 & 0 \\ 0 & 0 & 0 & 0 \\ 0 & 0 & 0 & 0 \\ 0 & 0 & 0 & 0 \end{bmatrix}$$

3.3.2. The Series Capacitor Compensated Transmission Line Model

The simple radial transmission system of the IEEE FBM in figure 3.1 can be represented by the AC equivalent RLC circuit as shown in figure 3.2 [80]. The total inductive reactance in the network is expressed as X_L while the total resistance is expressed as R_L.

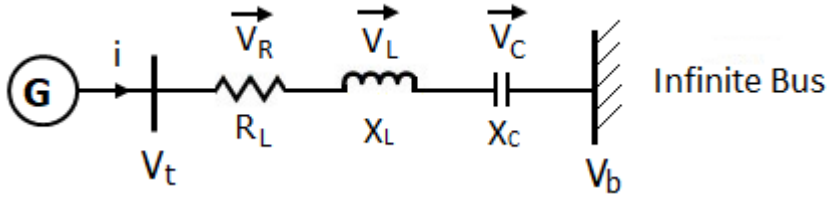

Figure 3.2: *AC equivalent circuit of the transmission system of the IEEE FBM in figure 3.1[80]*

The equation for the voltage across the resistance is given by:

$$\begin{bmatrix} V_{Rd} \\ V_{Rq} \end{bmatrix} = \begin{bmatrix} R_L & 0 \\ 0 & R_L \end{bmatrix} \begin{bmatrix} i_d \\ i_q \end{bmatrix} \tag{3.8}$$

Across the inductance, the voltage is given by:

$$\begin{bmatrix} V_{Ld} \\ V_{Lq} \end{bmatrix} = \begin{bmatrix} 0 & -\frac{w}{w_0} X_L \\ \frac{w}{w_0} X_L & 0 \end{bmatrix} \begin{bmatrix} i_d \\ i_q \end{bmatrix} + \begin{bmatrix} \frac{X_L}{w_0} & 0 \\ 0 & \frac{X_L}{w_0} \end{bmatrix} \begin{bmatrix} \frac{di_d}{dt} \\ \frac{di_q}{dt} \end{bmatrix} \tag{3.9}$$

Across the series capacitor, the voltage is given by:

$$\begin{bmatrix} \frac{dV_{Cd}}{dt} \\ \frac{dV_{Cq}}{dt} \end{bmatrix} = \begin{bmatrix} w_0 X_C & 0 \\ 0 & w_0 X_C \end{bmatrix} \begin{bmatrix} i_d \\ i_q \end{bmatrix} + \begin{bmatrix} 0 & w \\ -w & 0 \end{bmatrix} \begin{bmatrix} V_{Cd} \\ V_{Cq} \end{bmatrix} \tag{3.10}$$

The final series capacitor compensated transmission line equations then become:

$$\begin{bmatrix} \frac{dV_{Cd}}{dt} \\ \frac{dV_{Cq}}{dt} \\ V_{td} \\ V_{tq} \end{bmatrix} = [Att] \begin{bmatrix} V_{Cd} \\ V_{Cq} \end{bmatrix} + [Rt1] \begin{bmatrix} \frac{di_d}{dt} \\ \frac{di_q}{dt} \end{bmatrix} + [Rt2] \begin{bmatrix} i_d \\ i_q \end{bmatrix} + [Btt][V_b] \tag{3.11}$$

where

$$[Att] = \begin{bmatrix} 0 & w \\ -w & 1 \\ 1 & 0 \\ 0 & 1 \end{bmatrix}$$

$$[Rt1] = \begin{bmatrix} 0 & 0 \\ 0 & 0 \\ \frac{X_L}{w_0} & 0 \\ 0 & \frac{X_L}{w_0} \end{bmatrix}$$

$$[Rt2] = \begin{bmatrix} w_0 X_C & 0 \\ 0 & w_0 X_C \\ R_L & -\frac{w}{w_0} X_L \\ \frac{w}{w_0} X_L & R_L \end{bmatrix}$$

$$[Rt2] = \begin{bmatrix} 0 \\ 0 \\ \sin\delta \\ \cos\delta \end{bmatrix}$$

After linearization, equation 3.11 then becomes:

$$\begin{bmatrix} \frac{d\Delta V_{Cd}}{dt} \\ \frac{d\Delta V_{Cq}}{dt} \\ \Delta V_{td} \\ \Delta V_{tq} \end{bmatrix} = [At]\begin{bmatrix} \Delta V_{Cd} \\ \Delta V_{Cq} \end{bmatrix} + [R1]\begin{bmatrix} \frac{d\Delta i_d}{dt} \\ \frac{d\Delta i_q}{dt} \end{bmatrix} + [R2]\begin{bmatrix} \Delta i_d \\ \Delta i_q \end{bmatrix} + [Bt]\begin{bmatrix} \Delta w \\ \Delta\delta \end{bmatrix} \quad (3.12)$$

where

$$[At]=\begin{bmatrix} 0 & w_0 \\ -w_0 & 0 \\ 1 & 0 \\ 0 & 1 \end{bmatrix}$$

$$[R1]=\begin{bmatrix} 0 & 0 \\ 0 & 0 \\ \frac{X_L}{w_0} & 0 \\ 0 & \frac{X_L}{w_0} \end{bmatrix}$$

$$[R2]=\begin{bmatrix} w_0 X_C & 0 \\ 0 & w_0 X_C \\ R_L & -X_L \\ X_L & R_L \end{bmatrix}$$

$$[Bt]=\begin{bmatrix} V_{Cq0} & 0 \\ -V_{Cd0} & 0 \\ -\frac{X_L}{w_0} i_{q0} & V_{bq0} \\ \frac{X_L}{w_0} i_{d0} & V_{bd0} \end{bmatrix}$$

3.3.3. Modelling the Mechanical System of the Turbine-Generator Shaft

Figure 3.3 shows the two masses representing the generator rotor (G) and the low-pressure turbine section B (LPB) connected by an elastic shaft of stiffness coefficient K_{BG}. The dynamic model of the shaft system is then developed as follows, based on the approach in [80]. Considering the generator rotor for example:

$$Input torque: T_{BG} = k_{BG}(\delta_B - \delta) - k_{GX}(\delta - \delta_X)$$
$$Output torque: T_e$$
$$Damping torque: D_G \Delta w$$

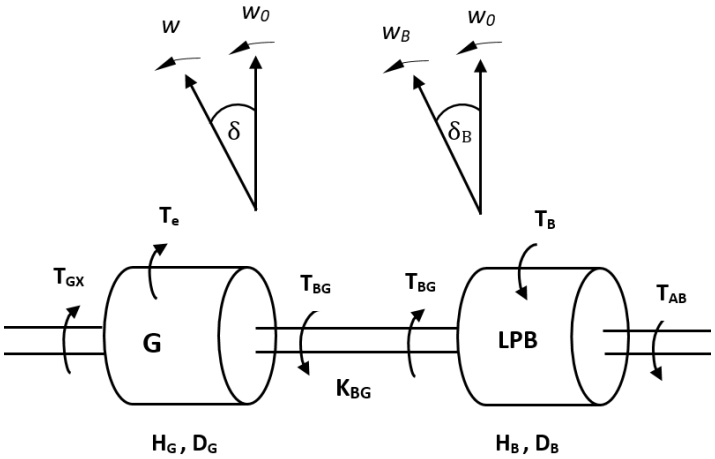

Figure 3.3: *The generator rotor (G) connected to the low pressure turbine section B (LPB)*

Thus, the differential equations for the generator become:

$$\begin{aligned} 2H_G \frac{d}{dt}\Delta w &= k_{BG}(\delta_B - \delta) - T_e - k_{GX}(\delta - \delta_X) - D_G \Delta w \\ \frac{d}{dt}\delta &= (\Delta w) w_o \end{aligned} \tag{3.13}$$

Likewise, for the exciter and other sections of the turbine

$$\begin{aligned} 2H_X \frac{d}{dt}\Delta w_X &= k_{GX}(\delta - \delta_X) - D_X \Delta w_X \\ \frac{d}{dt}\delta_X &= (\Delta w_X) w_o \end{aligned} \tag{3.14}$$

$$\begin{aligned} 2H_B \frac{d}{dt}\Delta w_B &= T_B + k_{AB}(\delta_A - \delta_B) - k_{BG}(\delta_B - \delta) - D_B \Delta w_B \\ \frac{d}{dt}\delta_B &= (\Delta w_B) w_o \end{aligned} \tag{3.15}$$

$$\begin{aligned} 2H_A \frac{d}{dt}\Delta w_A &= T_A + k_{IA}(\delta_I - \delta_A) - k_{AB}(\delta_A - \delta_B) - D_A \Delta w_A \\ \frac{d}{dt}\delta_A &= (\Delta w_A) w_o \end{aligned} \tag{3.16}$$

$$\begin{aligned} 2H_I \frac{d}{dt}\Delta w_I &= T_I + k_{HI}(\delta_H - \delta_I) - k_{IA}(\delta_I - \delta_A) - D_I \Delta w_I \\ \frac{d}{dt}\delta_I &= (\Delta w_I) w_o \end{aligned} \tag{3.17}$$

$$\begin{aligned} 2H_H \frac{d}{dt}\Delta w_H &= T_H - k_{HI}(\delta_H - \delta_I) - D_H \Delta w_H \\ \frac{d}{dt}\delta_H &= (\Delta w_H) w_o \end{aligned} \tag{3.18}$$

where T_A is the torque produced in the *LPA* section of the turbine in per unit as given in Appendix A.

The linearized equations of this mechanical system give the state equation of the form:

$$\frac{d}{dt}[\Delta X_{ms}] = [A_{ms}][\Delta X_{ms}] + [B_{ms}][\Delta U_{ms}] \tag{3.19}$$

where

$$[\Delta X_{ms}] = [w_H \quad \delta_H \quad w_I \quad \delta_I \quad w_A \quad \delta_A \quad w_B \quad \delta_B \quad w \quad \delta \quad w_X \quad \delta_X]^T$$

$$[\Delta U_{ms}] = [\Delta T_H \quad \Delta T_I \quad \Delta T_A \quad \Delta T_B \quad \Delta T_e]^T$$

$$[A_{ms}] = \begin{bmatrix} [A1] & [A2] \\ [A3] & [A4] \end{bmatrix}$$

$$[A1] = \begin{bmatrix} -\frac{D_H}{H_H} & -\frac{K_{HI}}{H_H} & 0 & \frac{K_{HI}}{H_H} & 0 & 0 \\ w_0 & 0 & 0 & 0 & 0 & 0 \\ 0 & \frac{K_{HI}}{H_I} & -\frac{D_I}{H_I} & -\frac{(K_{HI}+K_{IA})}{H_H} & 0 & \frac{K_{HI}}{H_I} \\ 0 & 0 & w_0 & 0 & 0 & 0 \\ 0 & 0 & 0 & \frac{K_{IA}}{H_A} & -\frac{D_A}{H_A} & -\frac{(K_{IA}+K_{AB})}{H_A} \\ 0 & 0 & 0 & 0 & w_0 & 0 \end{bmatrix}$$

$$[A2] = \begin{bmatrix} 0 & 0 & 0 & 0 & 0 & 0 \\ 0 & 0 & 0 & 0 & 0 & 0 \\ 0 & 0 & 0 & 0 & 0 & 0 \\ 0 & 0 & 0 & 0 & 0 & 0 \\ 0 & \frac{K_{AB}}{H_I} & 0 & 0 & 0 & 0 \\ 0 & 0 & 0 & 0 & 0 & 0 \end{bmatrix}$$

$$[A3] = \begin{bmatrix} 0 & 0 & 0 & 0 & 0 & \frac{K_{AB}}{H_B} \\ 0 & 0 & 0 & 0 & 0 & 0 \\ 0 & 0 & 0 & 0 & 0 & 0 \\ 0 & 0 & 0 & 0 & 0 & 0 \\ 0 & 0 & 0 & 0 & 0 & 0 \\ 0 & 0 & 0 & 0 & 0 & 0 \end{bmatrix}$$

$$[A4] = \begin{bmatrix} -\frac{D_B}{H_B} & -\frac{(K_{AB}+K_{BG})}{H_B} & 0 & \frac{K_{BG}}{H_B} & 0 & 0 \\ w_0 & 0 & 0 & 0 & 0 & 0 \\ 0 & \frac{K_{BG}}{H_G} & -\frac{D_G}{H_G} & -\frac{(K_{BG}+K_{GX})}{H_G} & 0 & \frac{K_{GX}}{H_G} \\ 0 & 0 & w_0 & 0 & 0 & 0 \\ 0 & 0 & 0 & \frac{K_{GX}}{H_X} & -\frac{D_X}{H_X} & -\frac{K_{GX}}{H_X} \\ 0 & 0 & 0 & 0 & w_0 & 0 \end{bmatrix}$$

Further details on combining the linearized equations for individual components to generate an overall small signal model of the SMIB power system of the IEEE FBM are given in [80].

3.3.4. Preliminary Eigenvalue Analysis for the IEEE FBM with Fixed Capacitors

By varying the compensating reactance from 0.002 pu to 0.5 pu in the IEEE FBM, the values of compensating reactance that result in the worst torsional interaction due to SSR are shown in figure 3.4 [80].

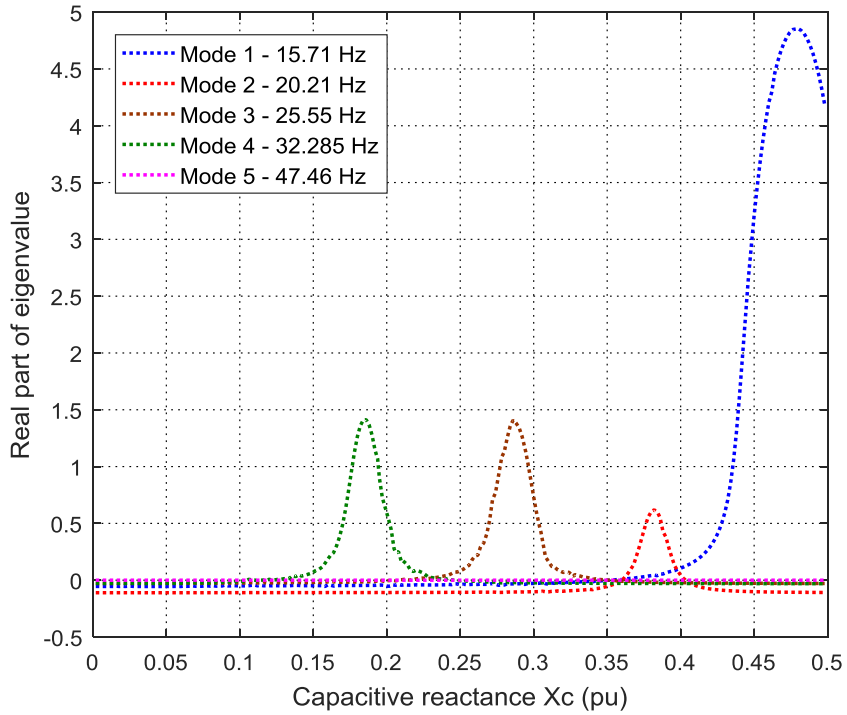

Figure 3.4: *Real components of the eigenvalues of the state matrix as the compensating reactance is varied from 0.002 pu to 0.5 pu in the IEEE FBM [80]*

The worst torsional interaction with Mode 4 of the turbine-generator shaft occurs around $X_C = 0.184$ pu, while those of Mode 3 and Mode 2 occur at around $X_C = 0.286$ pu and $X_C = 0.382$ pu respectively. Lastly, the worst ever torsional interaction that can be experienced in this study system is that of Mode 1 which occurs around $X_C = 0.48$ pu. Conversely, Mode 5 is observed to be stable throughout the range of X_C considered.

3.4. The Static Synchronous Series Compensator Modelling

This section presents modelling and design of the SSSC for PSCAD simulation. The SSSC scheme adopted in this thesis was proposed in [81], and has been used by other researchers for power flow control studies [82-83]. Introduction of the external damping controller around the SSSC based on this scheme was done in [84] for damping the low frequency inter-area oscillations in the power system. However, in practice, the power system oscillations are not limited to low frequency; torsional oscillations may also be present which may be spanning the entire subsynchronous frequency range. The SSSC consists of a sinusoidal pulse width modulation (SPWM) voltage source inverter (VSI) using power IGBTs with the switching frequency of 1260 Hz (i.e. $21 \times f_0$).

3.4.1. Voltage Source Inverter (VSI)

This is the critical component of the SSSC, which generates AC voltage from the fixed dc source by controlling the turn ON and turn OFF of the IGBTs. The frequency and magnitude of the AC voltage

can be controlled as required. Figure 3.5 shows the three phase VSI with parallel diodes that allow the flow of current when the corresponding IGBTs are in OFF state.

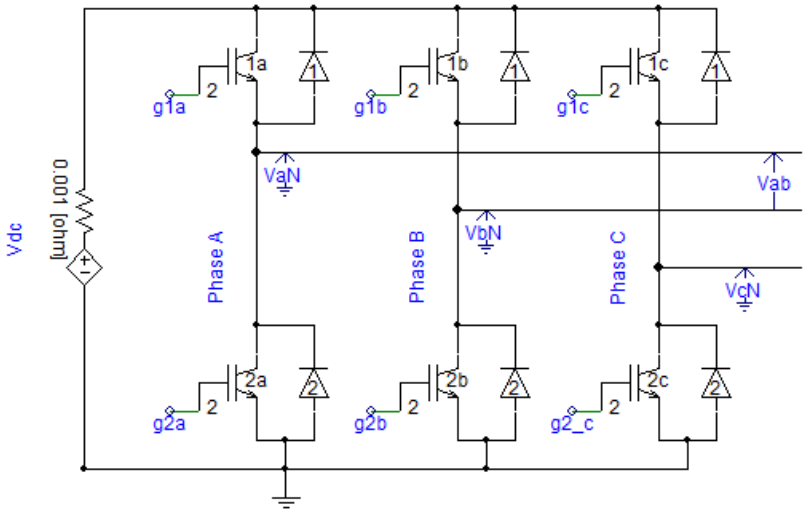

Figure 3.5: *The three-phase Voltage Source Inverter using power IGBT switches*

The SPWM technique generates the firing pulses for the IGBTs by comparing the modulating sinusoidal signal S_m with the triangular wave S_C. If S_m is greater than S_C, the upper switch is turned ON, else it is turned OFF. The phase angle of the output AC voltage is the same as that of the modulating signal S_m. The amplitude of the AC voltage from the inverter depends on the value of the dc voltage V_{dc} and the amplitude modulation index m_a with the latter being the ratio of the amplitude of the modulating signal to that of the triangular wave as given in equation 3.19. The fundamental components of the phase voltage and the line-to-line voltage are the obtained from equations 3.20 and 3.21 respectively.

$$m_a = \frac{|S_m|}{|S_C|} \tag{3.19}$$

$$V_{aN} = m_a \times \frac{V_{dc}}{2} \tag{3.20}$$

$$V_{ab} = m_a \times \frac{V_{dc}}{2}\sqrt{3} \tag{3.21}$$

The lower IGBT switch in each phase conducts complimentary to the upper IGBT switch in the same phase. Figure 3.6 shows the generation of firing pulses using an example of phase A with the modulation index of 0.8. The magnitude of the triangular wave S_C is arbitrarily chosen as 1.41, which is the square root of two.

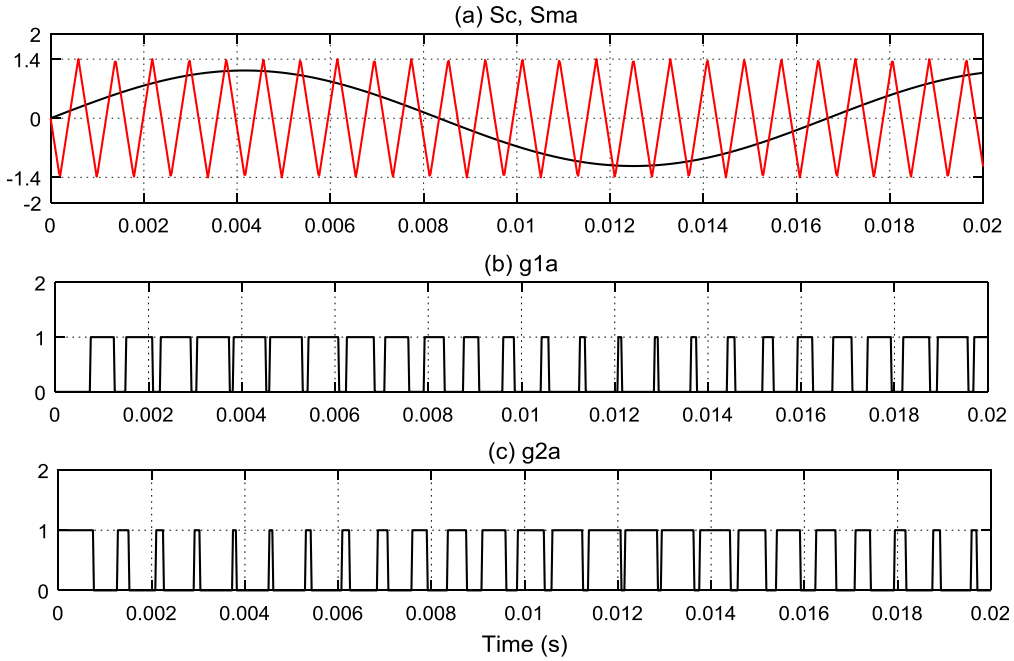

Figure 3.6: *The firing pulses for the IGBTs generated from SPWM*

The SSSC controls the magnitude of the injected voltage through modulation of the amplitude modulation index using the internal controls as discussed in the next subsection.

3.4.2. SSSC Internal Controls

For all the studies performed in this thesis, the reactance controlled type of SSSC is considered for capacitive mode of operation. The internal controls of the SSSC are shown in figure 3.7. These ensure that the SSSC injects, in series with the transmission line, a controllable voltage emulating a voltage drop across a capacitor. This is achieved by ensuring that the injected voltage (V_{SSSC}) lags the line current by 90°. The DC link voltage is maintained at the predetermined value V_{dc0} by ensuring that no active power is exchanged between the SSSC and the line, except a small amount that is rectified to charge the capacitor and to compensate for the inverter losses.

The magnitude of the voltage injected by the SSSC is determined by the variable modulating signal S_m calculated using equation 3.22.

$$|S_m| = I_{pk} X_{sssc} \frac{2\sqrt{2}}{V_{dc}} = I_{pk} X_{sssc} \frac{1}{V_{dc} K_{conv}} \tag{3.22}$$

where: I_{pk} or $|I|$ = peak value of line current

K_{conv} = gain of the inverter

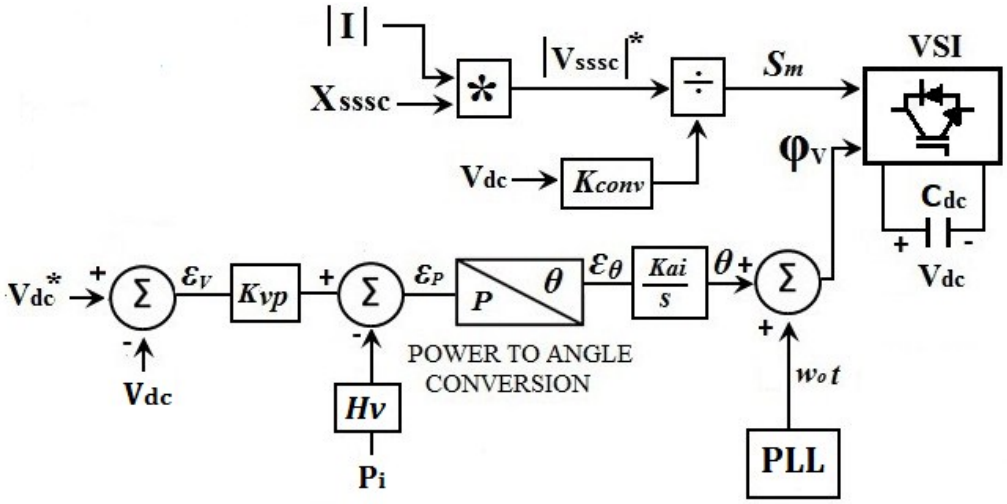

Figure 3.7: *Internal controls of the Static Synchronous Series Compensator*

The phase angle φ_v of the injected voltage is obtained from the two-loop angle calculator as shown in figure 3.7. The power to angle gain block ensures that the signal ε_Θ, driving the inner loop controller always equals the actual angular error between V_{dc} and the reference voltage V_{dc}^* (or V_{ref}) irrespective of the transmission line operating conditions as given in equation 3.23.

$$\varepsilon_\theta = \frac{1}{\frac{3}{2} I_{pk}^2 X_{sssc}} \varepsilon_P \tag{3.23}$$

The angle error ε_Θ is then taken through the PI controller to get the angle Θ, whose dynamics are defined by equation 3.24.

$$\frac{d\theta}{dt} = \frac{K_{ai}}{\frac{3}{2} I_{pk}^2 X_{sssc}} \left\{ K_{vp} \left(V_{dc}^* - V_{dc} \right) - P_i \right\} \tag{3.24}$$

Finally, the angle Θ, is added to the transmission voltage angle obtained using the phase locked loop (PLL), to get the required angle, φ_v. Further details regarding the internal controls of the SSSC are available in [81]. Figure 3.8 shows the single line diagram of the single machine infinite bus power system incorporating the SSSC connected to the transmission line adopted from the IEEE FBM. The DC source on the VSI is replaced by the storage device, which is the dc capacitor.

Table *3.1* gives the parameters and gains of the SSSC on a 892.4 MW, 500 kV, 60 Hz base, per unit calculations shown in Appendix B. The transmission line parameters are the same as those in the IEEE FBM are re given in table 3.2. The step-up transformer has its star winding leading the delta winding by 30°.

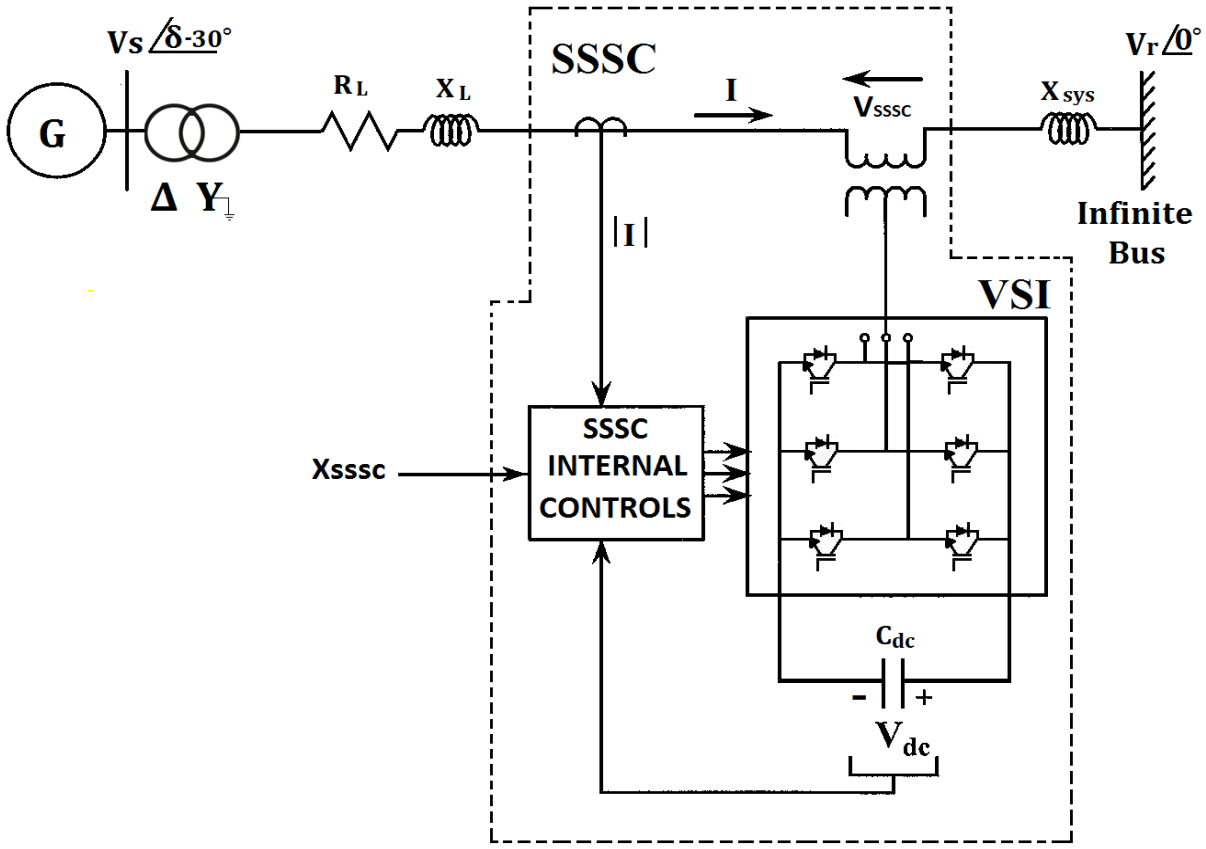

Figure 3.8: *The single machine infinite bus power system incorporating the VSI-based SSSC*

Table 3.1: Parameters of the SSSC

Parameter	***Value in Per Unit***	***Actual Value***
V_{dc0}	0.22494	70 kV
V_{dc}* or V_{ref}	0.1 V_{dc0}	7 kV
w_0	1.0	376.9911 rad/s
C_{dc}	0.12208	375 µF
K_{vp}	10.159	9711.91
K_{ai}	3.9*w_0	1470.27
H_p	0.3	0.3

Table 3.2: Parameters of the IEEE FBM Transmission line

Parameter	***Value in Per Unit***	***Actual Value***
X_L	0.50	162.9733 Ω
R_L	0.02	6.0832 Ω

3.4.3. Performance and validation of the SSSC Model

This subsection determines whether the SSSC can provide the required amount of series compensation in the 500 kV transmission network of figure 3.8, at the rated system frequency (i.e. 60 Hz). The susceptibility of the SSSC to the system disturbances is also evaluated. It should be noted that for the purpose of the investigations in this subsection, the SSSC is connected to the transmission network of figure 3.8 with the generator replaced by the three-phase AC voltage source of the same amplitude (i.e. 26 kV) while the infinite bus voltage is kept at 500 kV and the transmission angle is *delta* (δ).

Figure 3.9 shows the system response with the transmission angle *delta* (δ) set to 15.1° and compensating reactance at 81.40 Ω (i.e. 0.25 pu). To confirm that the SSSC is indeed capable of providing the required amount of series compensation, the power transferred over the line P_{tr} and the RMS value of line current I_{rms} in the SSSC compensated line (figure 3.9 (a)) are compared with those in a capacitor compensated line (figure 10 (b)). The results show that at steady state, the SSSC is capable of injecting the voltage that emulates the required capacitive reactance in series with the line.

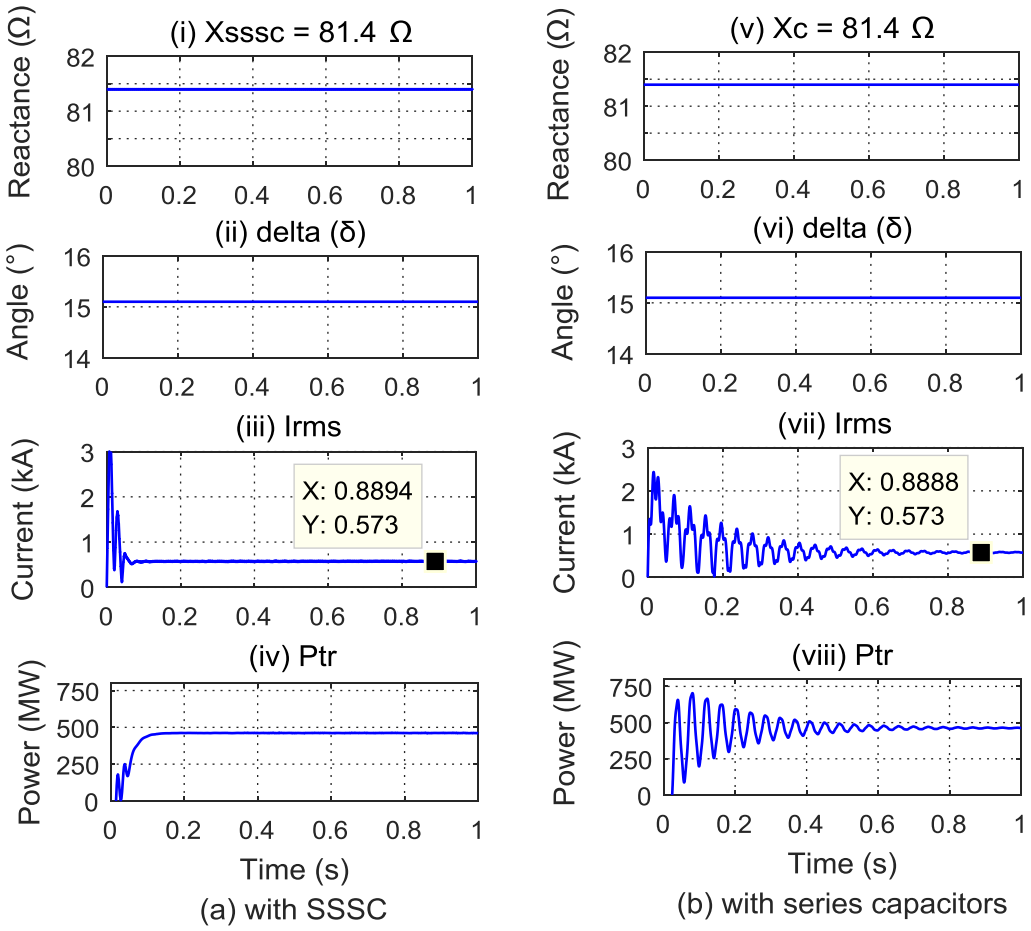

Figure 3.9: *Response of the SMIB power system, (a) compensated by the SSSC (b) compensated by conventional series capacitors*

Rapid controllability of the commanded compensating reactance X_{sssc} provided by the SSSC is demonstrated in figure 3.10. At t = 0.5 s, X_{sssc} is increased from 16.12 Ω to 32.56 Ω and then increased to 65.12 Ω at t = 0.65 s. X_{sssc} is further increased to 97.68 Ω at t = 0.8 s, decreased to 48.84 Ω at t = 0.95 s and finally decreased back to 16.28 Ω at t = 1.1 s, while δ is kept at 15.1° and V_{ref} at 7 kV. The results show that increasing X_{sssc} increases the injected voltage and the line current as well as the power transferred over the line as expected. This is because a larger portion of the line's inductive reactance gets cancelled, hence increasing the power transfer capability of the line. Conversely, reduction of the compensating reactance provided by the SSSC results in reduction of the power transferred over the line. The angle Θ_{iv} by which the line current leads the commanded value of the phase voltage *VinjA** to be injected by the SSSC into the line is maintained at 90° by as seen in figure 3.10 (e).

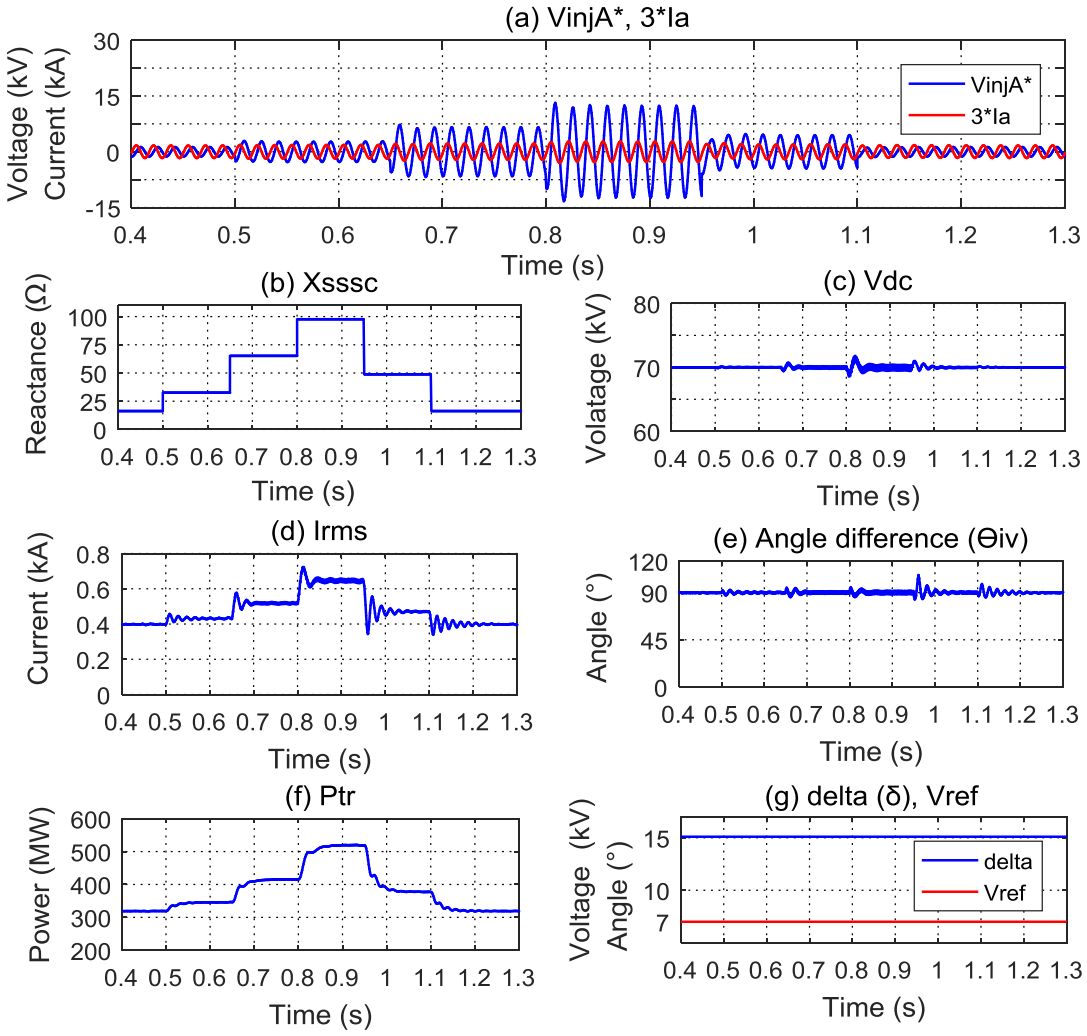

***Figure 3.10**: Simulated SSSC and system response to rapid change in the commanded SSSC compensating reactance X_{SSSC}*

Figure 3.11 shows the response of the SSSC when the transmission angle *delta* (δ) is increased from 15.1° to 27.1° at t = 0.5 s and then reduced back to 15.1° at t = 0.7 s, with the compensating reactance

X_{sssc} kept at 65.12 Ω (i.e.) and V_{ref} at 7 kV. The line current phasor I_a is scaled by a factor of three so that it can be compared with the commanded voltage phasor V_{injA}* to be injected by the SSSC. The SSSC is able maintain the DC link voltage at 70 kV and the injected voltage in lagging quadrature (i.e. lagging by 90°) with line current and as shown by figures 3.11 (d) and 3.11 (f) respectively. Furthermore, as the transmission angle *delta (δ)* is increased, the injected voltage, line current and the power dispatch (P_{tr}) over the line increase as shown in figures 3.11 (b) and 3.11 (g), which is in agreement with equation 1.1 (for δ below 90°).

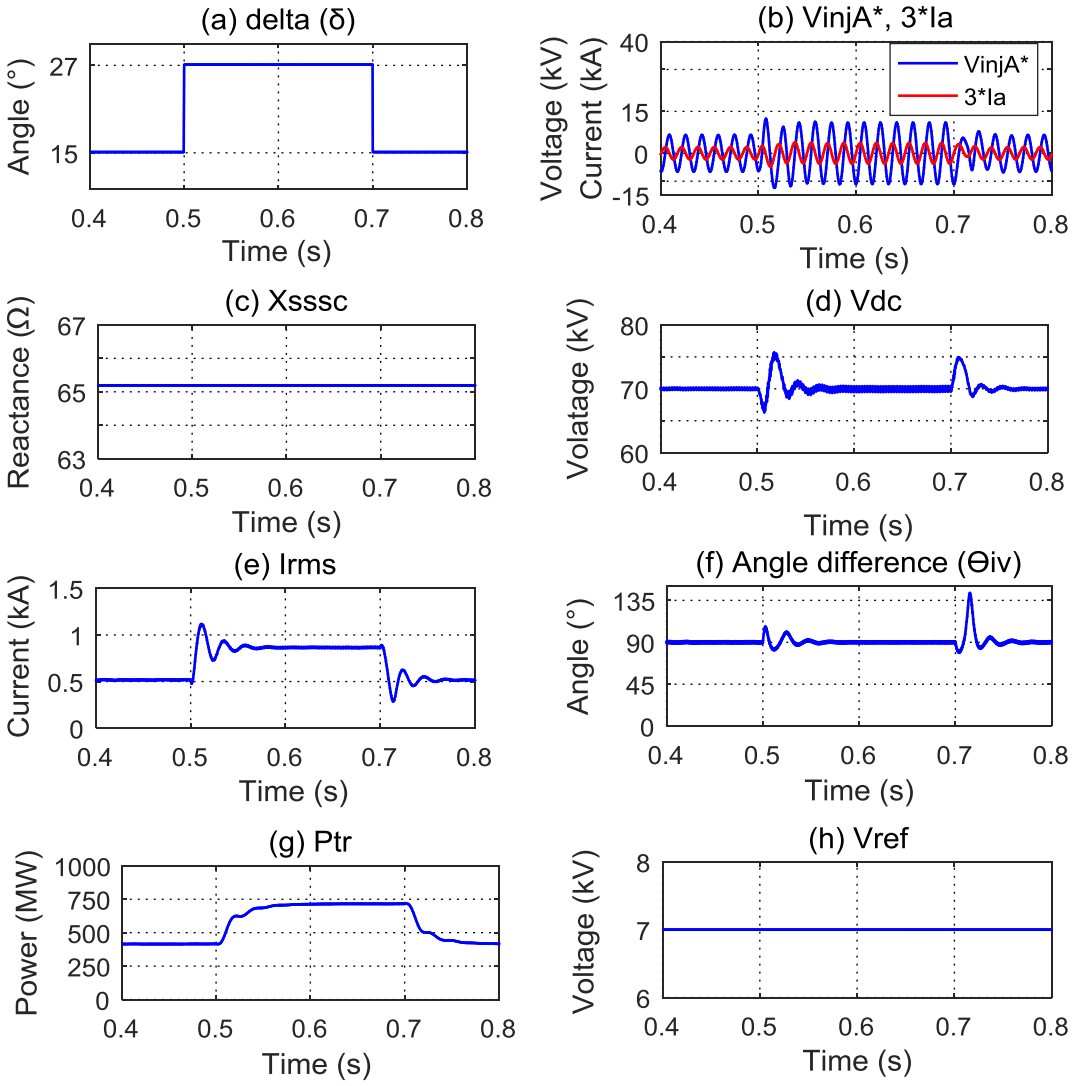

Figure 3.11: *Simulated response of the SSSC and the transmission system when the transmission angle is increased from 15.1° to 27.1° and then decreased back to 15.1°.*

Finally, the performance of the SSSC is evaluated when there is a step change in the DC link reference voltage V_{ref}. Figure 12 shows the response of the SSSC and the system when V_{ref} is increased from 7 kV to 7.5 kV at t = 0.5 s, and then decreased back to 7 kV at t = 0.7 s, while X_{SSSC} is kept at 81.40 Ω and δ at 15.1°. The results in figure 3.12 show that the SSSC is capable of withstanding the disturbances on the DC side of its inverter. The commanded value of the voltage to

be injected V_{injA}* and the power dispatched P_{tr} are maintained, showing that the inverter is able to maintain the required amount of series compensation of the transmission line.

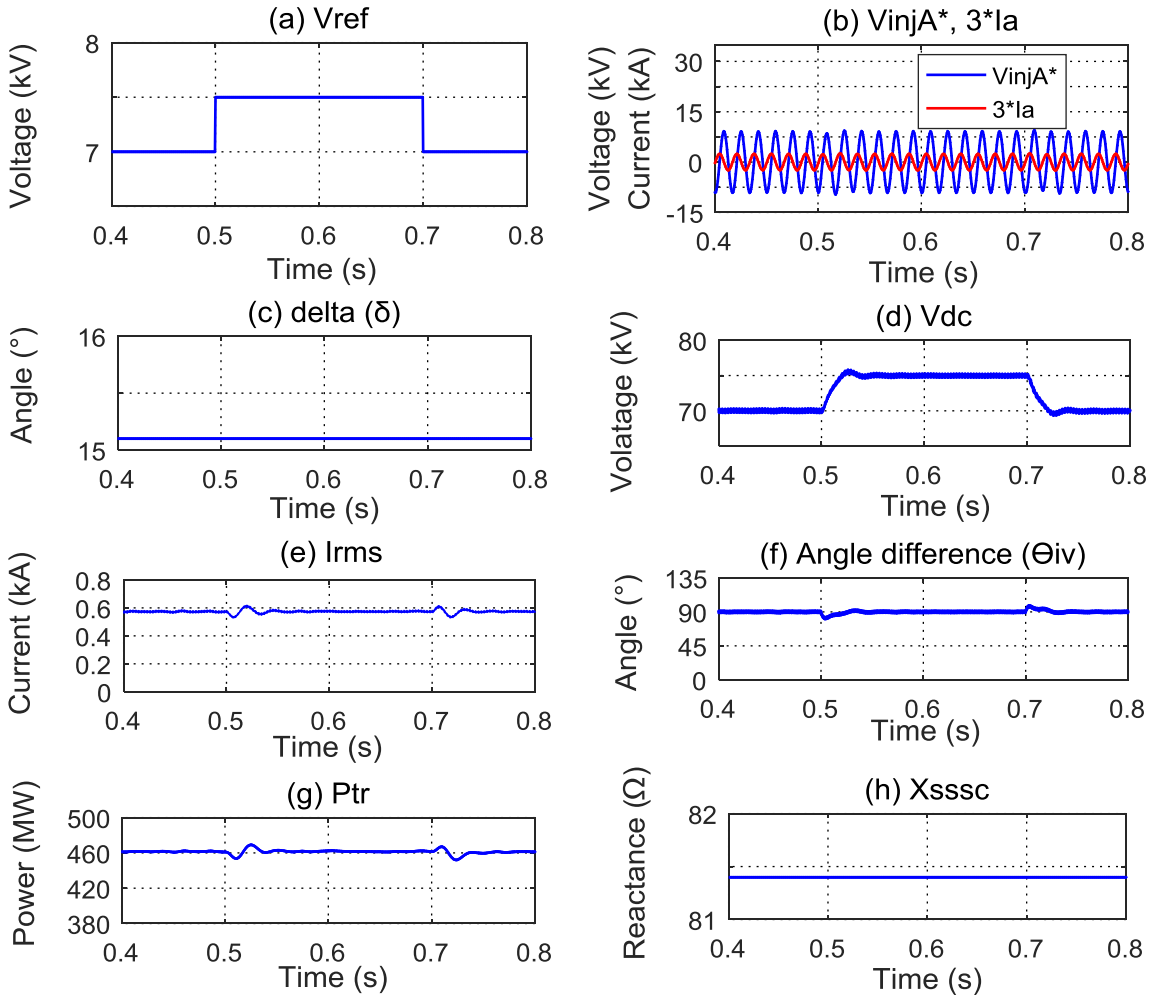

Figure 3.12: *Simulated system and SSSC response when V_{ref} is increased from 7 kV to 7.5 kV and then decreased back to 7 kV*

The performance of the SSSC developed in this section is presented in figures 3.10 – 3.12 are in agreement with those obtained earlier by others [79, 81, 84]. Hence, the results validate the model of the SSSC that has been developed in PSCAD for this thesis.

3.5. Conclusion

This chapter has presented mathematical modelling of the system under study, namely the IEEE first benchmark model for SSR analysis. Preliminary eigenvalue analysis in [80] has been used to predict the values of capacitive reactance expected to result in the worst torsional interaction with the turbine-generator shaft modes. This analysis technique is, however, computationally intensive [3], neglects non-linearity of the power system components such as power electronic switches if any are present. Therefore, in subsequent chapters, frequency scanning and non-linear time domain simulations will be

used to analyze SSR. Performance of the SSSC prototype has been evaluated in the presence of disturbances in the system. The results show that the SSSC has a well damped dynamic response and its dynamics are not susceptible to disturbances in the system. The effects that the SSSC internal controls have on the transmission network are investigated in the next chapter.

CHAPTER FOUR

RESONANT CHARACTERISTICS OF THE SERIES COMPENSATED TRANSMISSION NETWORK

4.1. Introduction

In the previous chapter, a detailed mathematical modelling of the study system was presented. This chapter aims at studying the resonant characteristics of the series compensated network to assess the potential risk of SSR. Initially, the harmonic impedance solution (HIS) is used to determine the resonant frequency of the series capacitor compensated network using linear circuit theory analysis. The frequency-response test (FRT) methodology proposed by other researchers in [18,87] for network impedance scanning is presented and validated against theoretical calculations for a series capacitor compensated network of the IEEE first benchmark model. Lastly, the FRT methodology is used to investigate whether the SSSC has a potential to excite SSR in the power system, and to investigate the impact of dual compensation on SSR characteristics of the transmission network.

In order to get a better understanding of the SSR characteristics of the SSSC, the resonant characteristics of the SSSC compensated transmission line are compared with those of the capacitor compensated line that are known to cause SSR problem in the power system [18,85,87].

4.2. Harmonic Impedance Scanning

Harmonic impedance scanning is a technique used to determine the net impedance of the transmission network (seen from behind the equivalent impedance of the generator under study) as a function of frequency. This method can be used to approximate the frequency of electrical resonance in a series compensated network. If the dip occurs in the magnitude of the system impedance, then there is a likelihood of subsynchronous interactions between such a transmission network and the mechanical systems of the nearby turbine-generator shafts.

4.2.1. Harmonic Impedance Solution (HIS)

This is a feature (component) available in PSCAD that allows impedance scanning of electrical systems [85]. This component generates the system impedance matrix in phase domain and then collapses it into an equivalent matrix as seen from the point of interface. For transmission line or cable models, this component uses the RLC data directly. However, for accurate representation of unbalanced transmission lines or Y-Δ transformers, the equations are solved in phase domain without using sequence networks. The process is repeated for each frequency in the range specified by the user in the parameter inputs to generate the impedance response in frequency domain. Figure 4.1 shows the use of the harmonic impedance solution to scan the impedance of the capacitor compensated IEEE FBM network, with the synchronous generator replaced by the three-phase AC voltage source of the same amplitude behind the generator's sub-transient reactance. The impedance

of this source is kept high during simulation to ensure that the impedance scanned corresponds to the transmission network impedance only.

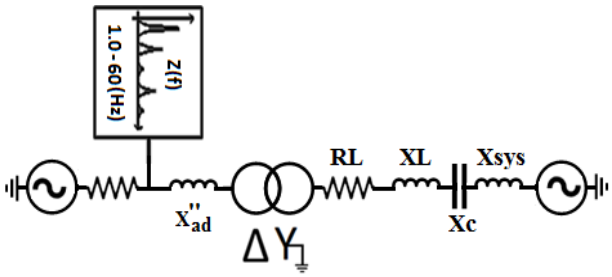

Figure 4.1: *Diagram showing the interface to harmonic impedance solution to scan the network impedance*

The output from the harmonic impedance solution is in a form of a text file consisting of frequency, magnitudes and phase angles of the sequence impedances. The data can be analysed in any external graphical analysis program, such as Excel, or MATLAB. The latter is used for the studies in this thesis. The assumptions made in the harmonic impedance solution calculations include the following:

(a) Transformer saturation and arresters are assumed to be in their unsaturated region.

(b) All power electronic devices are assumed to be in their OFF state.

Figure 4.2 shows harmonic impedance of the series capacitor compensated IEEE FBM with $X_C = 0.3707$ pu. The electrical resonant frequency, f_{er} at this degree of series compensation is 39.9 Hz. This will develop and an air gap electromagnetic torque at a complimentary (slip) frequency (i.e. $f_0 - f_{er}$) of 20.1 Hz, which is close to Mode 2 (at 20.21 Hz) of the shaft system. Thus, there is a risk of SSR due to torsional interaction through destabilization of this particular mode of oscillation.

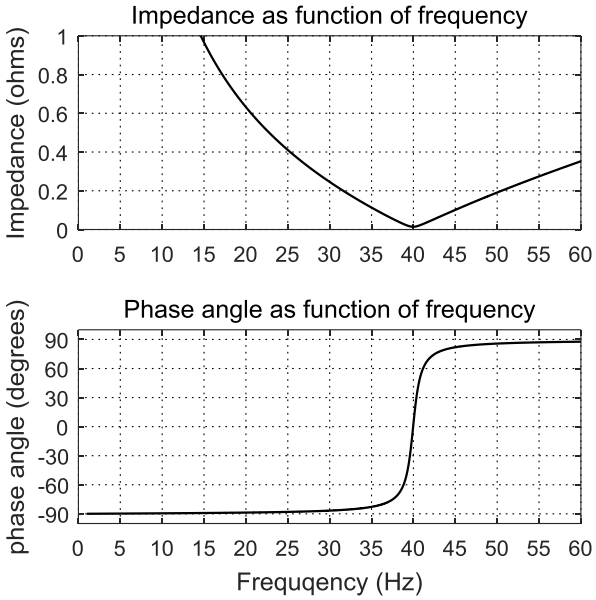

Figure 4.2: *Network impedance of the capacitor compensated IEEE FBM with $X_C = 0.3707$ pu*

Figure 4.3 (a) shows how the resonant frequency in the electrical network varies with the compensating capacitive reactance X_C in the IEEE FBM as predicted using the harmonic impedance solution. On the other hand, figure 4.3 (b) shows variation of the complimentary frequency (f_0 - f_{er}) of the air gap torque with capacitive compensating reactance. Figure 4.3 (b) also indicates the values of X_C at which the slip frequency of the electromagnetic torque coincides with the natural resonances of the IEEE FBM shaft system, which are expected to result in the worst torsional SSR interaction. Worst destabilization of Mode 1 is expected to be at X_C = 0.455 pu, Mode 2 at X_C = 0.367 pu, Mode 3 at X_C = 0.275 pu, Mode 4 at X_C = 178 pu and Mode 5 at X_C = 0.0365 pu. These results agree closely with the predictions presented in Chapter Three using eigenvalue analysis in [80].

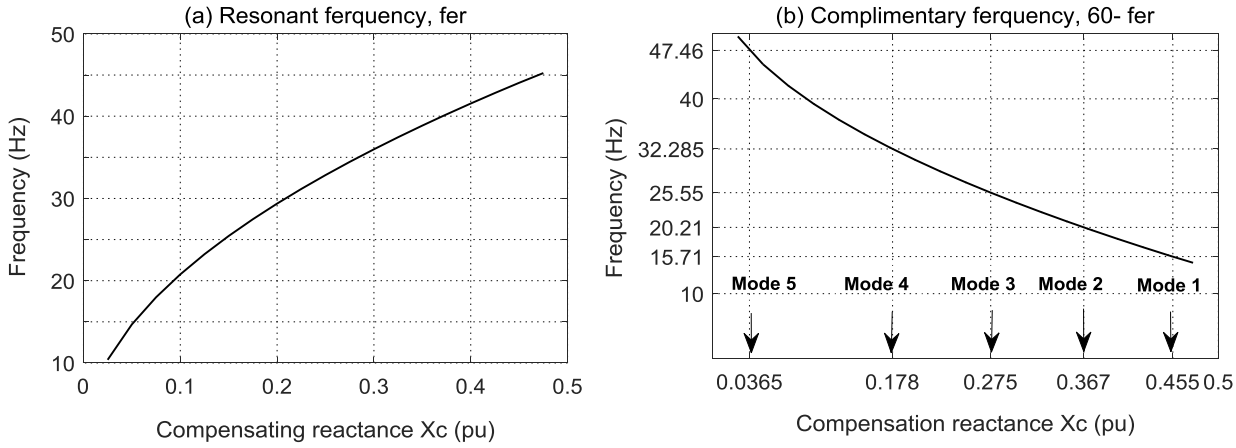

Figure 4.3: *Variation of electrical resonant frequency with compensating capacitive reactance obtained for the series capacitor compensated IEEE FBM*

This method is efficient since the magnitude and the phase of network impedance for the entire frequency range of interest can be obtained within a single simulation run, for a given operating point. However, due to assumption (b) above, this method cannot determine the effective impedance of the power electronic based devices such as FACTS controllers or even wind turbine-generators. Thus, it is not suitable for resonance studies in a transmission line incorporating the SSSC, hence why the use of the frequency-response test methodology is proposed.

4.2.2. Frequency-Response Test (FRT) methodology

As mentioned in the previous subsection, the major drawback of the harmonic impedance solution technique is its inability to determine the effective impedance of power electronic devices. So to determine the SSR characteristics of the SSSC, the frequency-response test methodology proposed in [87] is used and its equivalent circuit is shown in figure 4.4. Here the network impedance is monitored in the presence of subsynchronous currents that are deliberately injected into the system. The net impedance of the SSSC compensated transmission network of the IEEE FBM is determined as follows:

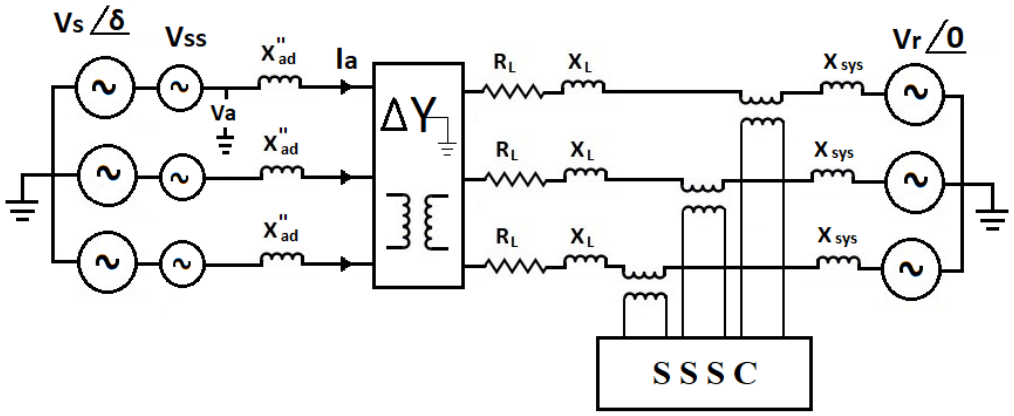

Figure. 4.4: *Diagram of the simulated frequency-response test (FRT) equivalent circuit*

(a) As with the harmonic impedance solution, the synchronous generator is replaced by the three-phase AC voltage source. The transmission network is fed with the normal transmission line voltage at its sending and receiving ends, which are separated by some transmission angle δ. A small subsynchronous voltage V_{SS} (10% of the sending-end voltage amplitude) is inserted in each phase at the sending end, as in figure 4.4. The frequency of the subsynchronous voltage is set to a value lower than the power system frequency.

(b) Steady-state response of the transmission line voltages and currents to this combination of subsynchronous and synchronous forcing voltages is obtained.

(c) The Fast Fourier Transform (FFT) analysis is carried out on time domain results to extract the magnitude and phase relationship between the voltage and current phasors so as to obtain the net impedance of the line at the given frequency.

(d) The frequency domain characteristics of the line are obtained by repeating the above steps (a) to (c) for a frequency range of interest.

4.2.2.1. Validation of the Frequency-Response Test Methodology

Before applying this technique to obtain resonant characteristics of the IEEE FBM transmission network in the presence of the SSSC, it is worth validating it to have confidence in it. This is achieved by comparing the results obtained using this method with the theoretical results from harmonic impedance solution for the series capacitor compensated IEEE FBM (i.e. replacing the SSSC in figure 4.4 with series capacitor banks).

Figure 4.5 shows comparison of the FRT and HIS techniques, showing harmonic impedance of the series capacitor compensated IEEE FBM for the values of X_C perceived to excite the torsional modes of the turbine-generator shaft from figure 4.3. The frequency-response test results are in agreement with the theoretical results. Furthermore, the network impedance exhibits a resonant minimum and becomes purely resistive at some subsynchronous frequency (i.e. less than f_0), and this is the root cause of SSR.

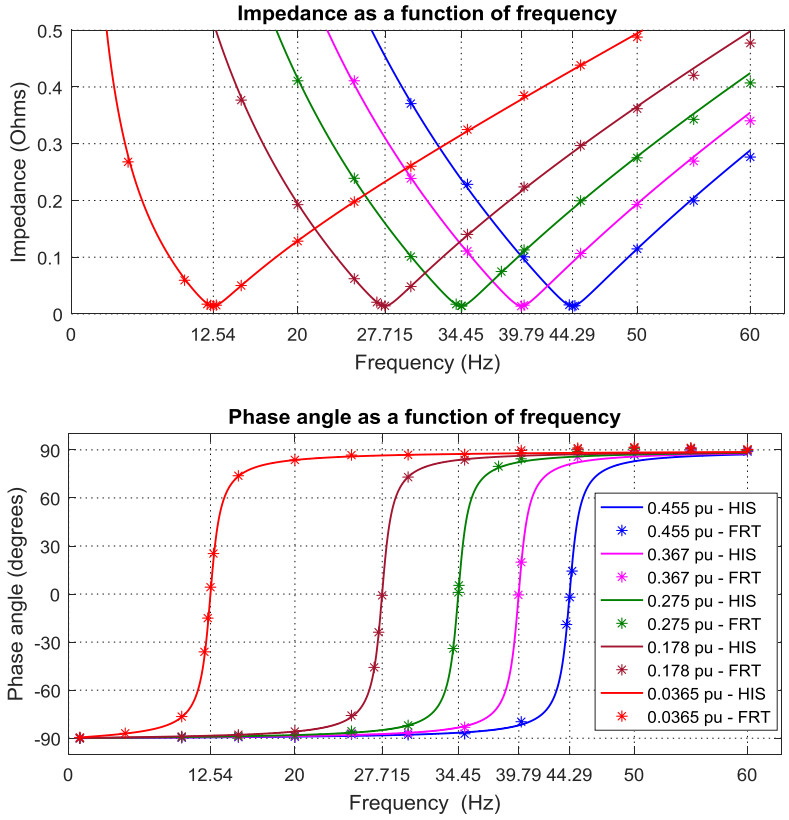

Figure 4.5: *Validation of the frequency-response test (FRT) methodology through comparison with the results from harmonic impedance solution (HIS)*

The network impedance changes from capacitive to inductive as the frequency is increased from 1 Hz to 60 Hz in each case, and the resonant frequency is the same as that obtained from equation 1.3 in Chapter One. Lastly, for all values of X_C considered, the minimum impedance is 0.01416 Ω, which is the line resistance seen from the armature of the generator.

4.3. Resonant Characteristics of the IEEE FBM incorporating the SSSC

This section investigates the resonant characteristics of the IEEE FBM transmission network in the presence of the SSSC. The objective here is to determine whether the SSSC has the potential to excite SSR on its own in the power system. The frequency-response test methodology is used to approximate the frequency of electrical resonance, f_{er}.

4.3.1. IEEE FBM Compensated with the SSSC only

Figure 4.6 shows the network impedance (magnitude on the left and the corresponding phase angle on the right) as a function of frequency, considering different values of compensating reactance, X_{SSSC}. From figure 4.6, two major similarities are noted from the SSSC compensated network and the one compensated by series capacitors. In both cases, the magnitude of the system impedance exhibits a resonant minimum at subsynchronous frequency and the resonant frequency increases with the degree

of series compensation. However, the magnitude of the network impedance at resonant frequency is larger with the SSSC compensation than with series capacitor compensation.

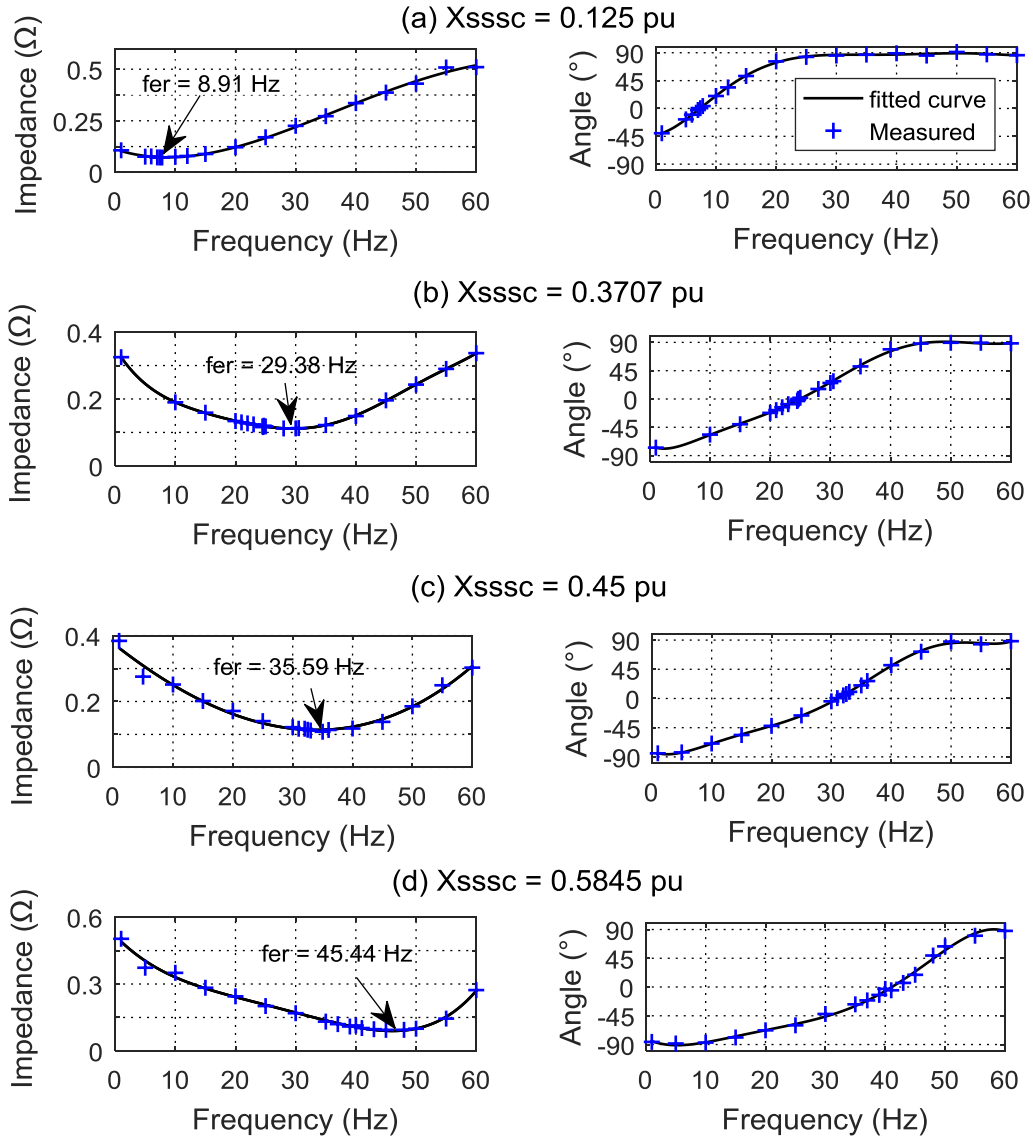

Figure 4.6: *Harmonic impedance of the SSSC compensated IEEE FBM*

The work of [85] has shown that the SSSC injects not only capacitive reactance but also some resistance at subsynchronous frequencies, and this reportedly adds positive damping to the subsynchronous oscillations.

Figure 4.7 shows variation of the resonant frequency with compensating reactance (X_{SSSC}) in the SSSC compensated IEEE FBM. The values of X_{SSSC} at which the slip frequency of the air gap torque matches the shaft resonances are also indicated. Comparison of figure 4.7 and figure 4.3 shows that the resonant frequency with the SSSC compensation is lower than that with series capacitors for a given degree of series compensation. As a result, the worst-case interactions with the shaft resonances each occurs at higher degree of compensation with the SSSC than with series capacitor banks.

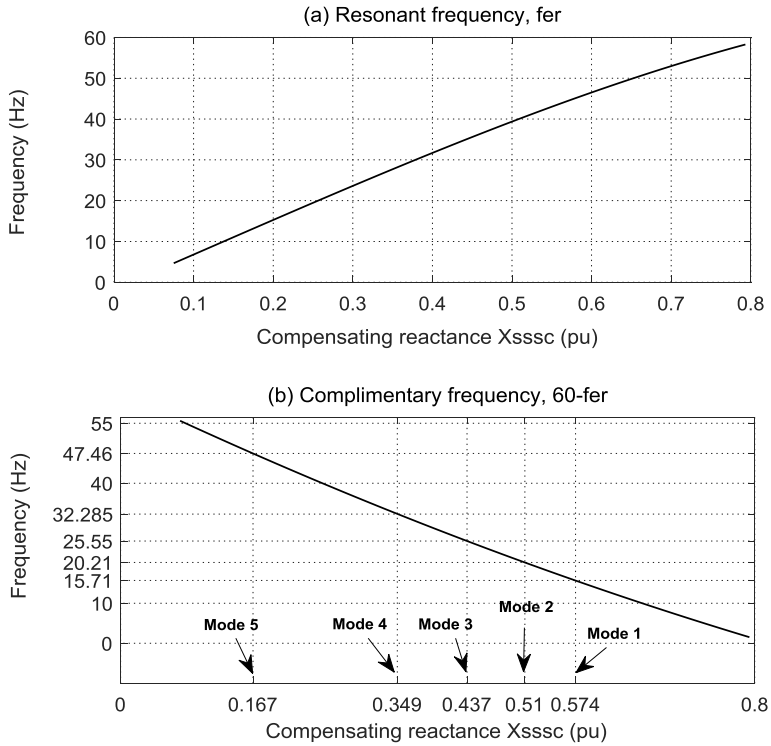

Figure 4.7: *Variation of electrical resonant frequency with compensating capacitive reactance for the SSSC compensated IEEE FBM*

The following subsection extends the frequency response test technique to the IEEE FBM with dual (hybrid) compensation, where series compensation is provided by the SSSC in conjunction with series capacitor banks.

4.3.2. IEEE FBM with Dual Compensation (SSSC and series capacitor banks)

Various studies in the literature have indicated that the cost of installing a SSSC is high due to the injection transformers [8, 17]. The study in [8] has shown that by using dual compensation (SSSC and series capacitors), the benefits of the SSSC can be realized at a lower cost. In this subsection, three case studies with dual compensation of the IEEE FBM are considered as given in *Table 4.1*.

In all cases studies, the total compensating reactance, X_{comp} is 0.3707 pu. For *Case 1a*, the SSSC accounts for 20 % (X_{SSSC} = 0.07414 pu) of total series compensating reactance while the other 80 % is provided by series capacitors (X_C = 0.29656 pu). For *Case 1b*, the SSSC provides 40 % (X_{SSSC} = 0.14828 pu) while series capacitors provide 60 % (X_C = 0.22242 pu) of the total series compensating reactance. Lastly, for *Case 1c*, 60% of total series compensating reactance is provided by the SSSC (X_{SSSC} = 0.22242pu) while the series capacitors account for 40% (X_C = 0.14828 pu) of total compensating reactance.

The harmonic impedance of the IEEE FBM with dual compensation is shown in figure 4.8 for the case studies 1a – 1c. The results show that as the ratio of X_{SSSC} to X_C is increased, the electrical resonant frequency of the transmission network decreases and the resonant impedance of the network

increases, thus better damping of SSR can be expected. For all the three cases considered, the net system impedance at rated system frequency (i.e. 60 Hz) is the same which implies that the total reactance provided by the SSSC and series capacitor banks is the same in all cases as expected. This confirms the SSSC's ability to provide the required amount of series compensation.

Table 4.1: Summary of the case studies for dual compensation

Case Study	X_{SSSC} (pu)	X_C (pu)	$\frac{X_{SSSC}}{X_{Comp}}$	***Total*** X_{Comp} (pu)
Case 1a	0.07414	0.29656	0.20	0.3707
Case 1b	0.14828	0.22242	0.40	0.3707
Case 1c	0.22242	0.14828	0.60	0.3707

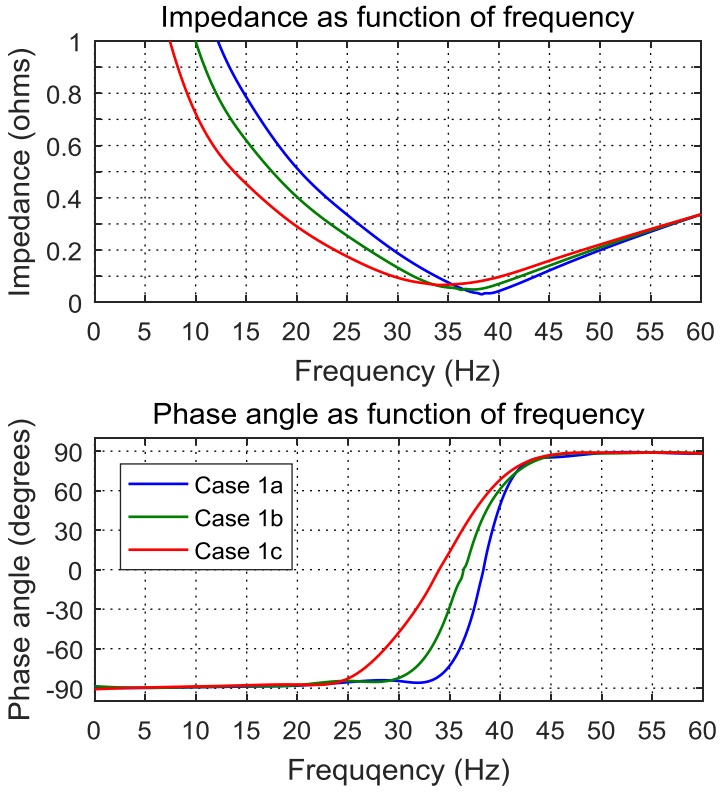

Figure 4.8: *Resonant characteristics of the dually compensated IEEE first benchmark model*

The resonant frequency in *Case 1a* is 38.29 Hz resulting in the complimentary frequency of 21.71 Hz for the air gap torque, which is close to Mode 2 of the turbine-generator shaft in the IEEE FBM. Likewise, for *Case 1b* and *Case 1c*, the resonant frequencies are 36.29 Hz and 34.15 Hz respectively, giving the complimentary frequencies of 23.71 Hz and 25.85 Hz. The latter is close to Mode 3 of the turbine-generator shaft, thus SSR due to destabilization of Mode 3 can be expected for *Case 1c*.

4.4. Conclusion

This chapter has presented the resonant characteristics of the series compensated transmission network of the IEEE FBM. SSR characteristics of the SSSC have been investigated using the harmonic impedance scanning technique. The results show that the SSSC can excite SSR on its own in the power system, since it provides capacitive reactance not only at the rated system frequency, but also at subsynchronous frequencies. This can cause an electrical resonance at subsynchronous frequencies, which may lead to SSR in the same manner that conventional series capacitors do. The impedance of the transmission network with dual compensation also exhibits a resonant minimum indicating the potential risk of SSR interaction with the nearby turbine-generator shafts. Therefore, prior to installing the SSSC in the power system, its SSR characteristics should be known as well the resonances of the nearby turbine-generator shafts.

Although resonant studies can predict the possibility of SSR interactions by approximating the frequency of electrical resonance, they do not demonstrate the severity of SSR instability. In the next chapter, the non-linear time domain simulations are presented to analyse SSR. The design of the supplementary subsynchronous damping controller for the SSSC to mitigate SSR is also presented.

CHAPTER FIVE

DAMPING CONTROLLER DESIGN AND ITS PERFORMANCE IN THE IEEE FIRST BENCHMARK MODEL

5.1. Introduction

The effects of the SSSC's internal controls on the dynamics of the transmission line have been investigated in the previous Chapter using the IEEE FBM transmission network. SSR characteristics of the SSSC were established in frequency domain using the harmonic impedance scanning technique. Comparison of the resonant characteristics of the SSSC compensated transmission line with those of a series capacitor compensated line has shown that the SSSC in not inherently immune to SSR, although it can provide some additional damping to the torsional oscillations in the system.

This chapter now presents a detailed design of the supplementary damping controller for the SSSC to damp SSR in cases where the damping provided by the SSSC is not adequate for small signal stability of the power system. The time domain transient simulations are presented to analyze the post-transient response of the power system and to assess the effectiveness of the damping controller in mitigating SSR in the IEEE FBM. In all graphical representations of the system response in time domain, LPA to LPB torque will be used to denote the torque in the section of the shaft connecting the low pressure turbine section A and the low pressure turbine section B. Similarly, generator to exciter torque will be used to denote the torque in the generator-exciter shaft.

5.2. Modulating Line Reactance to Damp Post-Transient Oscillations

The idea of damping SSR through modulation of the transmission line reactance originates from the quite primitive practice of switching the fixed series capacitor in or out of the line using circuit breakers [89]. The typical approach used was the 'bang-bang' control since the line reactance was varied in steps based on the algorithm below:

$$\begin{aligned} &Insert\ \ X_C\ if\ \ w - w_0 > 0 \\ &\mathrm{Re}move\ X_C\ if\ \ w - w_0 < 0 \end{aligned} \tag{5.1}$$

The main drawback of the bang-bang control approach has been that of the controller chatter whereby small deviations in the generator speed near steady state would result in an undesired operation of the controller. The SSSC and other series FACTS devices, on the other hand, provide controllable series compensation, a feature that may enable implementation of the above idea or the modification thereof in a continuously controllable fashion.

5.2.1. Input Signals for a SSSC-based SSR Damping Controller

Selection of the appropriate input signal(s) to the SSR damping controller is a fundamental aspect of the robust controller design. The chosen signal should contain the oscillation modes of interest (i.e. modes that may require damping) and be able to provide the required controllability at all times. In practice, the control signal may be synthesized from the local measurements on the transmission line (e.g. line power flow, node voltages) or from the remote signals in the generating environment (e.g. generator speed deviation). Although local signals may be readily available and at low cost, they may not contain all the desired oscillation modes and therefore may compromise the controller performance. Speed deviation of the generator contains all the critical oscillation modes of the turbine-generator shaft system and it has been a logical candidate for the controller input signal in most studies [17,63,89]. Although this is remote signal, advancements in fiber optics communication and global positioning system (GPS) made it possible to measure and send the signal to the control location, even in real time [89]. This thesis utilizes the generator speed deviation as the damping controller input signal as shown in figure 5.1.

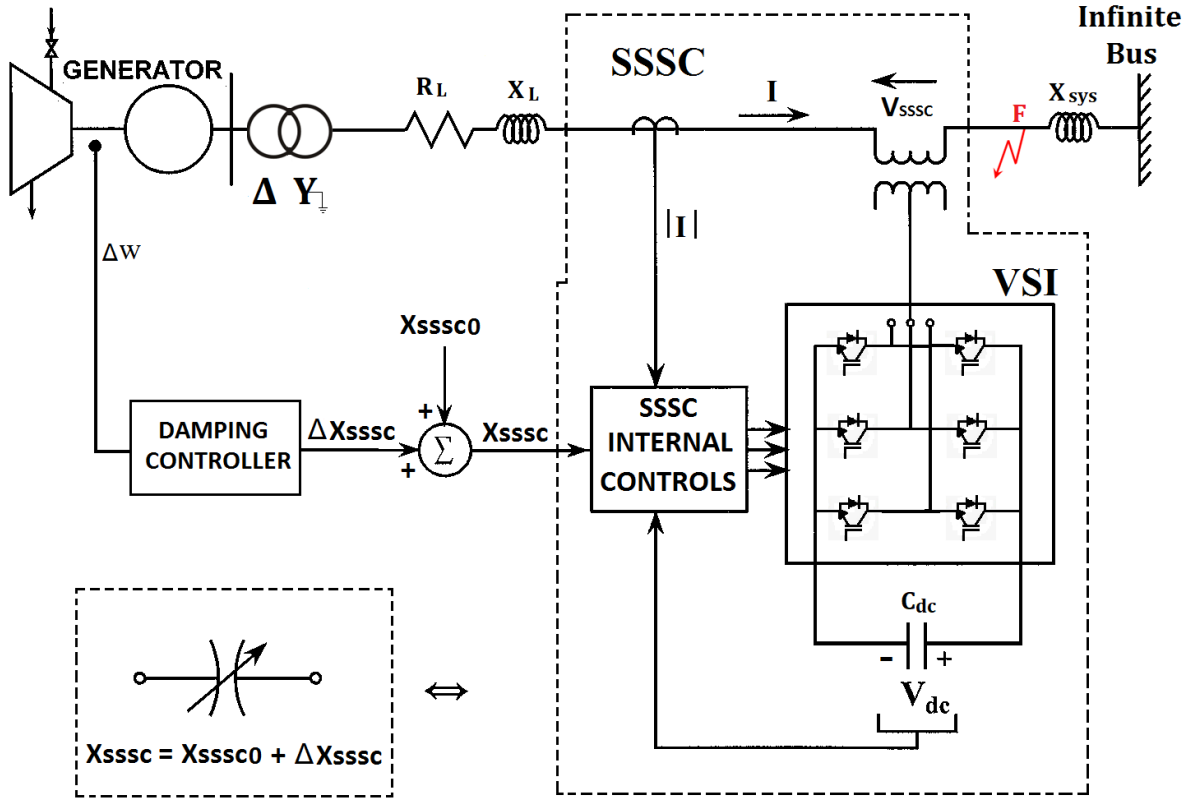

Figure 5.1: *Equivalent circuit of the IEEE FBM compensated by the SSSC that is equipped with the supplementary damping controller*

5.2.2. Structure and Design of the Supplementary Damping Controller

The power system response following a disturbance largely depends on the electrical torque in addition to other factors. The change in the synchronous machine electrical torque subsequent to a

system perturbation can be resolved into synchronizing and damping torque components denoted by $T_s\Delta\delta$ and $T_D\Delta w$ respectively, as given by equation 5.2.

$$\Delta T_e = T_s\Delta\delta + T_D\Delta w \tag{5.2}$$

where: T_s = synchronizing torque coefficient

T_D = damping torque coefficient

Synchronizing torque is the component in phase with the rotor angle deviation while the damping torque is the component in phase with the rotor speed deviation. In order to damp the torsional oscillations in the system, the external controller should be able to improve the damping torque component by ensuring that ΔT_e is almost in phase with rotor speed deviation, Δw.

If the generator rotor speed deviation Δw oscillates at some subsynchronous frequency due to torsional motion, the damping controller should modify the compensating reactance of the SSSC to produce a component of ΔT_e that is in phase with the original subsynchronous oscillation in rotor speed, Δw. The lead-lag structure is chosen to provide the phase compensation as it offers ease of online tuning and is therefore preferred by most power system utilities [89].

5.2.2.1. Single-mode Damping Controller

For a single-mode damping controller, the SSSC-based SSR damping controller is of the structure shown in figure 5.2 [89].

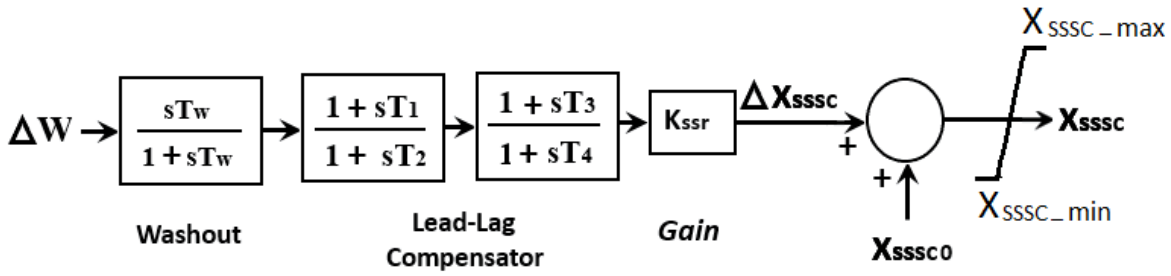

Figure 5.2: *The structure of the single-mode SSR damping controller for the SSSC [89]*

The first component in figure 5.2 is the signal washout, which acts as a high pass filter to ensure that only oscillatory components of Δw are allowed to pass unchanged. The value of this filter's time constant, T_W, is non-critical and can be between 1 s and 20 s [79,89]. In this thesis, the value of 10 s is used. The lead-lag compensator block compensates for the phase lag measured between the oscillation in generator speed and air gap torque. The value of series compensating reactance required from the SSSC at steady state is X_{SSSCO}. The controller output ΔX_{SSSC} is a modulated reactance, which is added to the steady state reactance X_{SSSCO} to give the commanded reactance, X_{SSSC}, which the SSSC should

provide, to modulate the generator electromagnetic torque and damp out subsynchronous oscillations. K_{ssr} is the gain of the controller.

Now, after the damping controller input signal and the structure have been chosen, the next step is to establish the approach for determining the phase angle between Δw and ΔT_e to be compensated for by the damping controller as well as the controller gain K_{ssr}. The following steps explicate the procedure for obtaining the phase lag between ΔT_e and Δw at a frequency of interest.

(a) A sinusoidal test signal of a small amplitude and a frequency of interest (frequency of the torsional mode to be damped) is injected into the ΔX_{sssc} input of figure 5.1 (without damping controller block).
(b) The steady state phase angle between the resulting torque oscillations ΔT_e and the controller input ΔX_{sssc} is measured using Fast Fourier Transform.

The inertia constant of the generator in the IEEE FBM is set to a very large value during the measurements above. This artificial decoupling technique prevents the steady state oscillations in ΔT_e to influence the rotor speed or rotor angle [17].

The suitable compensator (lead or lag) is then designed, from which the values of the time constants T_1 - T_4 are obtained, to counteract this phase difference. If ΔT_e leads ΔX_{sssc}, a lag compensator is required and if ΔT_e lags ΔX_{sssc}, then a lead compensator is required.
The controller in figure 5.2 with the parameters obtained above is then connected in the external loop of figure 5.1 (damping controller block). The range of values for K_{ssr} are considered and the one that gives satisfactory damping of the torsional mode of interest without destabilizing other critical modes is chosen.

5.2.2.2. Multi-modal Damping Controller

In cases where the subsynchronous oscillations arising in the power system are multi-modal in nature, a single-mode damping controller may not be adequate to damp all critical mode oscillations. The work of [17, 18] has shown that in such a case, the damping controller should be designed to provide damping of multiple torsional modes. Specifically, in [17], the design of a multi-mode damping controller is based on the dominant modes in the generator speed deviation. The approach in this thesis is similar to that in [18], which is based on all torsional modes, excluding Mode 5, which was found to be stable for all operating points considered as would be illustrated in time domain results.

The structure of the multi-modal damping controller, obtained by cascading individual mode controllers, is shown in figure 5.3, adopted from [19]. In addition to the lead compensators and gain blocks in each of the controller branches, there are bandpass filters to extract components of speed deviation at each of the critical torsional frequencies to be damped. The design of the phase

compensators for the multi-modal damping controller is done for each mode in turn, in a similar manner to that in the single-mode controller.

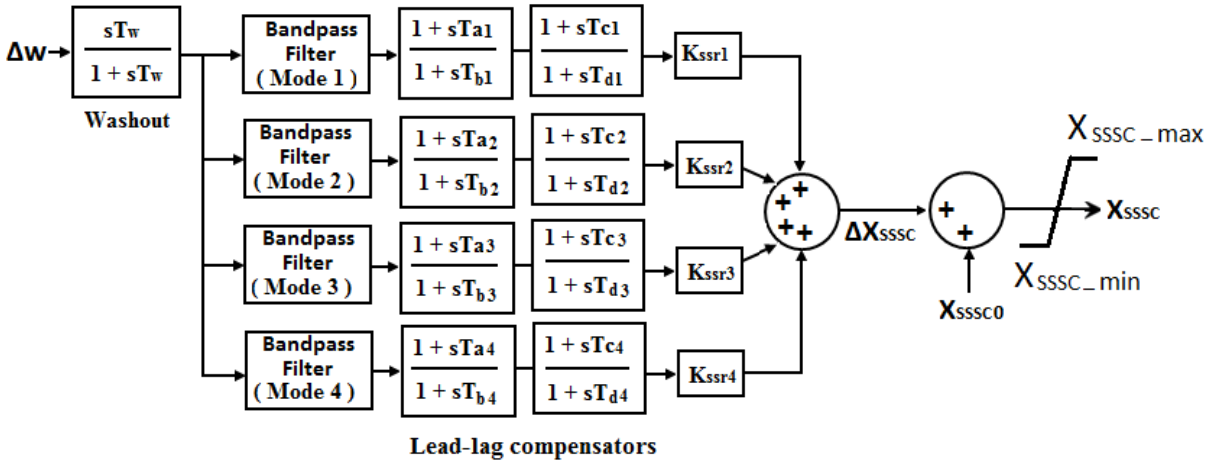

Figure 5.3: *The structure of the multi-mode SSR damping controller for the SSSC [19]*

Individual controller gains are determined as follows, using an example of K_{ssr1} for Mode 1:

(a) All other gains are set to zero (making their respective single-mode controllers ineffective).

(b) A range of values of K_{ssr1} is considered, and a value resulting in a satisfactory damping of Mode 1 without destabilizing other modes was determined (based on time domain simulations and Fast Fourier Transform analyses).

The other controller gains, $K_{ssr2} - K_{ssr4}$ are also determined in a similar manner, in turn.

5.3. SSR analysis in the IEEE FBM with a Single Transmission Line

This subsection investigates subsynchronous resonance in a single transmission line network of the IEEE FBM. Initially, the time domain simulations are presented to compare the performance of the SSSC with that of the conventional series capacitors. The single-mode damping controller is then designed to damp torsional oscillations caused by the SSSC alone. Lastly, the performance of the multimodal SSR damping controller is evaluated in the dually compensated IEEE FBM, using the three cases considered in the previous chapter.

5.3.1. Series Capacitors vs SSSC without Damping Controller

Figure 5.4 shows the system response to a three-phase to ground fault applied at 1.5 s and lasting for 4.5 cycles (0.075 s) for the IEEE FBM compensated with series capacitors (X_C = 0.3707 pu). The results show that following this disturbance, violent oscillations of growing amplitudes occur in the turbine-generator rotor and large twisting torques are observed in individual shafts of the rotor system. Within 4.5 seconds after the fault occurrence, amplitudes of the twisting torque in the shaft connecting

the Low Pressure turbine sections A and B exceed 10 pu while those of the generator to exciter shaft torque reach 10 pu. Deviations in the rotor speed exceed 20 rad/s and the Fast Fourier analysis in figure 5.5 shows that these are composed of Mode 1 (15.71 Hz) and Mode 2 (20.21 Hz), with Mode 2 being dominant. This finding is in agreement with that established in Chapter Four (subsection 4.2.1), which indicates that at this particular degree of compensation, the complimentary frequency of the air gap torque is 20.1 Hz which is very close to torsional Mode 2 of the turbine-generator shaft.

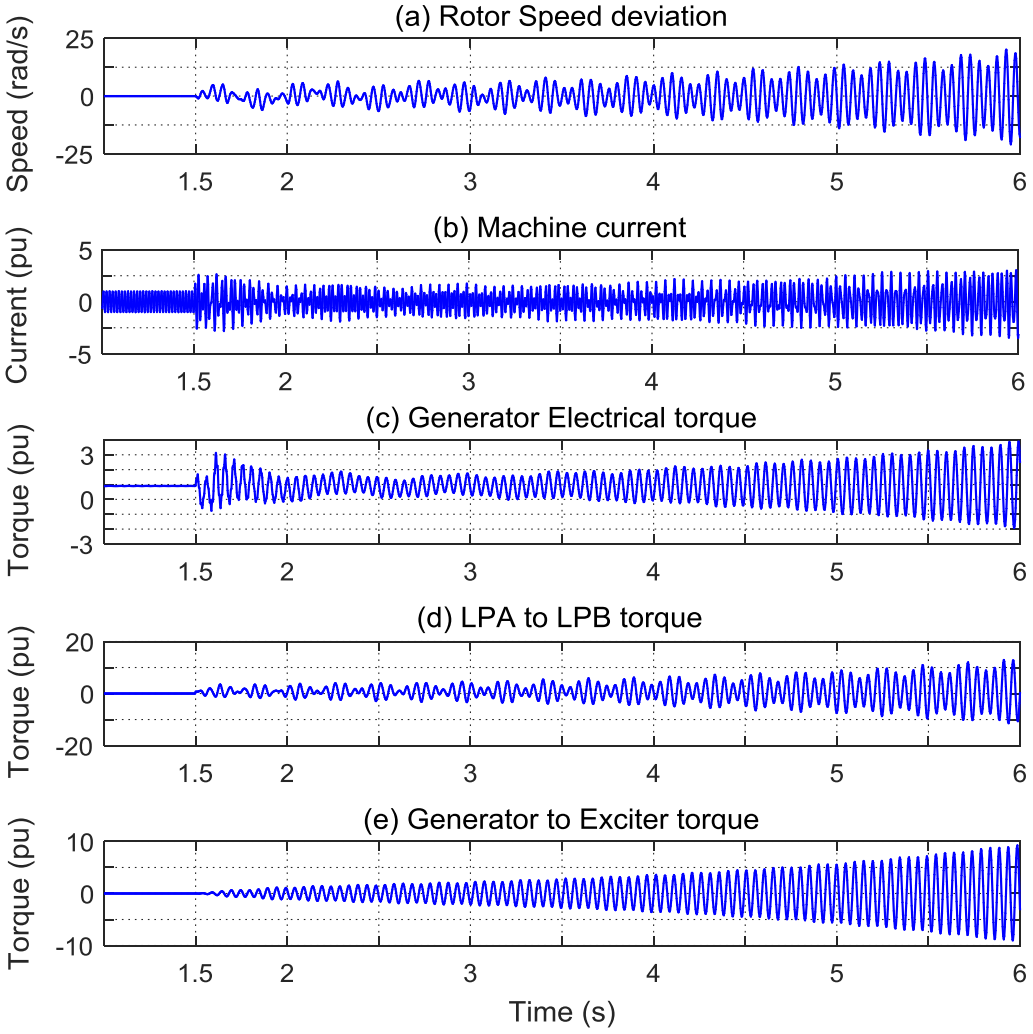

Figure 5.4: *The system response for the series capacitor compensated IEEE FBM, X_C = 0.3707 pu*

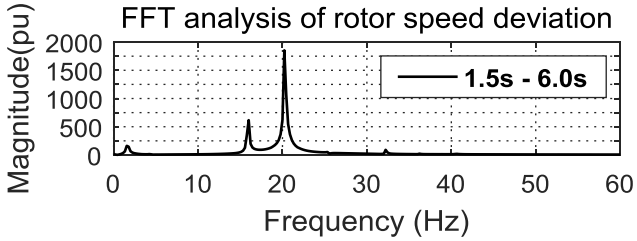

Figure 5.5: *FFT analysis of rotor speed deviation for the series capacitor compensated IEEE FBM, X_C = 0.3707 pu*

In figure 5.6, the speed deviation and twisting torques in various shafts sections of the turbine-generator rotor are shown when compensation is provided by the SSSC (X_{SSSC} = 0.3707 pu), instead of a conventional series capacitor (X_C = 0.3707 pu). Comparison of figure 5.6 with figure 5.4 shows that the torsional oscillations with the SSSC compensation do not grow as rapidly as they do with conventional capacitors, indicating the capability of the SSSC to add some positive damping at subsynchronous frequencies. However, the SSSC still excites SSR as established in the previous Chapter. FFT analysis of the rotor speed deviation in figure 5.7 shows that SSR in this case is caused by destabilization of Mode 1 and Mode 4, with Mode 4 being the dominant mode of oscillation. Thus, damping of SSR for this particular case requires adequate damping of Mode 4.

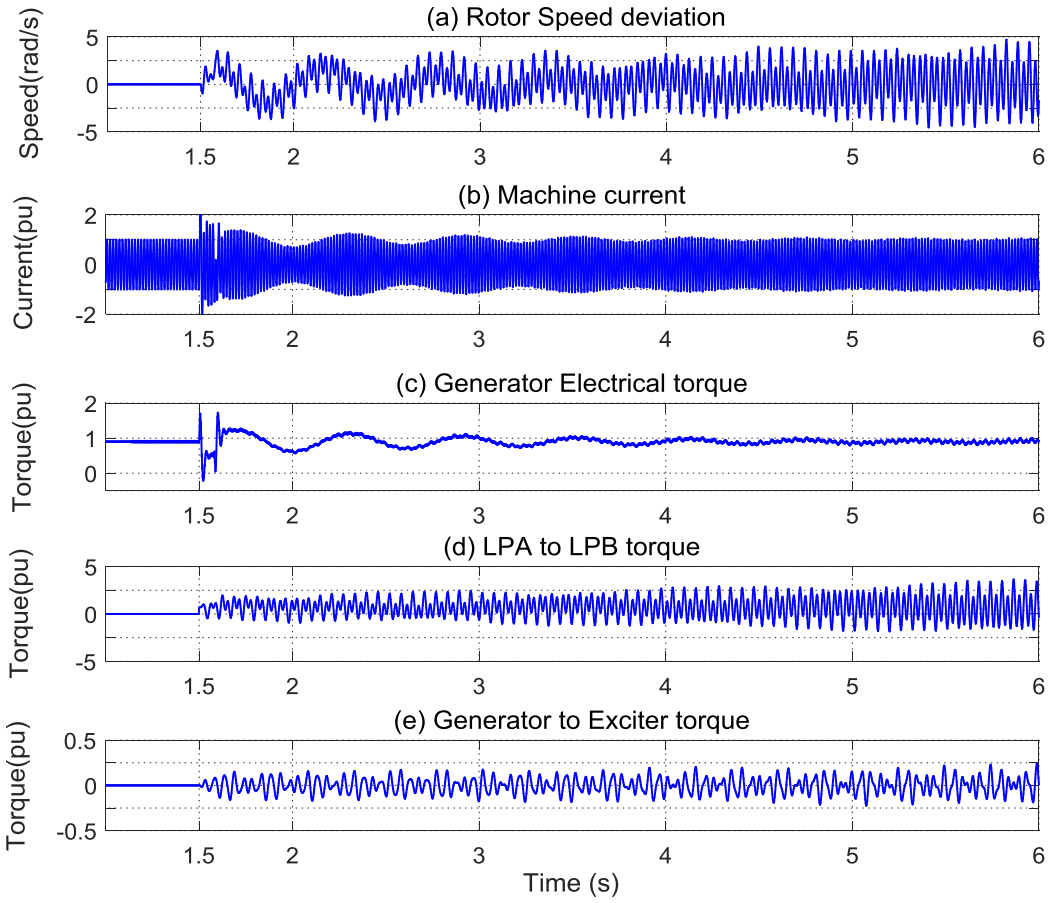

Figure 5.6: *The system response for the SSSC compensated IEEE FBM without damping controller,* X_{SSSC} *= 0.3707 pu*

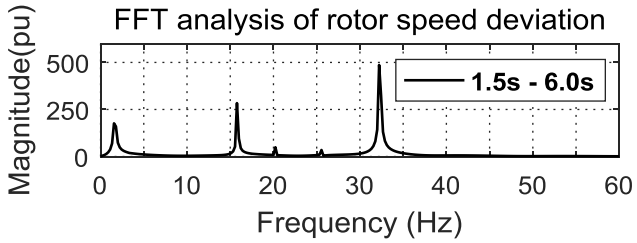

Figure 5.7: *FFT analysis of rotor speed deviation for the SSSC compensated IEEE FBM,* $X_{SSSC} = 0.3707$ *pu*

5.3.2. Damping Controller for a SSSC compensated IEEE FBM

After observing that Mode 4 (at 32.285 Hz) is dominant for the SSSC compensated IEEE FBM when $X_{SSSC} = 0.3707$ pu, the single mode damping controller is designed using the approach in subsection 5.2.2. For sufficient damping of this torsional mode, the controller output ΔX_{SSSC} should modulate the change in electrical torque ΔT_e such that it is almost in phase with the oscillations in the rotor speed Δw around 32.285 Hz (i.e. 202.947 rad/s). The steps taken are summarized as follows:

(a) A small sinusoidal test modulation signal at a frequency of 32.285 Hz was applied at input ΔX_{SSSC} (see figure 5.1) to the SSSC after the system entered steady state.

(b) This caused oscillations in generator electromagnetic torque from which ΔT_e was measured.

(c) It was found that ΔT_e lags ΔX_{SSSC} by 41.474˚ at 32.285 Hz, requiring the lead compensator that provides $\varphi_{max} = 41.474$˚ at $w_n = 202.947$ rad/s.

From the lead compensator point of view, this angle can be compensated using a single lead compensator of the form $M_4(s) = \dfrac{1+T_1 s}{1+T_2 s}$.

The lead compensator parameters can be expressed as follows:

$$M_4(s) = \frac{1+\tau s}{1+(\alpha\tau)s} \tag{5.3}$$

where:

$$\sin\varphi_{max} = \frac{1-\alpha}{1+\alpha} \tag{5.4}$$

$$\tau = \frac{1}{w_n\sqrt{\alpha}} \tag{5.5}$$

Now, from equation 5.4,

$$\alpha = \frac{1-\sin\varphi_{\max}}{1+\sin\varphi_{\max}} = 0.203167$$

Now, from equation 5.5,

$$\tau = \frac{1}{w_n\sqrt{\alpha}} = 0.010932 \;\Rightarrow \alpha\tau = 0.002221$$

The required compensator is thus as follows, and its bode diagram is given in Appendix B.

$$M_4(s) = \frac{1+0.010932s}{1+0.002221s}$$

The system response with Mode 4 damping controller is shown in figure 5.9, with two different values of the controller gain, $K_{ssr} = 2$ *and* $K_{ssr} = 5$.

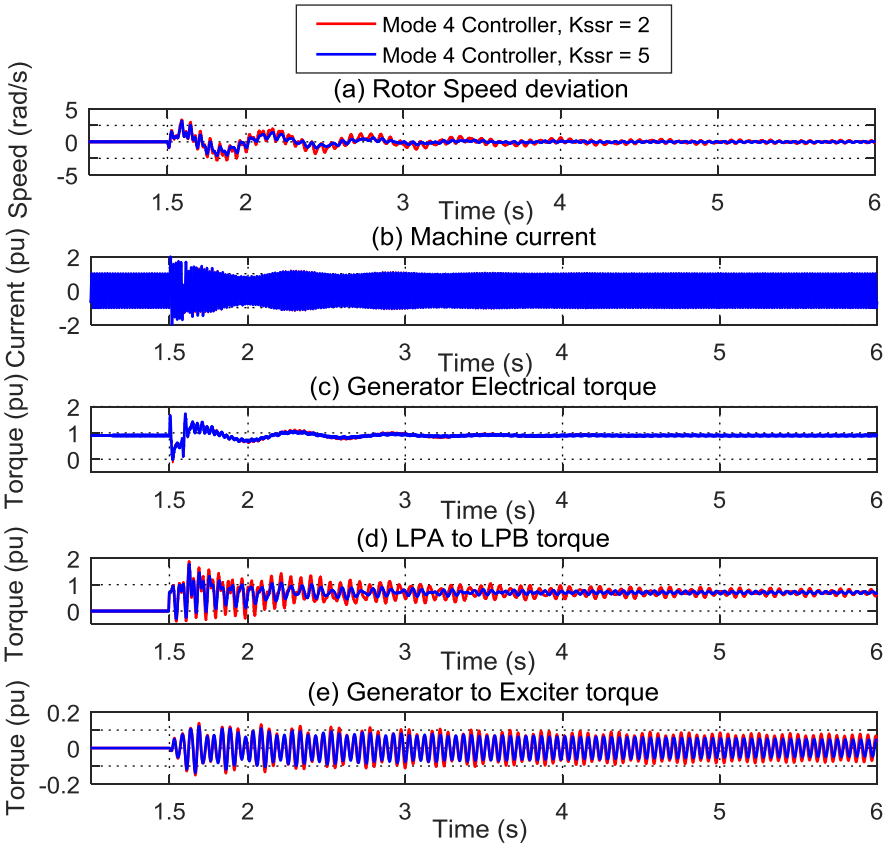

Figure 5.8: *The system response for the SSSC compensated IEEE FBM with Mode 4 damping controller,* $K_{ssr4} = 5$, $X_{SSSC} = 0.3707$ *pu*

The results of figure 5.8 show that the designed Mode 4 damping controller is able to damp the torsional oscillations and stabilize the system. As the value of the damping controller gain is increased from $K_{ssr} = 2$ to $K_{ssr} = 5$, the torsional modes become more stable and the damping rate of SSR oscillations increases. However, further increase in K_{ssr} worsens the destabilization of other modes, so the optimum value of $K_{ssr} = 5$ is chosen in this case. From figure 5.8 (e), it is apparent that even with this higher value of the controller gain ($K_{ssr} = 5$), the damping of the oscillations in the shaft

connecting the generator and the exciter is slow, and the FFT analysis (not shown here) show that these are Mode 2 frequency oscillations. The following subsection investigates SSR in a dually compensated IEEE FBM.

5.3.3. Analyzing SSR in a Dually Compensated IEEE FBM

As was mentioned in the previous Chapter, dual compensation using the SSSC in conjunction with fixed series capacitors may assist electric power transmission utilities to utilize the controllability of the SSSC at a lower cost. In this subsection, SSR characteristics are studied for the three case studies established Chapter Four (*Case 1a – Case 1c* in Table 4.1). Here the torsional oscillations turn out to be multimodal in nature since both the SSSC and conventional series capacitors contribute towards SSR, hence the multimodal damping controller is used.

5.3.3.1. Case Study 1a

Figure 5.9 shows the response of the IEEE FBM power system for *Case 1a* (i.e. $X_{SSSC}/X_{Comp} = 0.20$) without and with a SSSC-based multimodal SSR damping controller, whose parameters are given in Table 5.1.

Table 5.1: Multimodal Damping Controller Parameters for Case 1a

Mode	***Lead/Lag compensator***	*Gain*
1	$\frac{1+0.0074758s}{1+0.013745s}$	1.2
2	$\frac{1+0.007379s}{1+0.0084044s}$	1.8
3	$\left(\frac{1+0.017046\ s}{1+0.002254\ s}\right)\times\left(\frac{1+0.017046\ s}{1+0.002254\ s}\right)\times\left(\frac{1+0.0098722\ s}{1+0.0038827\ s}\right)$	0.5
4	$\left(\frac{1+0.01354\ s}{1+0.001793\ s}\right)\times\left(\frac{1+0.01354\ s}{1+0.001793\ s}\right)\times\left(\frac{1+0.006664\ s}{1+0.0036434\ s}\right)$	0.4

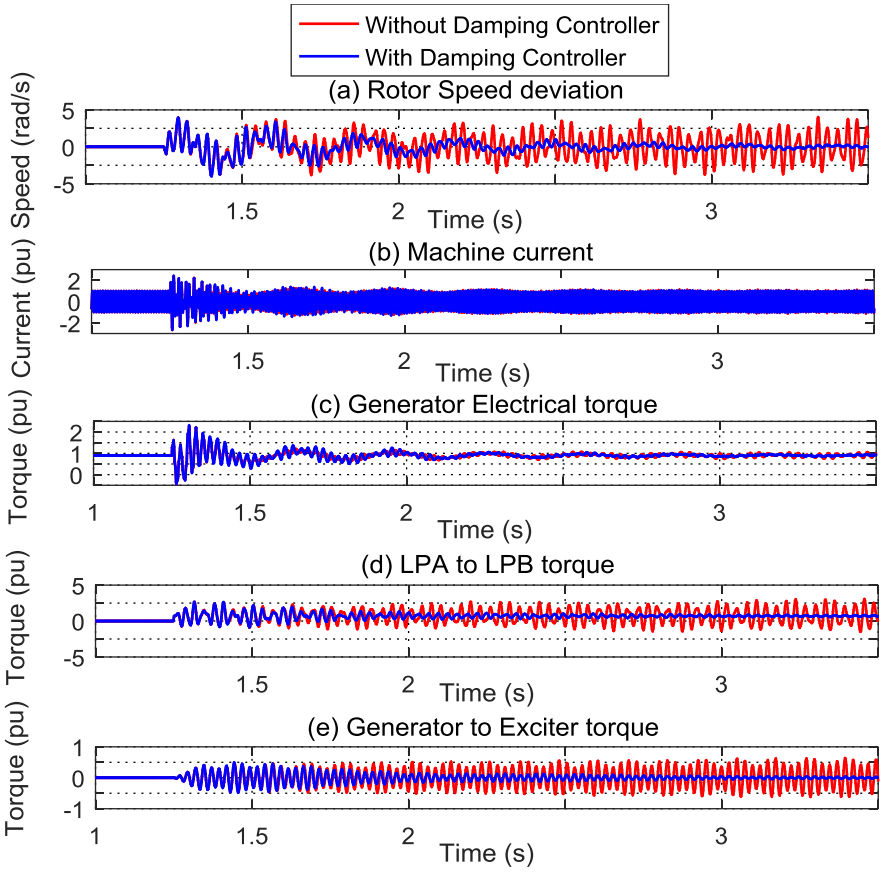

Figure 5.9: *The system response for the dually compensated IEEE FBM for Case 1a (X_{SSSC} = 0.07414 pu, X_C = 0.29656 pu) without and with multimodal damping controller*

The results of figure 5.9 thus show that the damping controller is capable of damping the torsional oscillations and stabilize the power system though modulation of the SSSC reactance around the steady state value of 0.07414 as shown in figure 5.10.

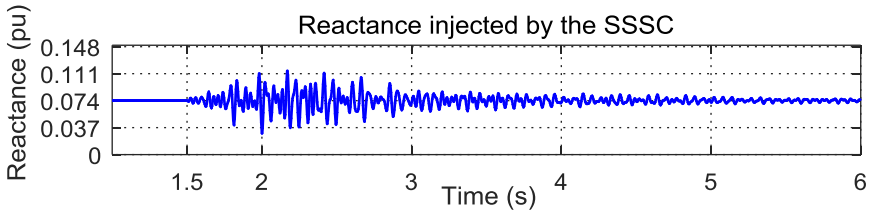

Figure 5.10: *The reactance provided by the SSSC for Case 1a with damping controller*

The Fast Fourier Transform analysis of the rotor speed deviation and the twisting torques in different sections of the turbine-generator shaft are shown in figure 5.11. As seen in figure 5.11 (i), the rotor speed deviation is dominated by Mode 1 (i.e. 15.71 Hz) oscillations, Mode 3 and Mode 4 oscillations are critically stable while there is a slight growth in Mode 2 oscillations. The twisting torque in the shaft connecting the low pressure turbine sections A and B (figure 5.11 (iv)) shows dominance of

Mode 1 while Mode 2 (at 20.21 Hz) is dominant in the generator to exciter shaft torque (see figure 5.11(v)).

5.2.1.1. Case Study 1b

In this case study, the ratio of X_{SSSC}/X_{Comp} is increased to 0.40 as shown in table 4.1. The system response in time domain is presented in figure 5.12 without and with the multimodal damping controller and the SSSC reactance with damping controller is shown in figure 5.13. The controller parameters used here are given in Table 5.2. The results thus show that the multimodal damping controller is able to damp SSR and bring the system back to its stable operation. Modal analysis of the signals in figure 5.12 is given in figure 5.14.

Table 5.2: Multimodal Damping Controller Parameters for Case 1b

Mode	***Lead/Lag compensator***	*Gain*
1	$\frac{1+0.0076953s}{1+0.0133531s}$	1.6
2	$\frac{1+0.0067447s}{1+0.0091949s}$	3.2
3	$\left(\frac{1+0.017046\ s}{1+0.002254\ s}\right)\times\left(\frac{1+0.017046\ s}{1+0.002254\ s}\right)$	0.7
4	$\left(\frac{1+0.01354\ s}{1+0.001793\ s}\right)\times\left(\frac{1+0.01354\ s}{1+0.001793\ s}\right)\times\left(\frac{1+0.0070014\ s}{1+0.0034678\ s}\right)$	0.18

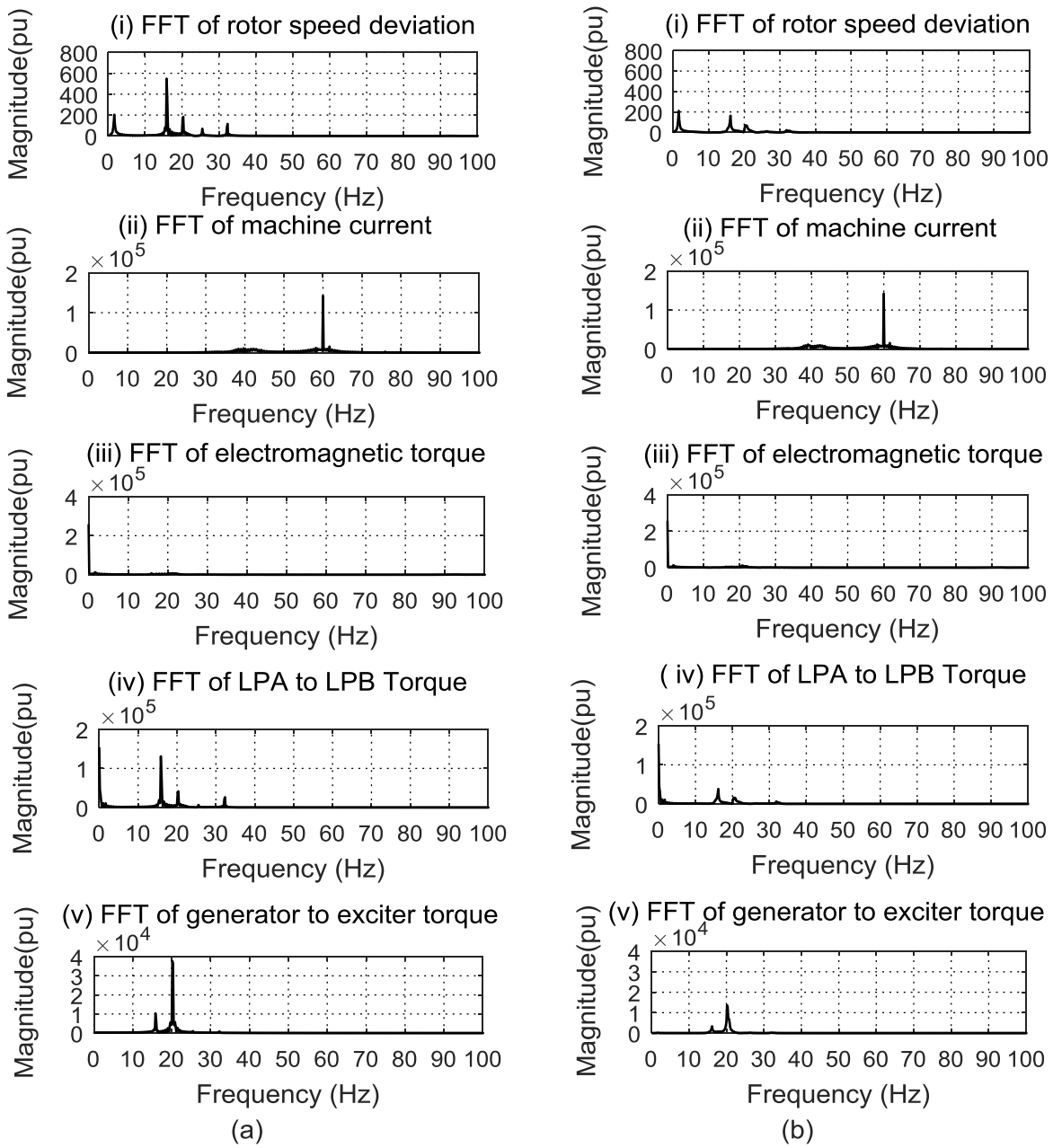

Figure 5.11: *FFT analyses for the dually compensated IEEE FBM of Case 1a (X_{SSSC} = 0.07414 pu, X_C = 0.29656 pu); (a) without damping controller, (b) with damping controller*

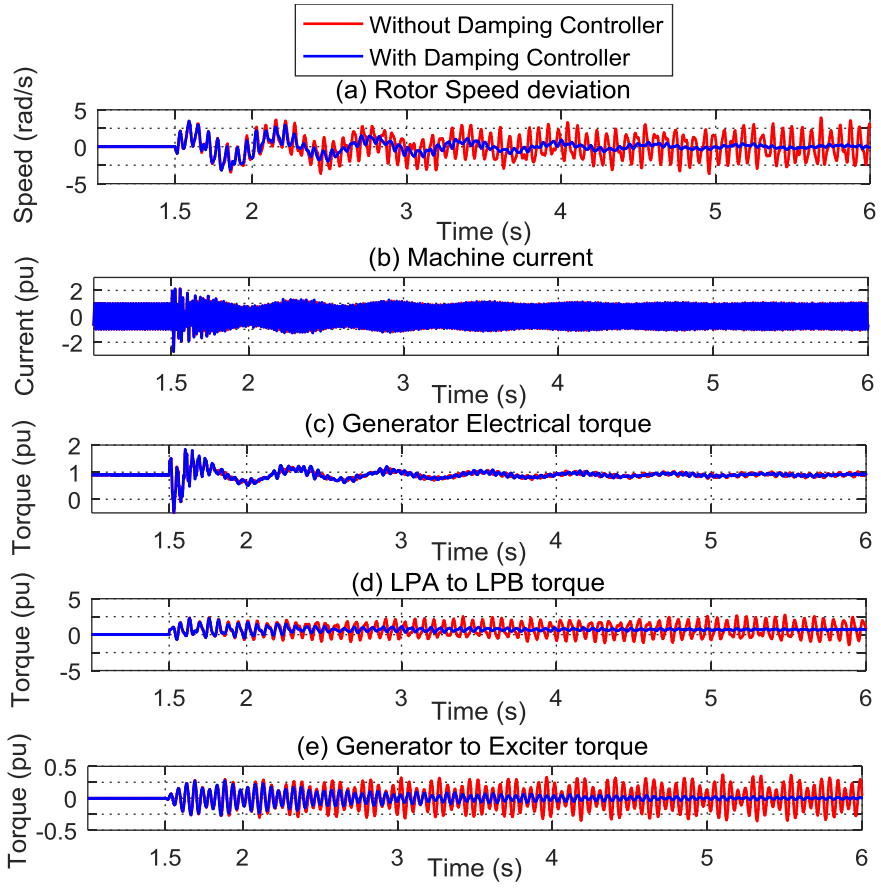

Figure 5.12: *The system response for the dually compensated IEEE FBM of Case 1b (X_{SSSC} = 0.14828 pu, X_C = 0.22242 pu) without and with multimodal damping controller*

Comparing figures 5.11 and 5.14, it is observed that as the ratio X_{SSSC}/X_{Comp} is increased from 0.20 to 0.40, there is a reduction of Mode 1 and Mode 2 components while there is a slight increase in Mode 3 and Mode 4 components in the rotor speed deviation and LPA to LPB shaft torque. For the generator to exciter torque, Mode 2 component is reduced by half while Mode 1 component remains unchanged.

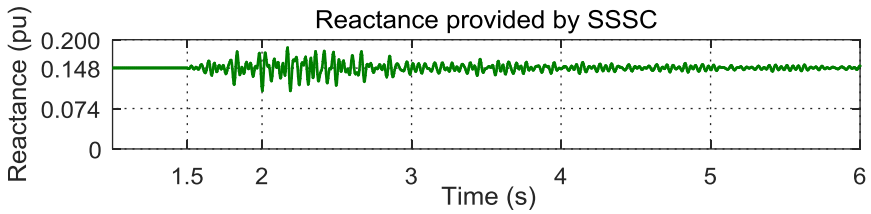

Figure 5.13: *The reactance provided by the SSSC for Case 1b with damping controller*

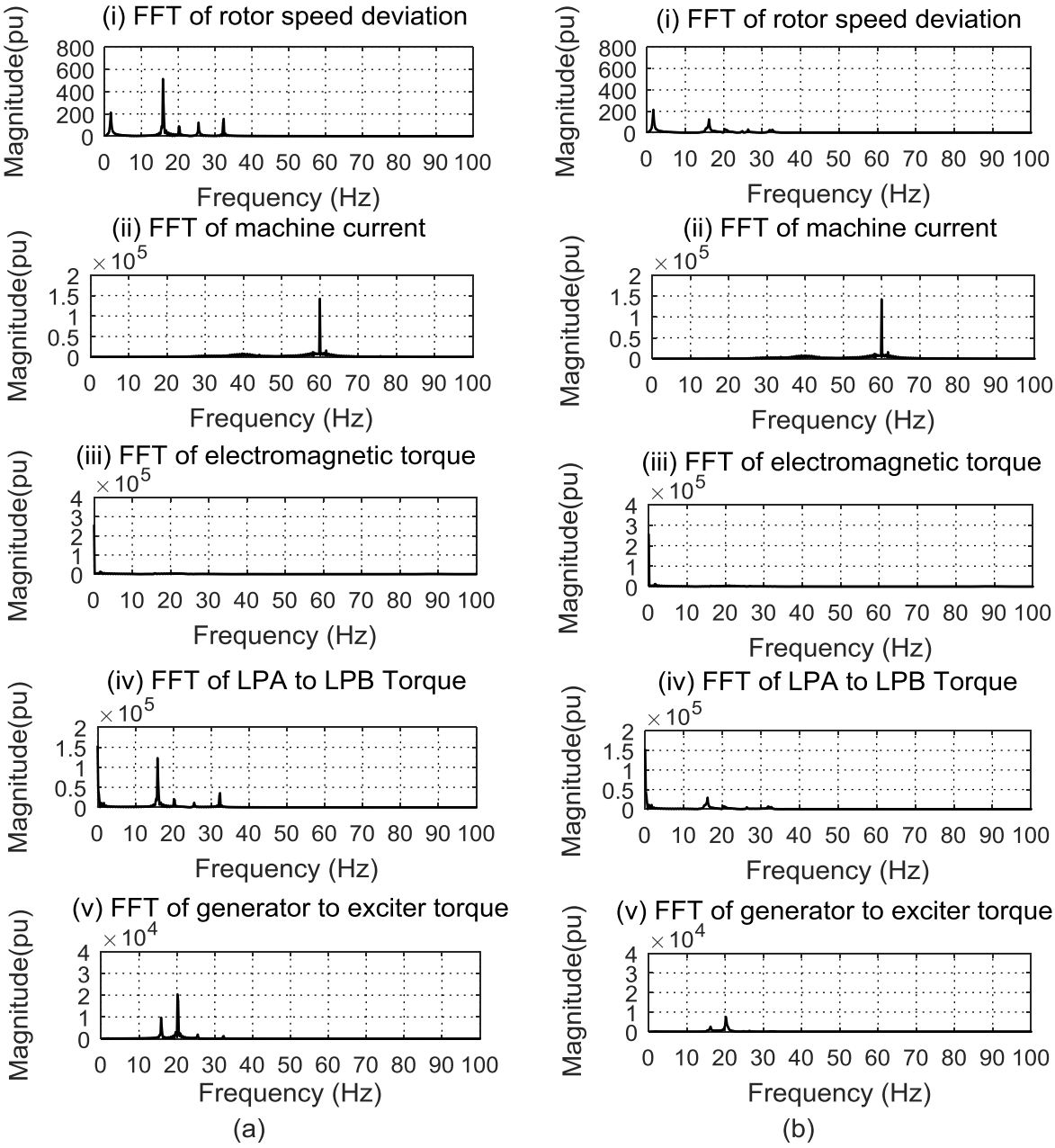

Figure 5.14: *FFT analyses for the dually compensated IEEE FBM of Case 1b; (a) without damping controller, (b) with damping controller*

5.2.1.2. Case Study 1c

The last case study in the IEEE FBM with a single transmission line considers the ratio $X_{SSSC}/X_{Comp} = 0.60$, while the total compensation is still kept at 0.3707 pu. The system response for this case study (i.e. *Case 1c*) is shown in figure 5.15 without and with a damping controller whose parameters are given in Table 5.3. Figures 5.16 and 5.17 show the reactance provided by the SSSC (with damping controller) and FFT analysis of the system variables respectively.

Table 5.3: Multimodal Damping Controller Parameters for Case 1c

Mode	***Lead/Lag compensator***	*Gain*
1	$\frac{1+0.0078263s}{1+0.013129s}$	1.6
2	$\frac{1+0.0065737s}{1+0.0094341s}$	3
3	$\left(\frac{1+0.015932\ s}{1+0.0024072\ s}\right)$	0.7
4	$\left(\frac{1+0.015628\ s}{1+0.0015536\ s}\right)\times\left(\frac{1+0.015628\ s}{1+0.0015536\ s}\right)\times\left(\frac{1+0.007922\ s}{1+0.0030647\ s}\right)$	0.18

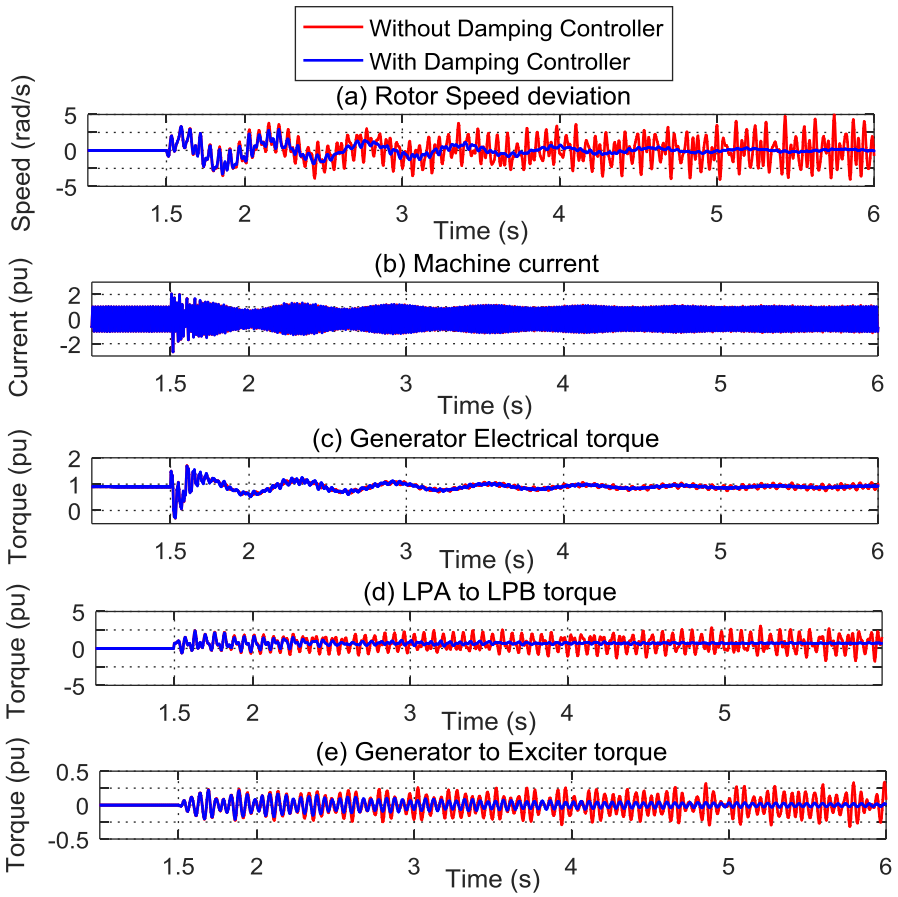

Figure 5.15: *The system response for the dually compensated IEEE FBM of Case 1c (X_{SSSC} = 0.22242 pu, X_C = 0.14828 pu) without and with multimodal damping controller*

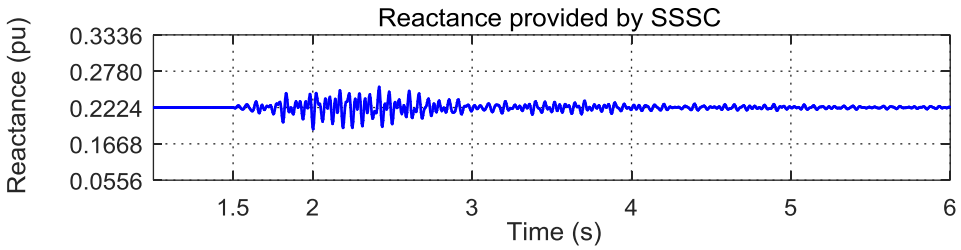

Figure 5.16: *The reactance provided by the SSSC for Case 1c with damping controller*

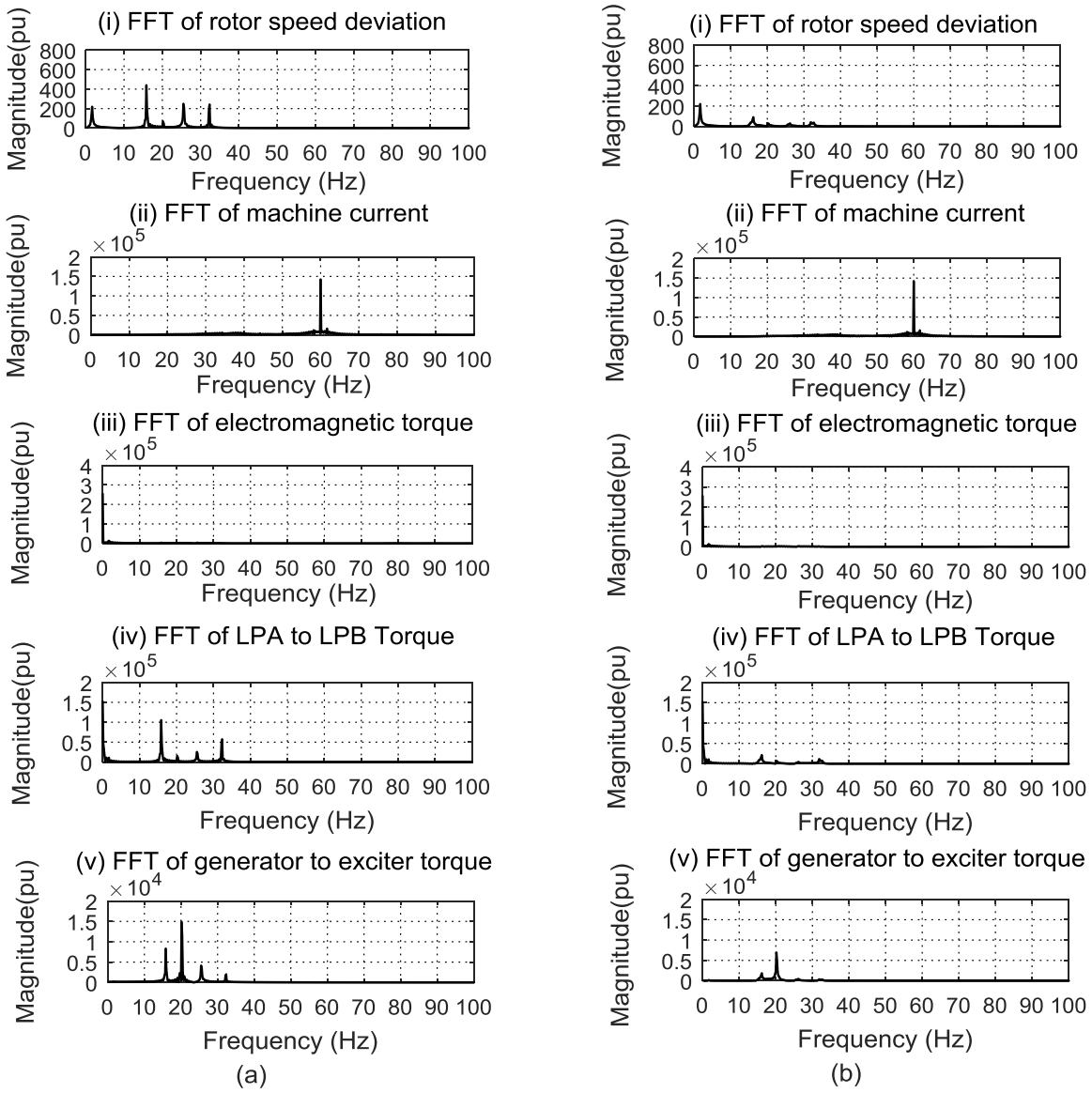

Figure 5.17: *FFT analyses for the dually compensated IEEE FBM of Case 1c; (a) without damping controller, (b) with damping controller*

It is observed in figures 5.17 (a) and 5.14 (a) that increasing the ratio X_{SSSC}/X_{Comp} from 0.40 to 0.60 increases the damping of Mode 1 and Mode 2 components in the generator rotor speed deviation

although this comes at the cost of weakening the damping of Mode 3 and Mode 4 components. The same observation is made in the LPA to LPB torque as well as in the generator to exciter torque.

The results for *Case 1a – Case 1c* show that as the ratio of X_{SSSC} to X_{Comp} is increased, the torsional interaction with the lower frequency modes (i.e. Mode 1 and 2) is reduced while that with the higher frequency modes (i.e. Mode 3 and 4) in increased. These findings are in agreement with those in Chapter Four, which indicated an increase in the complimentary frequency (f_0 - f_{er}) of the air gap torque from 21.71 Hz to 25.85 Hz as the ratio X_{SSSC}/X_{Comp} is increased from 0.20 to 0.60.

In practice, in real world transmission system, due to the relatively high cost of FACTS devices, most transmission lines would still employ conventional series capacitors with only a few lines likely to include a FACTS series compensator such as the SSSC. Hence in the next section, the concept of the damping controller around the SSSC to damp SSR is extended to the modified IEEE FBM with two parallel transmission lines originating from the same substation.

5.3. Modified IEEE FBM with a two parallel Transmission Lines

The study system used in this section is the modified IEEE FBM, whose parameters are the same as those in the original IEEE FBM except that in this case, the transmission network consists of two parallel transmission lines. This modification is done to allow incorporation of the SSSC in one line and conventional series capacitors in the other (adjacent) transmission line as shown in figure 5.18. For all case studies in this section, the post-disturbance response of the power system is monitored following a three phase to ground fault.

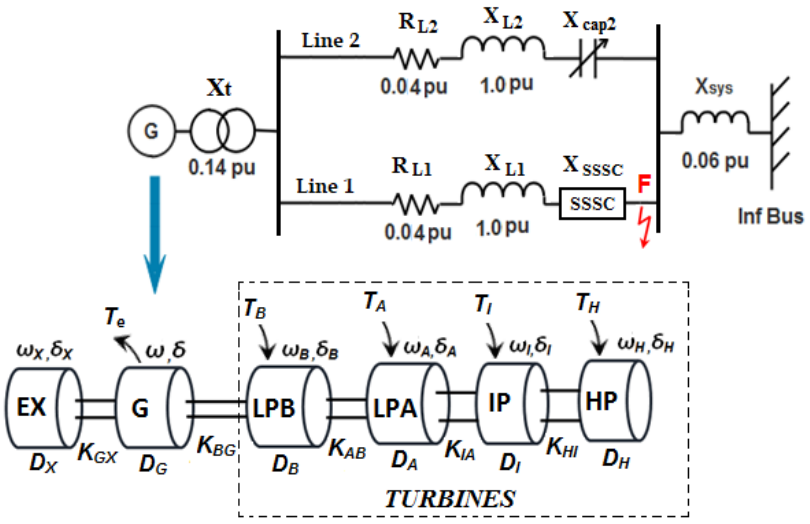

Figure 5.18: *The modified IEEE FBM with two parallel transmission lines*

Initially, the time domain simulations and FFT analyses are used to study SSR when one of the two transmission lines is compensated while the other line is left uncompensated as in Cases *2a* and *2b* in

Table 5.4. The possibility of using the supplementary damping controller around the SSSC to mitigate SSR in the presence of series capacitor in an adjacent transmission line is also explored in Cases *2c-2f*.

Table 5.4: Summary of the case studies for modified IEEE FBM

Case Study	***Compensation Details***	
	Transmission Line 1	***Transmission Line 2***
Case 2a	Uncompensated	X_{C2} = 0.70 pu
Case 2b	X_{SSSC} = 0.70 pu	Uncompensated
Case 2c	X_{SSSC} = 0.70 pu	X_{C2} = 0.70 pu
Case 2d	X_{SSSC} = 0.35 pu	X_{C2} = 0.70 pu
Case 2e	X_{SSSC} = 0.35 pu	X_{C2} = 0.55 pu
Case 2f	X_{SSSC} = 0.35 pu, X_{C1} = 0.35 pu	X_{C2} = 0.70 pu

5.3.1. One Line Compensated and the other Line left Uncompensated

Figure 5.19 shows the power system response of the Modified IEEE FBM system for *Case 2a* where Line 2 is compensated by conventional capacitors (X_{C2} = 0.70 pu) while Line 1 is not compensated following a three-phase to ground fault. At this particular value of compensation, rapidly growing oscillations are observable in the rotor speed deviation as well as in various sections of the turbine-generator shaft. These oscillations are mainly due to destabilization of torsional Mode 1 as shown by the FFT analysis in figure 5.19 (b). The amplitudes of oscillations in rotor speed deviation reach about 200 rad/s within 4.5 s post a fault. Thus if no mitigating measures are taken the detrimental shaft damage due to SSR. Supersynchronous frequency (i.e. above system frequency) components are observed in the machine current including Mode 5 components which is also present in the electromagnetic torque.

For comparison, *Case 2b* considers compensation by the SSSC in Line 1 (X_{SSSC} = 0.70 pu) while Line 2 is left uncompensated and the power system response is shown in figure 5.20, following the three phase to ground fault. Even with the SSSC compensation, SSR still occurs although not to the same extent as with series capacitors compensation as seen from the amplitudes of rotor speed deviation and the stress in the various shaft sections.

In practical transmission system, it is more likely to be the case that higher loading may be required for both lines such that both may have to be compensated. The next subsection considers a case where

both transmission lines are compensated and evaluates the ability of the damping controller in damping torsional oscillations due to SSR in each case.

5.2.1. Both Lines Compensated: SSSC in Line 1 and Series Capacitors in Line 2

Figure 5.21 shows the system response for Case *2c* with both Line 1 and Line 2 compensated by 0.70 pu with the SSSC in Line 1 (i.e. X_{SSSC} = 0.7 pu) and fixed capacitors in Line 2 (i.e. X_{C2} = 0.7 pu) following a three-phase to ground fault. FFT analysis of the rotor speed deviation for three time intervals for this case study are shown in figure 5.22 without and with the multimodal damping controller whose parameters are given in Table 5.5.

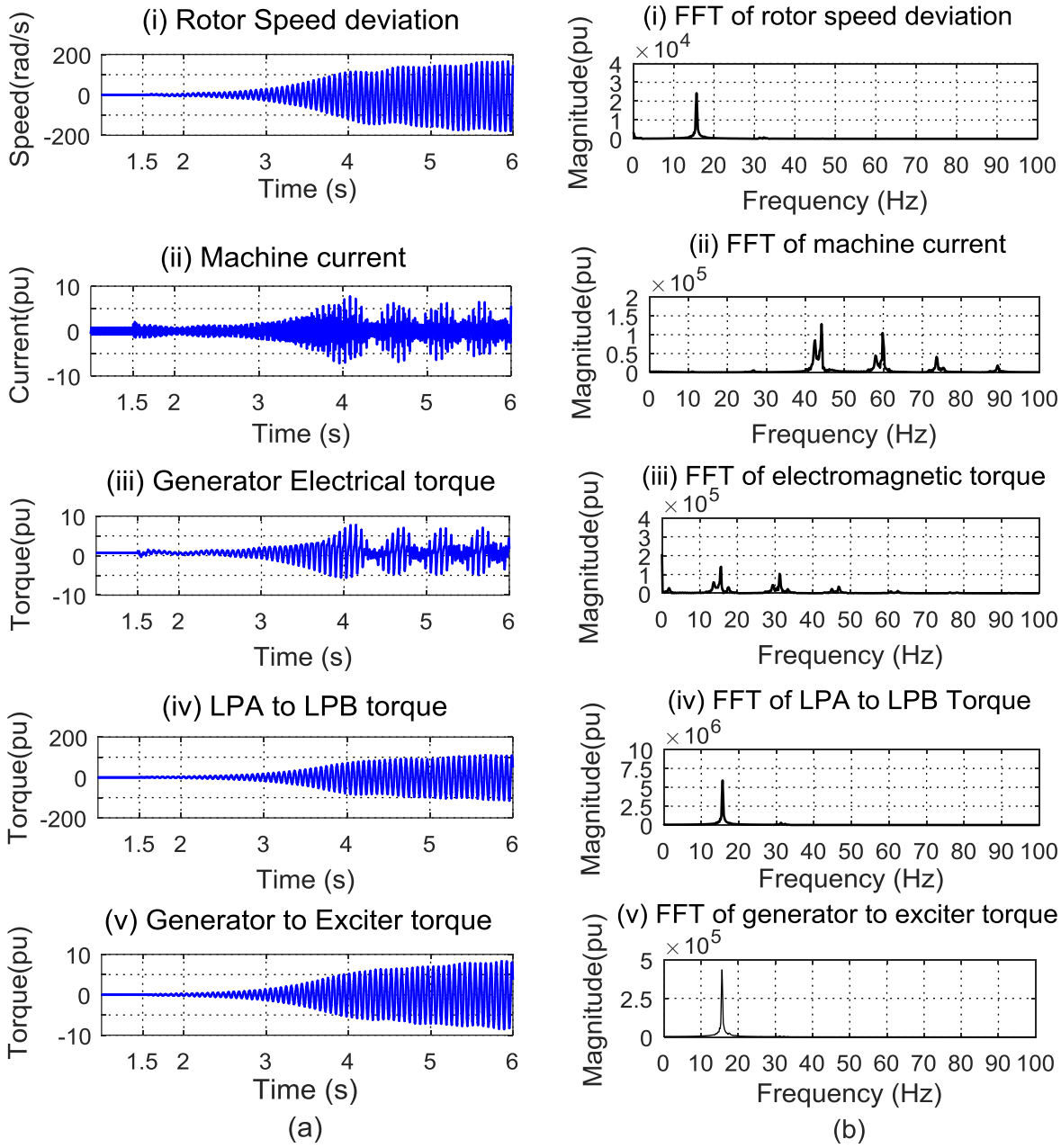

Figure 5.19: *System response in the presence of series capacitors in Line 2 (X_{C2} = 0.7 pu) and Line 1 left uncompensated; (a) time domain simulations, (b) FFT analyses*

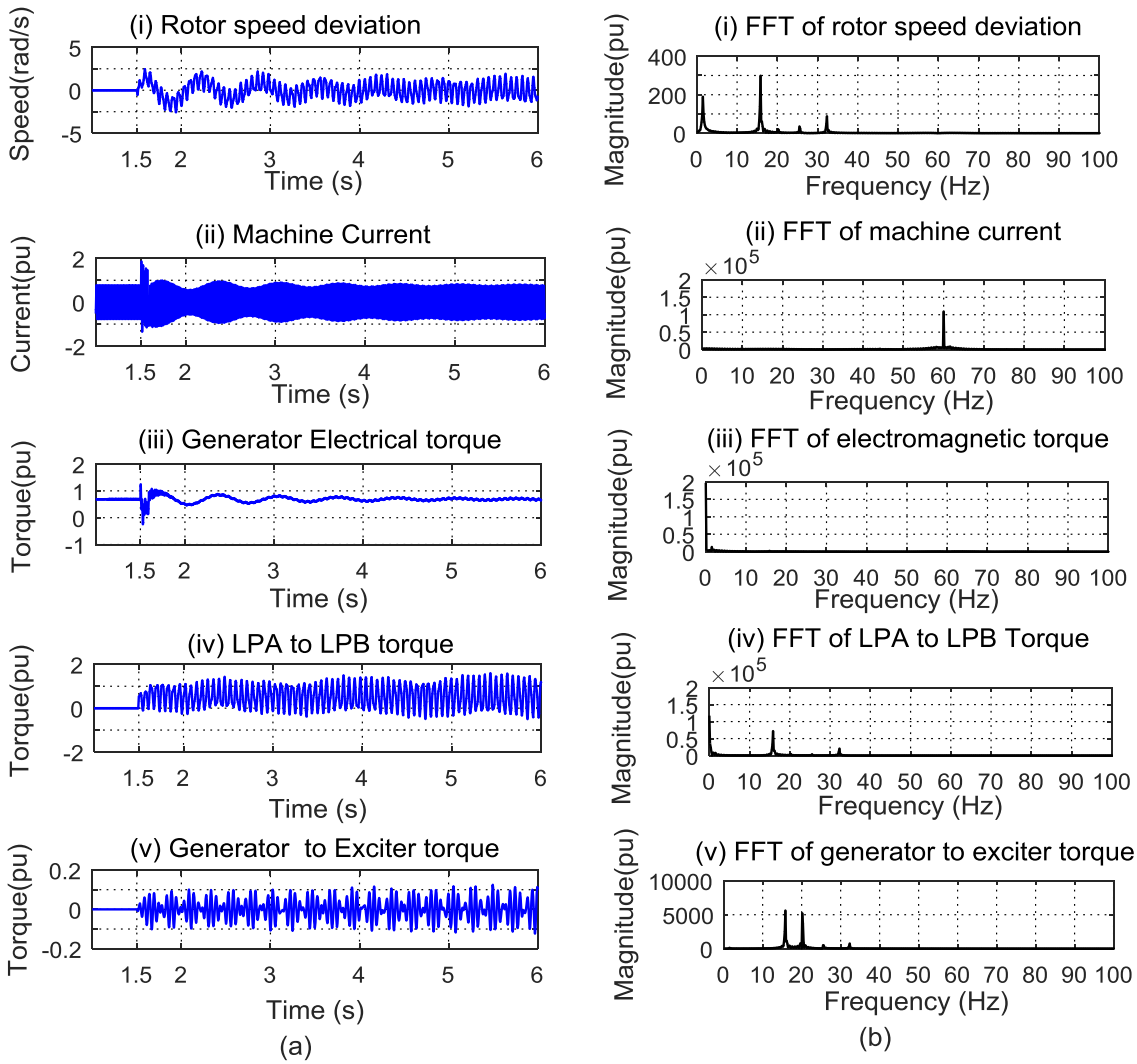

Figure 5.20: *System response in the presence of the SSSC in Line 1 (XSSSC = 0.70 pu) and Line 2 left uncompensated; (a) time domain simulations, (b) FFT analyses*

Table 5.5: Multimodal Damping Controller Parameters for Case 2c

Mode	***Lead/Lag compensator***	*Gain*
1	$\frac{1+0.0060496s}{1+0.016986s}$	4
2	$\frac{1+0.0056440s}{1+0.010988s}$	30
3	$\frac{1+0.0072248s}{1+0.0052935s}$	1.5
4	$\frac{1+0.013538s}{1+0.0017934s} \times \frac{1+0.0061355s}{1+0.0039572s}$	0.7

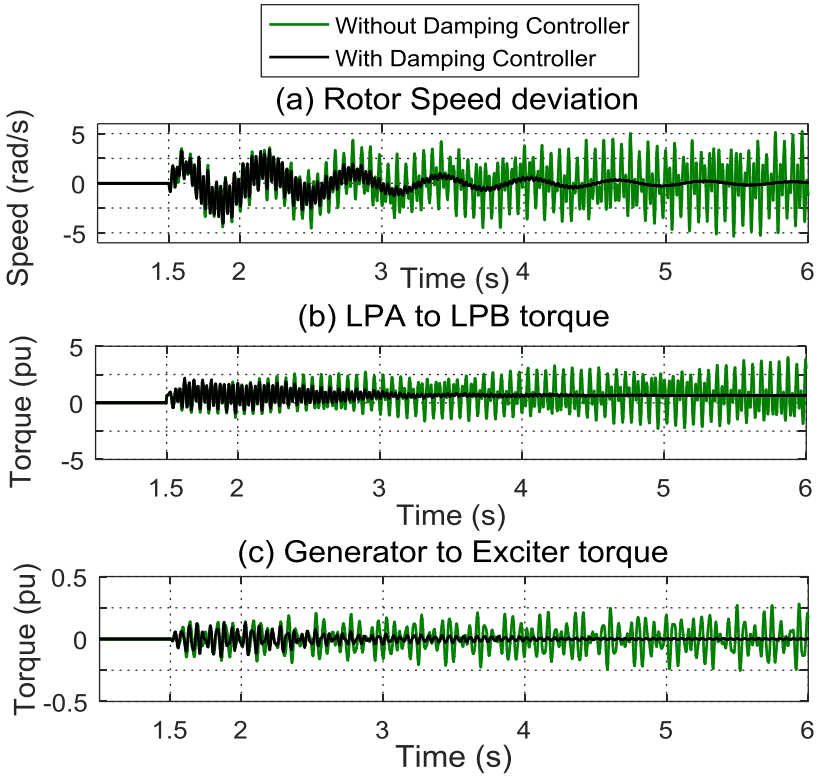

Figure 5.21: *Time domain simulations showing system response in the presence of the SSSC in Line 1 (X_{SSSC} = 0.70 pu) and capacitors in Line 2 (X_{C2} = 0.70 pu)*

The results in figures 5.21 and 5.22 show instability of Mode 1, Mode 3 and Mode 4 with Mode 1 and Mode 4 being dominant. However, the results also demonstrate that with the activation of the damping controller, the torsional oscillations are positively damped and the system is able to return back to its stable operation.

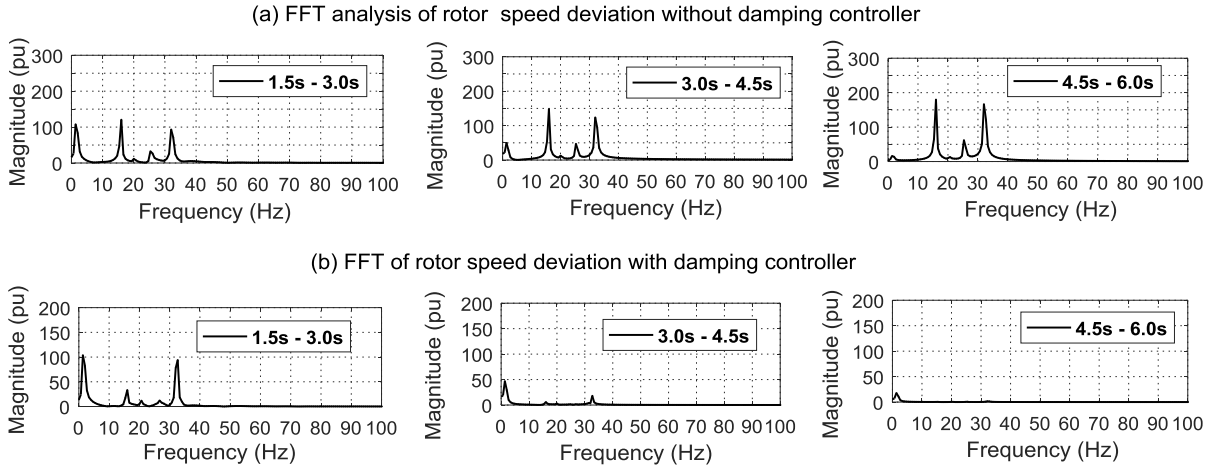

Figure 5.22: *FFT analyses of the rotor speed deviation with SSSC in Line 1 (X_{SSSC} = 0.70 pu) and capacitors in Line 2 (X_{C2} = 0.70 pu); (a) without damping controller, (b) with damping controller*

From the practical point of view, providing compensating reactance of 0.70 pu from the SSSC will require higher rating for the device and will be a costlier option. Case *2d* then considers a scenario where Line 1 is compensated by 0.35 pu provided by the SSSC while the series capacitor in Line 2 provides 0.70 pu. The post-fault system response with this configuration are given in figures 5.23 and 5.24 in the form of time domain simulations and FFT analysis respectively, without and with a damping controller whose parameters are provided in Table 5.6.

Table 5.6: Multimodal Damping Controller Parameters for Case 2d

Mode	***Lead/Lag compensator***	*Gain*
1	$\frac{1+0.0034196s}{1+0.030049s}$	13
2	$\frac{1+0.0051276s}{1+0.012095s}$	25
3	$\frac{1+0.00448s}{1+0.0857s}$	5
4	$\frac{1+0.0040022s}{1+0.060665s}$	5

At this operating point, rapidly growing oscillations in the rotor speed deviation are observed following a three-phase to ground fault as well as in the LPA to LPB and generator to exciter shaft torques. These torsional oscillations are comprised mainly of Mode 1 component as seen in figure 5.24. Comparison of the results from figures 5.19 and 5.23 shows that even without the action of the damping controller, presence of the SSSC in Line 1 does add some positive damping to the torsional oscillations due to the conventional series capacitor in Line 2, although the damping is not adequate to restore the power system stability. Upon activation of the damping controller, the oscillations are damped out and the system is stabilized.

With X_{SSSC} kept at 0.35 pu, the capacitive reactance in Line 2 is reduced to 0.55 pu as given by Case *2e* in Table 5.4 and the results for this operating condition are shown in figure 5.25 following a three-phase to ground fault. Here, poorly damped torsional oscillations are observed in the rotor speed deviation and shaft torques. These oscillations do not show rapidly growing amplitudes but they are sustained. Continuous occurrence of these oscillations in the turbine-generator shaft may develop some cracks, which will result in the shaft failure due to fatigue; therefore, they need to be damped.

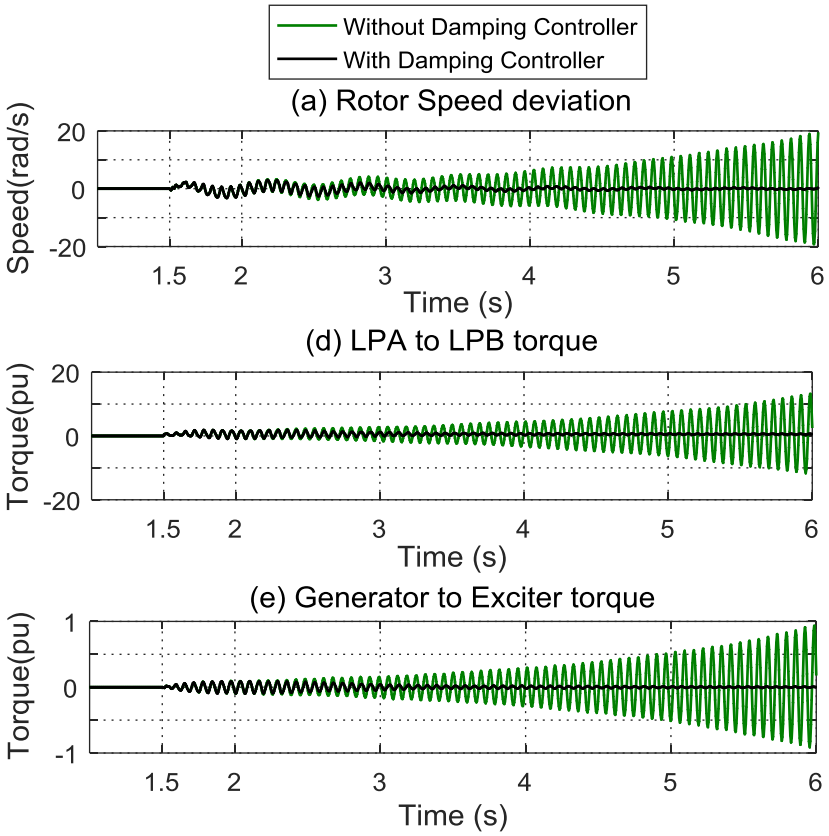

Figure 5.23: *Time domain simulations showing system response in the presence of the SSSC in Line 1 (X_{SSSC} = 0.35 pu) and capacitors in Line 2 (X_{C2} = 0.70 pu)*

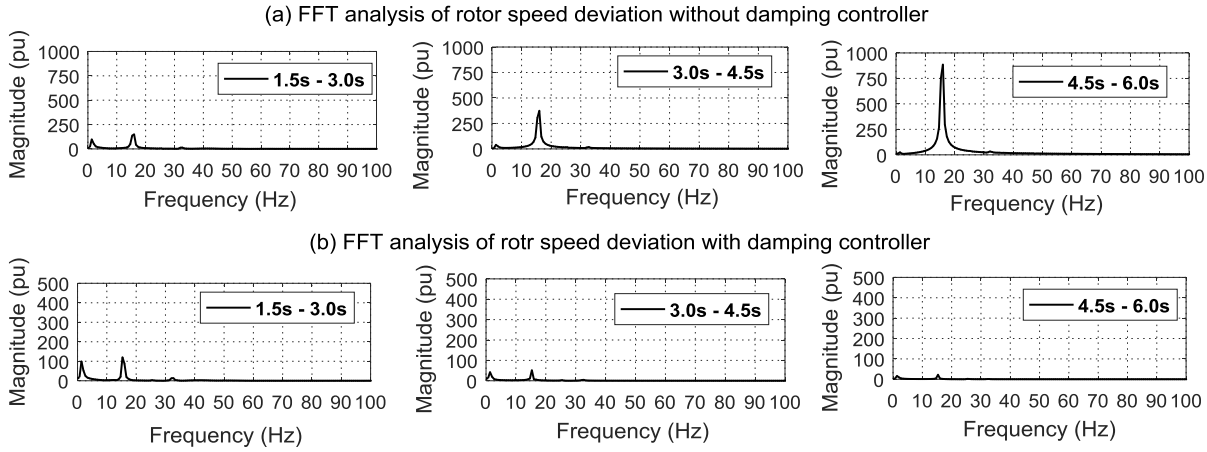

Figure 5.24: *FFT analyses of the rotor speed deviation with SSSC in Line 1 (X_{SSSC} = 0.35 pu) and capacitors in Line 2 (X_{C2} = 0.70 pu); (a) without damping controller, (b) with damping controller*

Figures 5.25 and 5.26 show that the multimodal-damping controller of parameters in Table 5.7 is able to damp out these oscillations and stabilize the power system.

Table 5.7: Multimodal Damping Controller Parameters for Case 2e

Mode	***Lead/Lag compensator***	*Gain*
1	$\frac{1+0.006903s}{1+0.014885s}$	40
2	$\left(\frac{1+0.003262\ s}{1+0.019012\ s}\right)\times\left(\frac{1+0.006795\ s}{1+0.009127\ s}\right)$	45
3	$\frac{1+0.009118s}{1+0.004206s}$	5
4	$\frac{1+0.004032s}{1+0.0060219s}$	5

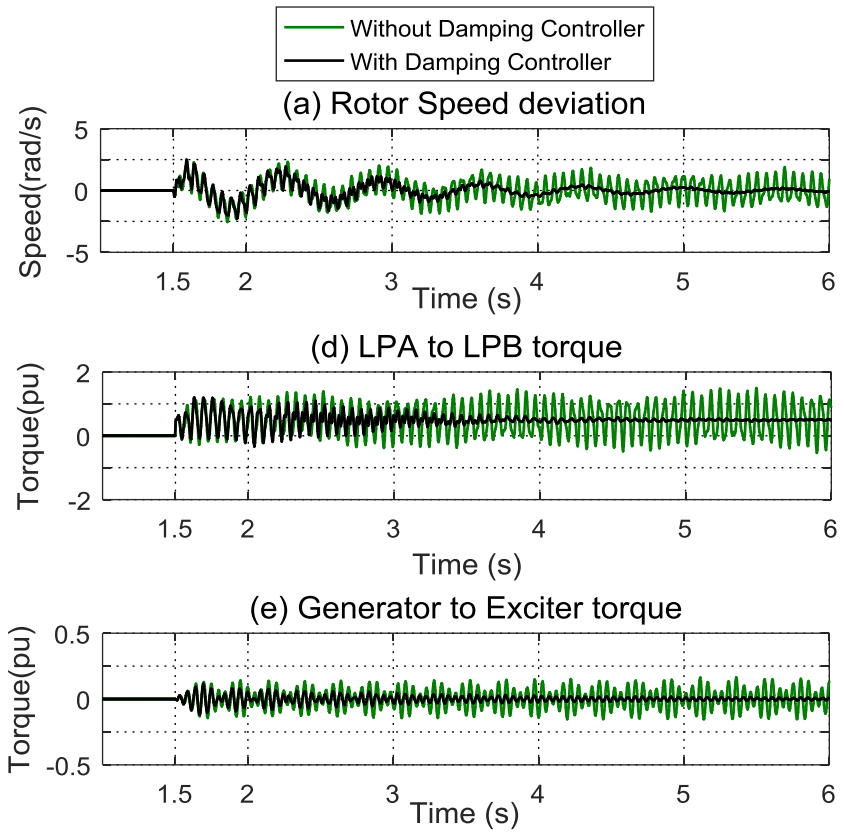

Figure 5.25: *Time domain simulations showing system response in the presence of the SSSC in Line 1 (X_{SSSC} = 0.35 pu) and capacitors in Line 2 (X_{C2} = 0.55 pu)*

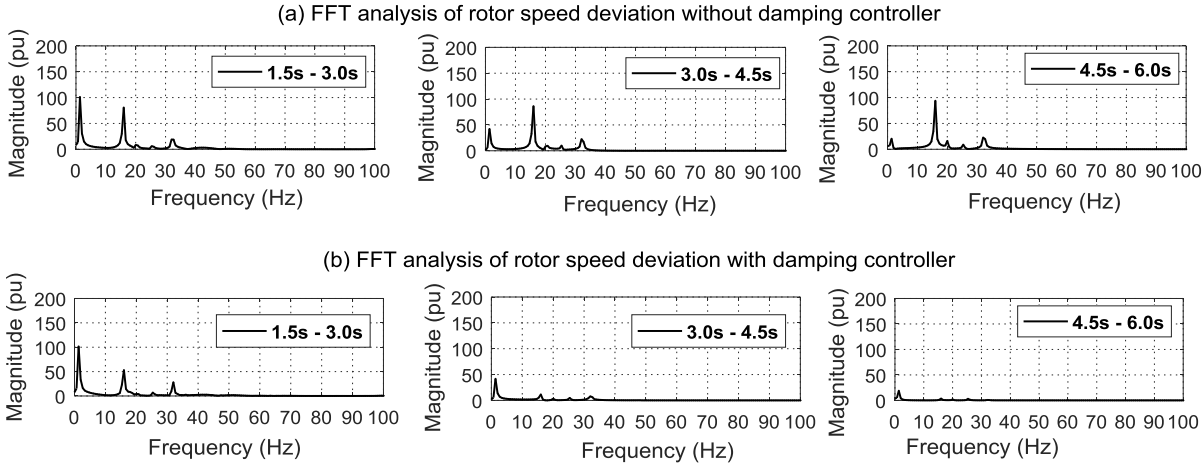

Figure 5.26: *FFT analyses of the rotor speed deviation with SSSC in Line 1 (X_{SSSC} = 0.35 pu) and capacitors in Line 2 (X_{C2} = 0.55 pu); (a) without damping controller, (b) with damping controller*

The last case study in Table 5.4 (i.e. Case *2f*) considers a scenario where transmission Line 2 is compensated by series capacitor while Line 1 is dually compensated. In this case, the capacitive reactance in Line 2 is kept at 0.70 pu and Line 1 is dually compensated (X_{SSSC} = 0.35 pu, X_{C1} = 0.35 pu). This case is much similar to *Case 2c* since in both cases, the total compensating reactance in each transmission line is 0.70 pu. The power system response and the FFT analysis of the rotor speed deviation for *Case 2f* are shown in figures 5.27 and 5.28 respectively following a three-phase to ground fault. Figure 5.28 shows that following the disturbance, subsynchronous oscillations in the generator rotor speed deviation is dominated by Mode 1 and Mode 3 for *Case 2f*. On the other hand, for *Case 2c*, the oscillations in the generator rotor speed deviation are dominated by Mode 1 and Mode 4. Activation of the damping controller with the parameters given in Table 5.8 successfully damps out the unstable torsional modes and brings the power system back to its stable operation.

Table 5.8: Multimodal Damping Controller Parameters for Case 2f

Mode	***Lead/Lag compensator***	*Gain*
1	$\frac{1+0.00659s}{1+0.01559s}$	5
2	$\frac{1+0.005706s}{1+0.01866s}$	20
3	$\left(\frac{1+0.01623\ s}{1+0.002364\ s}\right)\times\left(\frac{1+0.01623\ s}{1+0.002364\ s}\right)$	2
4	$\left(\frac{1+0.0119\ s}{1+0.002042\ s}\right)\times\left(\frac{1+0.0119\ s}{1+0.002042\ s}\right)\times\left(\frac{1+0.007922\ s}{1+0.0030647\ s}\right)$	2

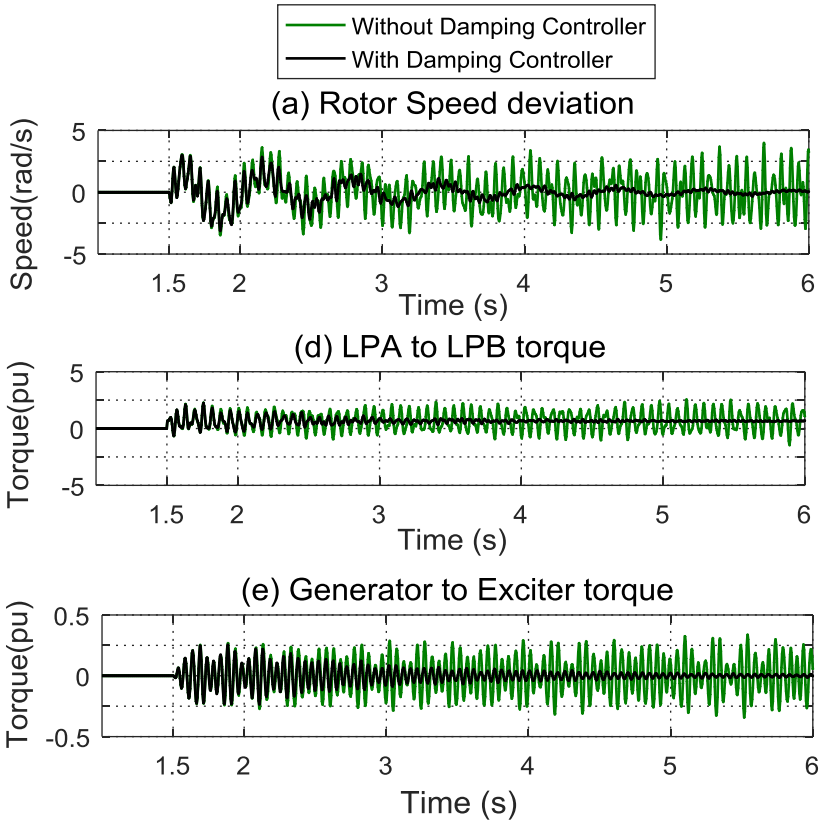

Figure 5.27: *Time domain simulations showing system response with hybrid compensation in Line 1 (X_{SSSC} = 0.35 pu, X_{C1} = 0.35 pu) and capacitors in Line 2 (X_{C2} = 0.70 pu)*

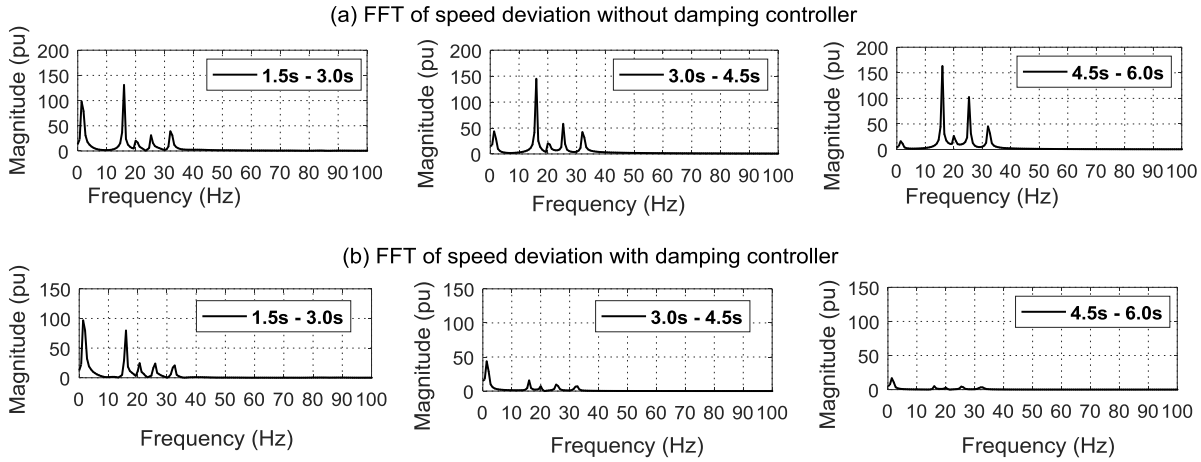

Figure 5.28: *FFT analyses of the rotor speed deviation with hybrid compensation in Line 1 (X_{SSSC} = 0.35 pu, X_C = 0.35 pu) and capacitors in Line 2 (X_C = 0.70 pu); (a) without damping controller, (b) with damping controller*

5.3. Conclusion

This chapter has presented the background to the damping of torsional oscillations through modulation of the transmission line reactance. The chapter has outlined the detailed steps required to deduce the phase difference between the oscillations in the generator rotor and the resulting electromagnetic torque in the air gap of the synchronous generator using time domain simulations in PSCAD. This technique was then used to design the SSSC-based SSR damping controller to mitigate SSR either due to the SSSC itself or due to the SSSC and the conventional series capacitors in the IEEE first benchmark model for SSR analysis. The results show that the damping controller with properly chosen parameters can successfully mitigate SSR. However, it is worth noting that the resonant frequency of the network changes from one combination of the SSSC and series capacitors to another even if the total amount of series compensation is maintained. This, as a result, requires that the controller parameters be modified to yield the best performance in each case. The idea was then extended to the modified IEEE first benchmark model with two parallel transmission lines with the presence of series capacitors in an adjacent transmission line. The results have shown that for different operating points of series compensation provided by the SSSC in Line 1, and together with additional conventional series capacitor in both Line 1 and 2, the supplementary controller around the SSSC is still capable of adding positive damping to the torsional oscillations caused by the multiple sources of SSR in both transmission lines 1 and 2 as shown by the Case Study *2f*.

CHAPTER SIX

CONCLUSIONS AND FUTURE WORK

In recent years, strengthening of transmission networks becomes imperative in order to improve their efficiency and relief transmission bottlenecks to meet the ever-growing electric power demands. This, as a result, reduces the reliance of these networks on existing generating units and minimizes the need to construct the new ones. The electric power industry is also seeing an increased penetration of renewable energy sources including hydro, wind, and solar, due to the global coercion on power plants to reduce their carbon footprint and the fear of depleting the non-renewable natural resources. Thus, in addition to efficient and reliable operation, future electric grids should be in a position to accommodate these variable energy sources along with the stability challenges that they bring. The conventional technology that has been used to increase the power transfer capability of transmission lines is that of fixed series capacitor banks operated by electromechanical switches. However, these switches cannot react quickly to counteract power system transients. Furthermore, series capacitors can cause electrical resonance in the transmission line resulting in violent torsional oscillations (due to SSR) and subsequent shaft failure in the nearby turbine-generators. SSR protection technologies provide necessary safety to the turbine-generators against shaft failure through tripping of the affected equipment (i.e. generators) or SSR escalating devices (i.e. conventional series capacitors), without damping the unstable torsional oscillations. Under severe conditions, the loss of power supply ensues with these techniques, which negatively affects the reliability of the supply.

The SSSC, which is a member of the power electronic based FACTS devices, can improve the capacity of the transmission line by providing controllable series compensation. In addition, this device can add positive damping to the torsional oscillations when installed in one of the transmission lines in an interconnected power system. However, the SSSC also has the potential to excite SSR on its own in the power system. In addition, the damping provided by the SSSC may not always be adequate to offset the negative damping in the system, and in such cases, supplementary damping controls may be added to mitigate SSR by modulating the line reactance to ensure continuous supply of electric power to the consumers. The damping controller design requires that the power system operating conditions be known together with the torsional modes of the nearby turbine-generator shafts.

Although the price tag associated with the SSSC is reportedly high due to the injection transformers, exhaustive work is being done by other researchers to achieve a transformerless version of the device. This initiative, together with the use of dual compensation, present an opportunity of utilizing the SSSC at a much lower cost in future.

6.1. Summary of the Results

The findings of the research work undertaken in this thesis are summarized as follows:

- In Chapter Three, we presented the mathematical modelling of the IEEE first benchmark model developed by other researchers in [80] to show the values of conventional capacitor compensation expected to cause the worst SSR instability in the power system. The model of the reactance-controlled type SSSC which is used for studies in this thesis is also presented in terms of its internal controls when operating in capacitive mode. Validation of the SSSC model was done in subsection 3.4.3 by showing that it satisfies the following; (i) it can provide the required amount of series compensation, (ii) it is able to maintain the required voltage at the DC side of the inverter, (iii) it has well damped dynamic response and (iv) its dynamics are not susceptible to the disturbances in the transmission system, which makes it robust.
- In Chapter Four, we studied the resonant characteristics of the SSSC compensated IEEE first benchmark model, utilizing the frequency response test (FRT) methodology which was validated against the harmonic impedance theoretical solution (HIS). From these resonant characteristics, we established that the SSSC can actually cause electrical resonance in the transmission line and thus it has a potential to cause SSR by exciting the torsional modes of the turbine-generator shaft system. However, it was observed that excitation of each torsional mode is expected to occur at higher degrees of compensation with the SSSC in comparison with conventional series capacitor compensation. For a case of dual compensation in subsection 4.3.2, the resonant impedance was seen to increase as the ratio X_{SSSC}/X_{Comp} was increased from 0.20 to 0.60. This in turn improves the damping torque component of the generator speed deviation, providing better damping of SSR. However, this comes with a higher price tag, presenting a trade-off between cost and performance which the transmission planner should be aware of. The results in subsection 4.3.2 also confirm the ability of the SSSC model to provide the required amount of series compensation at system frequency (i.e. 60 Hz).
- In Chapter Five, the design of the SSSC-based supplementary damping controller was presented. The criteria for choosing the controller structure and the its input signal was also discussed. Initially, in section 5.3, the original IEEE first benchmark model for SSR analysis is used. The results in this section have shown that a single mode damping controller can effectively damp SSR if there is only one source of SSR in the system (e.g. SSSC alone). This is because the torsional oscillations following a fault tend to have only one dominant mode. However, when the transmission line is dually compensated (i.e. with SSSC and conventional series capacitors), the post-fault torsional oscillations are multimodal in nature. Damping of SSR in such cases is achieved by using a multimodal damping controller as presented in Case

Studies *1a, 1b* and *1c*. It has also been discovered that an increase in the ratio X_{SSSC}/X_{Comp} improves damping of lower frequency modes (i.e. Mode 1 and Mode 2) at a cost of Mode 3 and Mode 4. This finding agrees with that in Chapter Four which shows a decrease in f_{er} (hence an increase in $f_0 - f_{er}$) as X_{SSSC}/X_{Comp} is increased.

The use of a SSSC-based damping controller is then extended to a parallel transmission line network in section 5.4. Here a modified IEEE first benchmark model with two transmission lines originating from the same substation is used to study SSR. The results in this section have shown that the presence of the SSSC alone in Line 1 can add some positive damping to the post-fault torsional oscillations due to conventional series capacitor in Line 2 (comparison of *Case 2a* with *Cases 2c* and *2d*). However, this damping is not sufficient to restore the system stable operation hence a need for supplementary damping controller. It has been shown in *Cases 2c, 2d* and *2e* that a damping controller can mitigate SSR due to the SSSC in one line and that due to conventional series capacitor in an adjacent transmission line. The results have also been demonstrated that a properly designed damping controller can mitigate SSR even in a case where Line 1 is dually compensated using an SSSC and a conventional series capacitor while Line 2 is compensated by a conventional series capacitor.

6.2. Suggestions for Possible Future Work

For future work considerations, the following aspects relating to the work covered in this thesis can be explored:

- In Chapter Five, we developed both the single mode and multi-modal supplementary damping controllers to damp torsional oscillations in the power system. The parameters of supplementary damping controller required for optimum performance were obtained through online tuning. These parameters were found to be dependent on the operating point of the power system namely the degree and type of compensation. Extension of this aspect of the work can be done by developing an intelligent self-tuning controller.
- Deducing from the current trends in electric power transmission, future grids will be made of heavily loaded and meshed transmission networks, most probably consisting of interconnected HVDC links and series compensated AC lines. Future studies may investigate SSR in such a scenario and determine whether the supplementary damping controls around the SSSC can damp torsional oscillations that may arise in the presence of an HVDC link in adjacent transmission line.

APPENDIX A - IEEE FIRST BENCHMARK MODEL

A1. Per-Unit Base

Table A1: Base Parameters

Parameter	***Grid side*** **(HV)**	***Generator side*** **(LV)**
Base power (3 phase)	892.4 MVA	892.4 MVA
Base voltage (phase-neutral)	311.192 kV	15.01 kV
Base impedance	325.55 Ω	0.7575 Ω
Base current	955.8 A	19.82 kA

A2. System Parameters

The IEEE FBM was originally created by the IEEE Subsynchronous Resonance Working Group [12] in 1977 and the parameters used were adopted from the Navajo Project in USA, based on 892.4 MVA generators and 500 kV transmission line with system frequency of 60 Hz. The synchronous generator is modelled by two damper windings in the *q*-axis and one damper winding in the *d*-axis.

Table A2: Synchronous generator parameters in pu (base 892.4 MVA)

Parameter	***Value*** (pu)	***Parameter***	***Value*** (pu)
X_d	1.79	X_{mq}	1.58
X_q	1.71	X''_q	0.2
R_a	0.0	X_p	0.13
X'_d	0.169	τ'_{d0}	4.3 s
X'_q	0.228	τ'_{q0}	0.85 s
X''_d	0.135	τ''_{d0}	0.032 s
X_{md}	1.66	τ''_{q0}	0.050 s

Table A3: Single line transmission network parameters in pu (base 892.4 MVA)

Parameter	***Positive sequence*** (pu)	***Zero sequence*** (pu)
R_L	0.02	0.50
X_L	0.50	1.56
X_{sys}	0.06	0.06

Table A4: Rotor Circuit parameters in pu (base 892.4 MVA)

Parameter	***D-axis*** (pu)	***Q-axis*** (pu)
w_0R_f	0.53	5.3
x_f	0.062	0.326
w_0R_k	1.54	3.1
x_k	0.0055	0.095
X_a	1.66	1.58
x_L	0.13	0.13

Table A5: Shaft Inertias and spring constants in pu on the Generator base (892.4 MVA)

Inertia	***Inertia constant*** H (s)	***Shaft section***	***Spring constant*** K (pu Torque/rad)	***Torque Fraction***
HP turbine	0.092897			a_H = 0.30
		HP-IP	7277	
IP turbine	0.155589			a_I = 0.26
		IP-LPA	13168	
LPA turbine	0.858670			a_A = 0.22
		LPA-LPB	19618	
LPB turbine	0.884215			a_B = 0.22
		LPB-G	26713	
Generator	0.868495			-
		G-Ex	1064	
Exciter	0.0342165			-

The torque developed in various sections of the turbine are as follows:

$$T_H = a_H \frac{w_0}{w_H} P_m \; ; \quad T_I = a_I \frac{w_0}{w_I} P_m \; ; \quad T_B = a_B \frac{w_0}{w_B} P_m \; ; \quad T_A = a_A \frac{w_0}{w_A} P_m \; ;$$

$$w_H = w_0 + \Delta w_H \; ; \quad w_I = w_0 + \Delta w_I \; ; \quad w_B = w_0 + \Delta w_B \; ; \quad w_A = w_0 + \Delta w_A$$

Table A6: Step-up transformer parameters in pu (base 892.4 MVA)

Parameter	***Value***
Rated Power	892.4 MVA
Nominal Frequency	60 Hz
Rated Voltage (LV)$_{L-L}$	26 kV
Rated Voltage (HV)$_{L-L}$	539 kV
Vector Group and Phase Shift	YNd1
Positive Sequence Impedance	0.14 pu
Zero Sequence Impedance	0.14 pu

A3. Original IEEE FBM with a Single Transmission Line

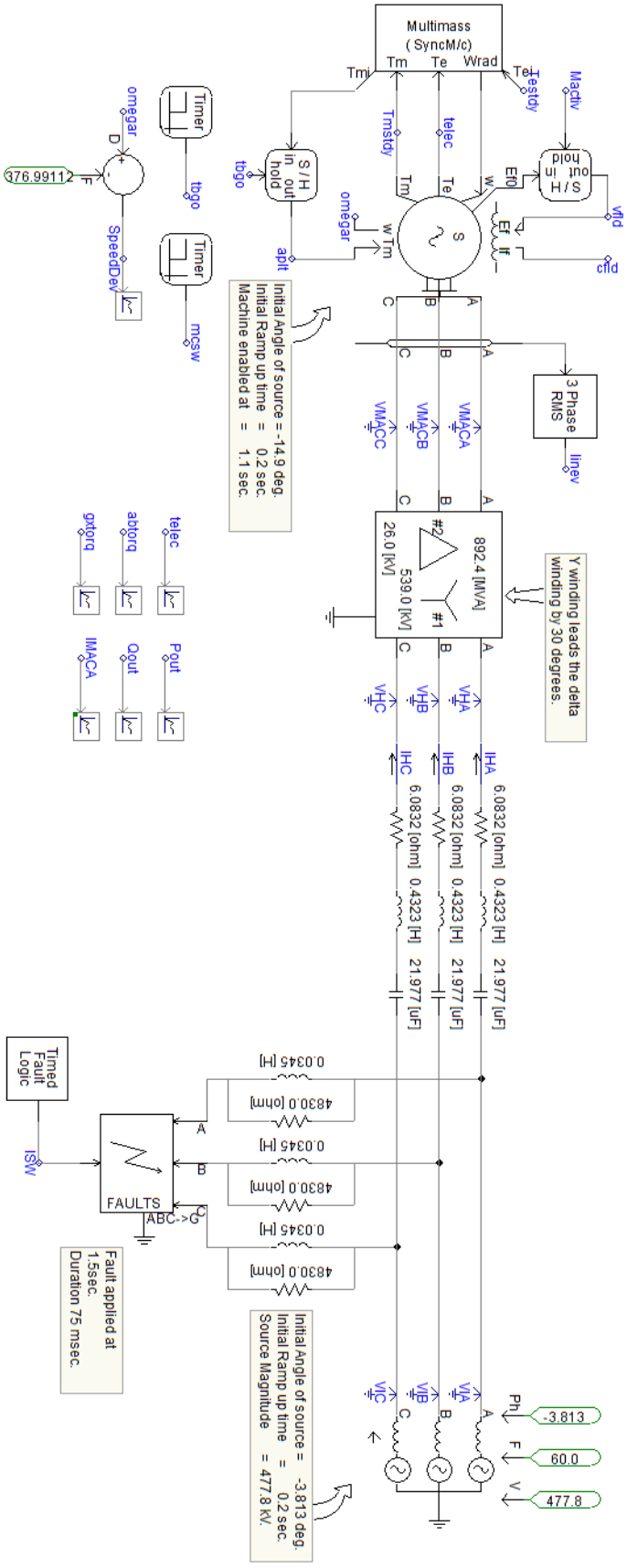

Figure A1: The IEEE first benchmark model in PSCAD

A4. SSR Characteristics of the Series Capacitors in the IEEE FBM

Harmonic Impedance Solution

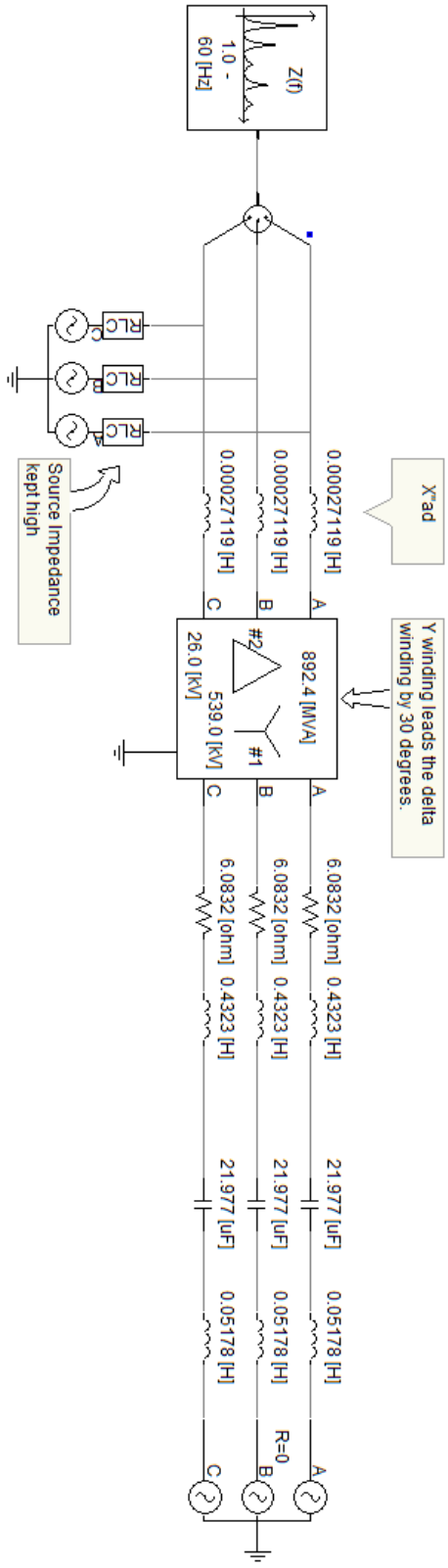

Figure A2: Scanning the network impedance of the capacitor compensated IEEE FBM using Harmonic Impedance Solution in PSCAD

Frequency Response Test Methodology

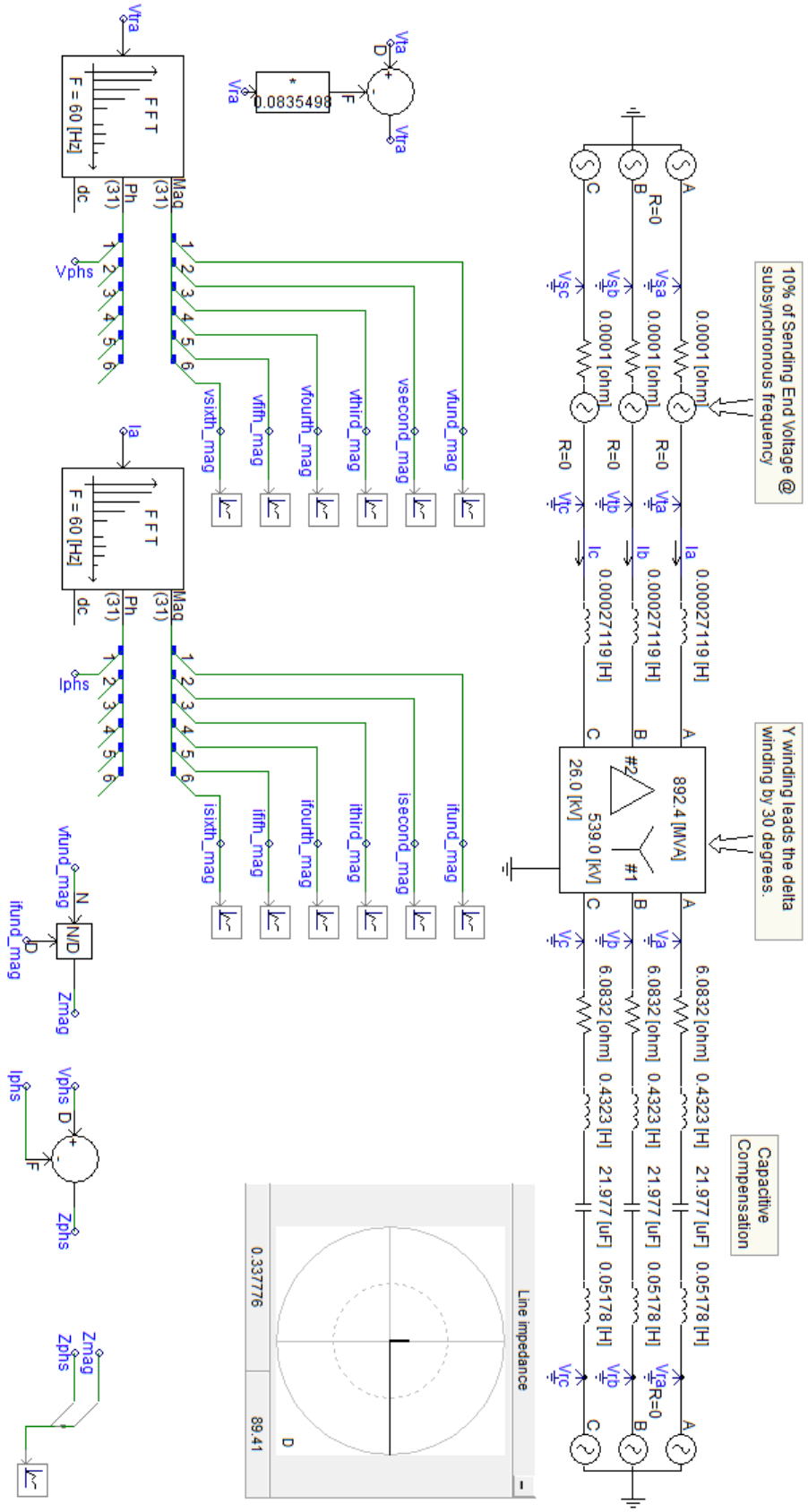

Figure A3: Frequency Response test methodology simulation in PSCAD

APPENDIX B - THE SSSC MODEL AND DAMPING CONTROLLER

B1. Parameters of the SSSC

The SSSC parameters are calculated using the grid side per unit base values in Appendix A.

K_{vp}^{Base} = Base Current = 955.8 A

$K_{ai}^{Base} = 1$

Table B1: Parameters of the SSSC

Parameter	***Value in Per Unit***	***Actual Value***
V_{dc0}	0.22494	70 kV
V_{dc}* or V_{ref}	0.1 V_{dc0}	7 kV
w_0	1.0	376.9911 rad/s
C_{dc}	0.12208	375 µF
K_{vp}	10.159	9711.91
K_{ai}	3.9*w_0	1470.27
H_p	0.3	0.3

B2. The SSSC Compensated IEEE FBM

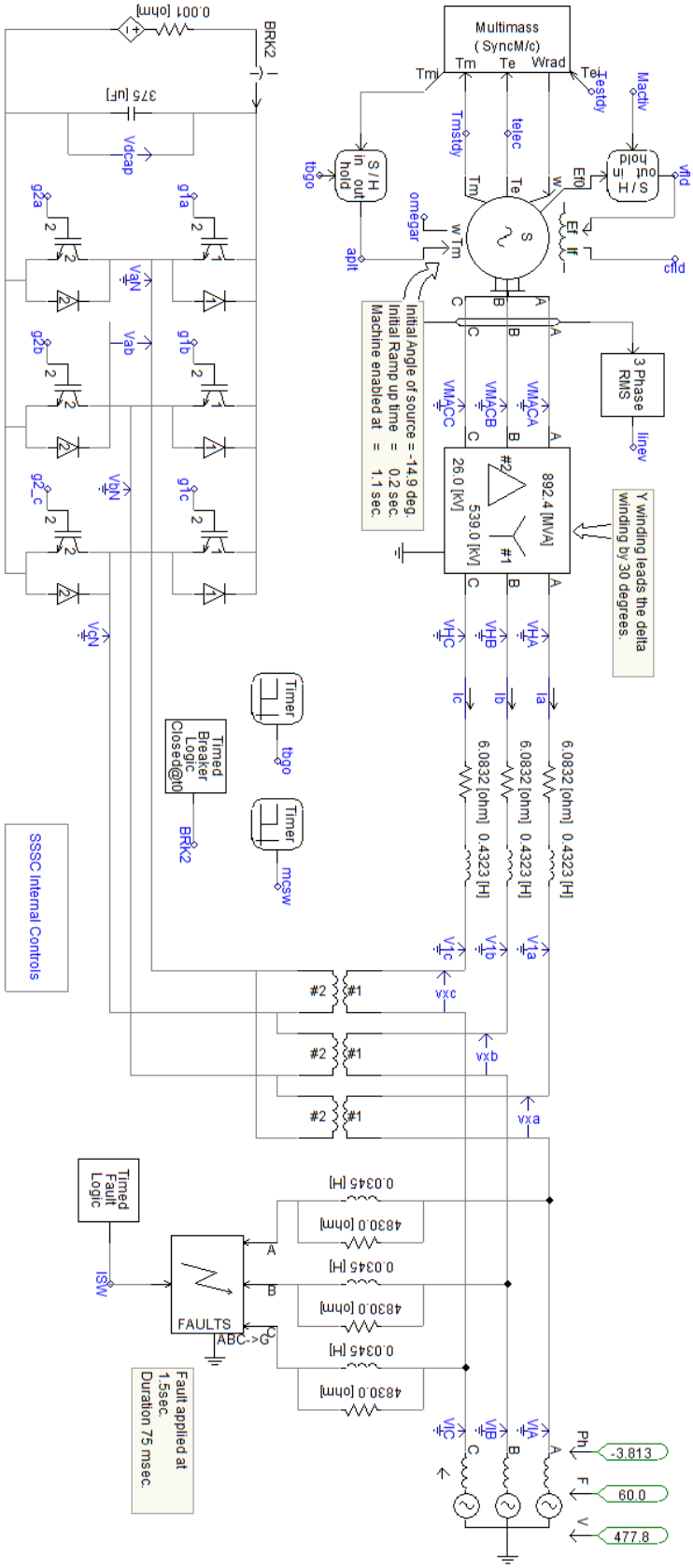

Figure B1: The IEEE first benchmark model in PSCAD

Internal Controls of the Static Synchronous Series Compensator

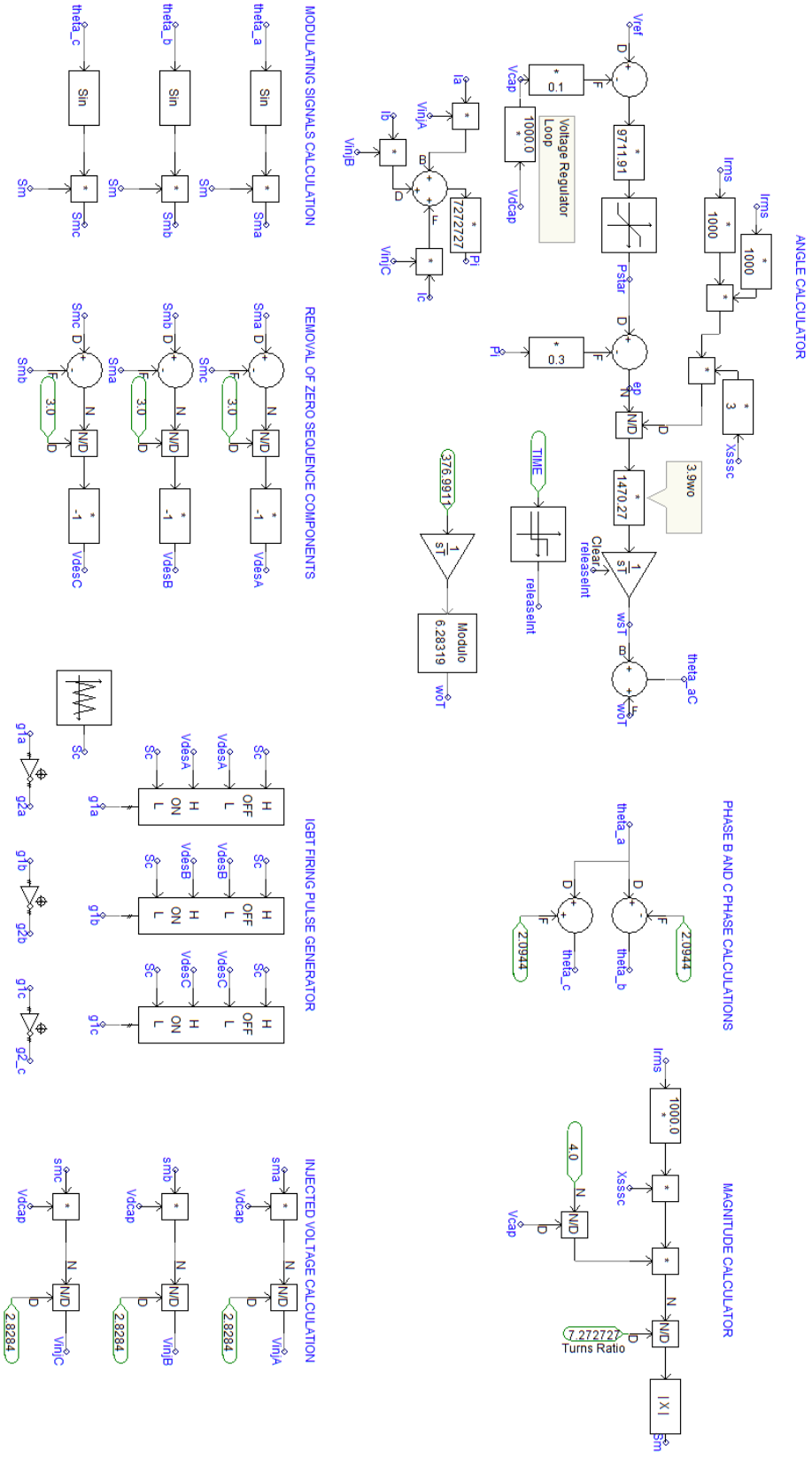

Figure B2: Internal Controls of the Static Synchronous Series Compensator

B3. Testing Performance of the SSSC

To evaluate whether the SSSC can provide the required compensating reactance, the following system model was used:

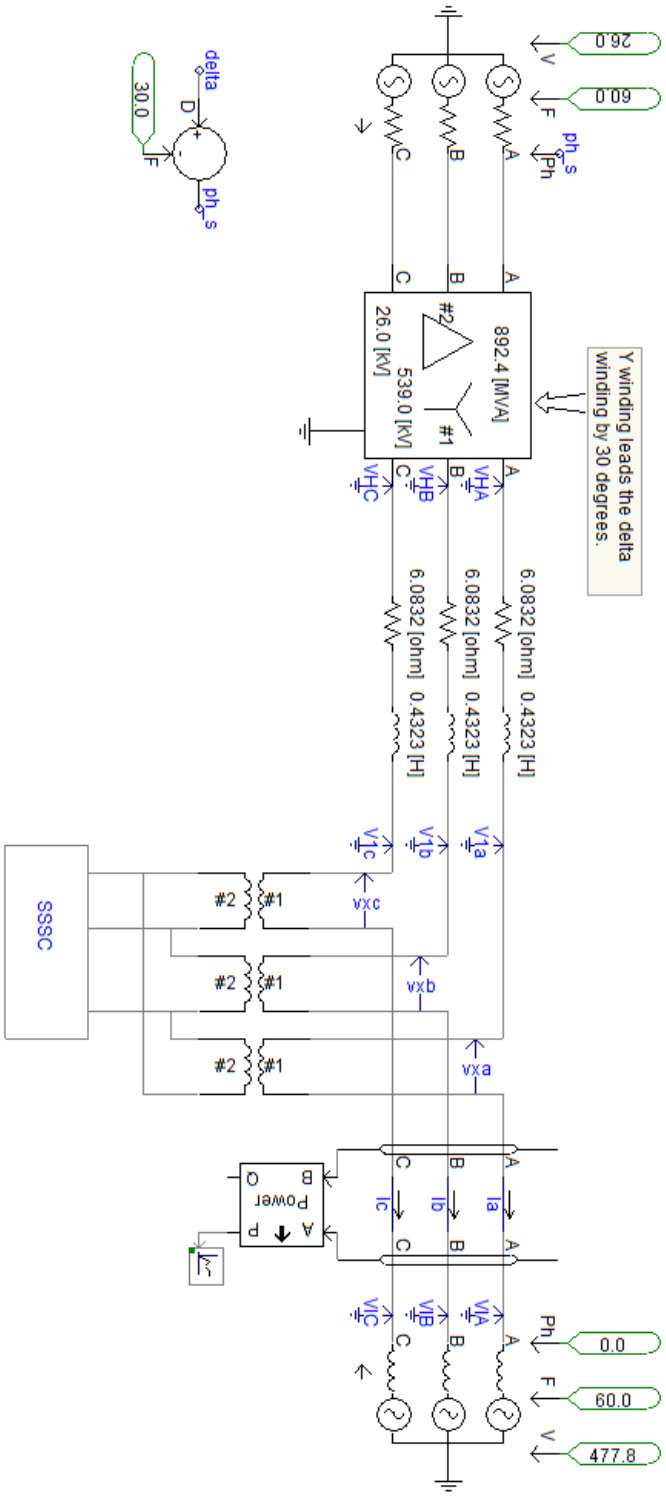

Figure B3: The Single Machine Infinite bus system used to simulate the performance of the SSSC

B4. SSR Characteristics of the SSSC in the IEEE FBM

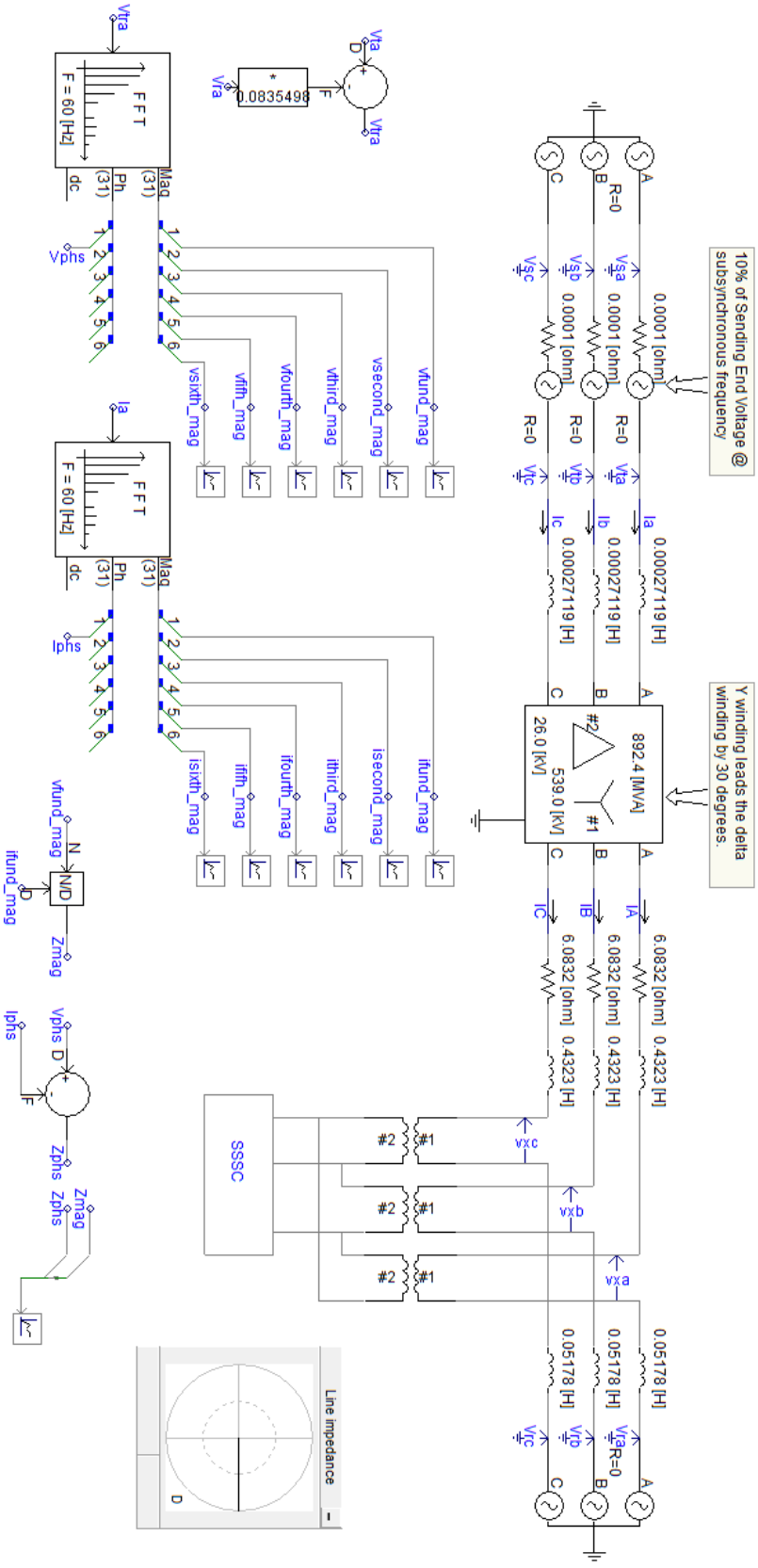

Figure B4: The Frequency Response Test for the SSSC compensated network

B5. Supplementary SSR Damping Controller

For the SSSC compensated IEEE FBM in Chapter 5 (subsection 5.3.2), the phase lag between ΔT_e and the modulating signal ΔX_{SSSC} was found to be 41.474°. The required lead compensator to provide this angle (at 32.285 Hz) was obtained to be as follows:

$$M_4(s) = \frac{1 + 0.010932s}{1 + 0.002221s} \tag{A1}$$

Bode diagram of this lead compensator is given in figure B5.

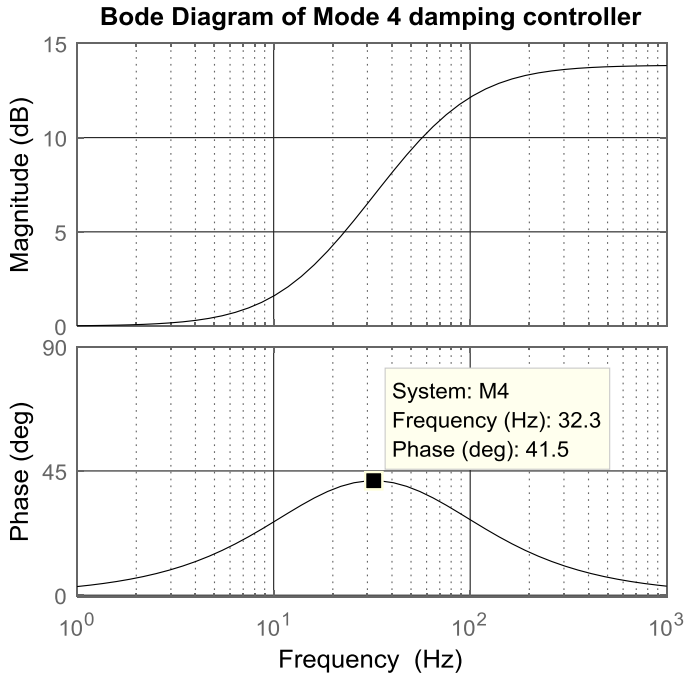

Figure B5: The lead compensator used for Mode 4 damping controller

B6. Modified IEEE FBM with Parallel Transmission Lines

Table B2: Double line transmission network parameters in pu (base 892.4 MVA)

Parameter	***Positive sequence*** (pu)
R_L	0.04
X_L	1.00

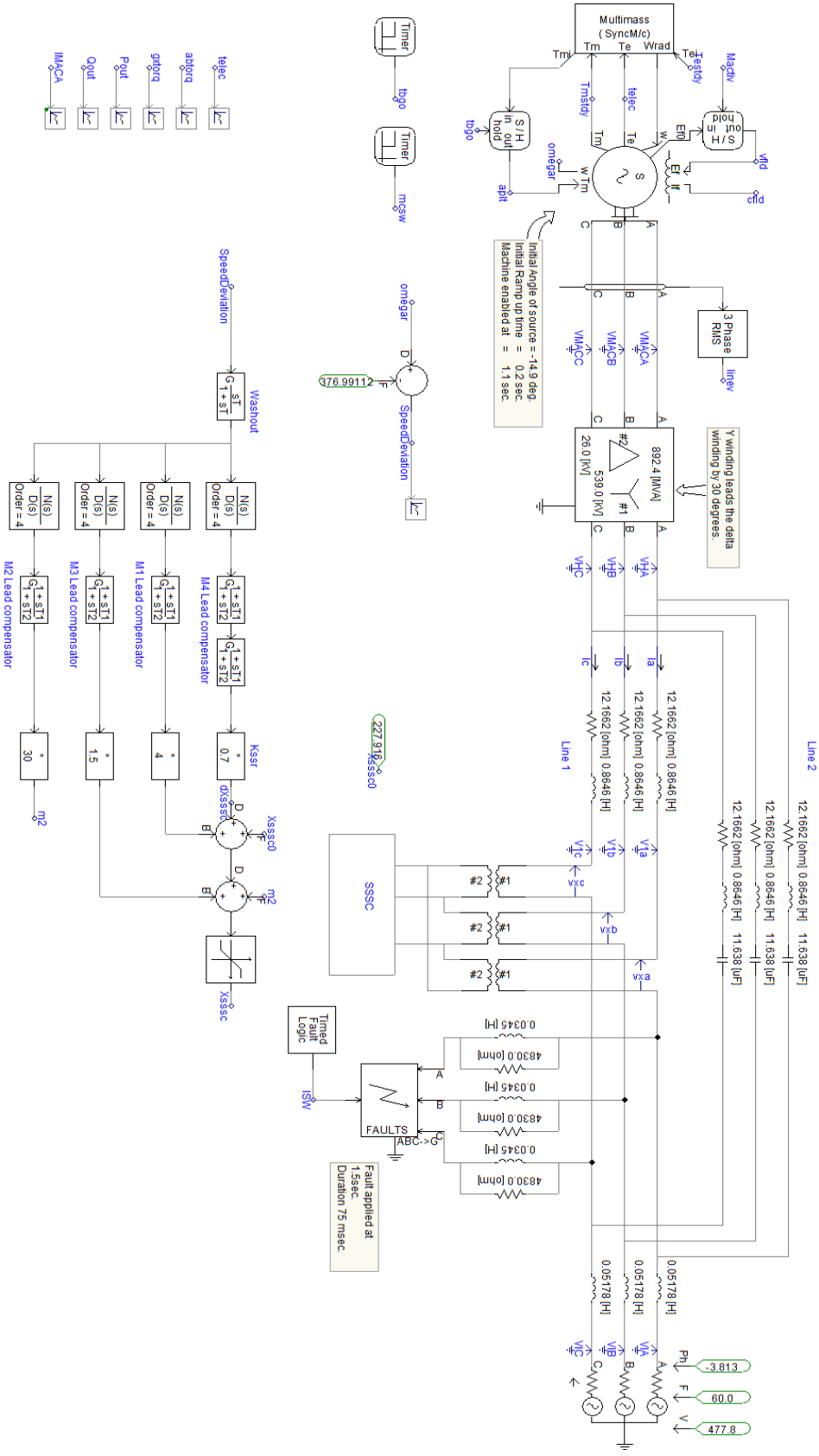

Figure B6: The modified IEEE FBM with multimodal damping controller in PSCAD

REFERENCES

1. United Nations, Department of Economic and Social Affairs, Population Division (2017). World Population Prospects: The 2017 Revision, custom data acquired via website. (https://esa.un.org/unpd/wpp/DataQuery/). Last Accessed 03 August 2017.

2. T.F. Garrity, "Innovation and trends for future electric power systems", *Power Systems Conference, 2009. PSC'09*, March 2009, pp. 1-8.

3. R. Pillay Carpanen, "Analysis of the Impact of a FACTS-Based Power Flow Controller on Subsynchronous Resonance", *PhD Thesis*, University of KwaZulu-Natal, 2012.

4. X.F. Wang, Y. Song and M. Irving, "Modern power systems analysis," *Springer Science & Business Media*, 2010.

5. I. Mayordomo, T. Dräger, P. Spies, J. Bernhard and A. Pflaum, "An overview of technical challenges and advances of inductive wireless power transmission." *Proceedings of the IEEE*, Vol 101(6), June 2013, pp. 1302-1311.

6. M.P. Thakre, V. S. Kale, K. R. Dhenuvakonda, B. S. Umre and A. S. Junghare, "Study and mitigation of subsynchronous oscillations with SSC based SSSC", *Journal of Power and Energy Engineering*, Vol 3(9), September 2015, p. 33.

7. C.M. Leoaneka, "Dynamic Performance of Numerical Distance Protection Relays in Heavily Series Compensated Networks", *Master of Engineering Dissertation*, University of KwaZulu-Natal, 2009.

8. D.H. Baker, E.G. Boukarim, R. D'Aquila and R. J. Piwko, "Subsynchronous resonance studies and mitigation methods for series capacitor applications", *Power Engineering Society Inaugural Conference and Exposition in Africa, 2005 IEEE*. IEEE, July 2005, pp. 386-392.

9. F.A. Jowder, B.T. Ooi, "Series compensation of radial power system by a combination of SSSC and dielectric capacitors", *IEEE Transactions on Power Delivery,* Vol 20(1), January 2005, pp. 458-465.

10. K.R. Padiyar, "Analysis of Subsynchronous Resonance in Power Systems", *Springer Science & Business Media*, Vol 471, 1999.

11. D. Mondal, A. Chakrabarti and A. Sengupta, "Power system small signal stability analysis and control", *Academic Press*, April 2014, p. 55

12. IEEE SSR working group, “First benchmark model for computer simulation of subsynchronous resonance”, *IEEE transactions on power apparatus and systems*, Vol *96*(5), 1977, pp. 1565-1572.

13. Y.H. Song and A. Johns, “Flexible ac transmission systems (FACTS)”, *Institution of Engineering and Technology*, 1999.

14. D.N. Walker, C.E.J. Bowler, R.L. Jackson and D.A. Hodges, “Results of subsynchronous resonance test at Mohave”, *IEEE Transactions on Power Apparatus and Systems*, Vol *94*(5), September 1975, pp. 1878-1889.

15. V.B. Virulkar and G. V. Gotmare, “Subsynchronous Resonance in Series Compensated Wind Farm: A review”, *Renewable and Sustainable Energy Reviews*, March 2016, pp. 1010-1029.

16. N. Acharya, A. Sode-Yome and N. Mithulananthan, “Facts about Flexible AC Transmission systems (FACTS) controllers: Practical Installations and Benefits”, *Australasian Universities Power Engineering Conference (AUPEC), Australia*, 2005, pp. 533-538

17. F.W. Huang, B. S. Rigby, R. G. Harley, “Static Synchronous Series Compensator Control for Active Damping of Generator Torsional Oscillations”, *Proceedings of the International Conference on Advanced Power System Automation and Protection APAP2004, Jeju, South Korea*, October 2004, pp. 610-615.

18. F.W. Huang, “Modelling and Analysis of Inverter-based FACTS devices for Power System Dynamic Studies”, *PhD thesis*, University of KwaZulu-Natal, Durban, South Africa, 2006.

19. X. Zheng, J. Zhang and C. Wang, “Active damping controller design for SSSC to mitigate subsynchronous resonance”, *IEEE Power and Energy Society General Meeting,* July 2010, pp. 1-6.

20. R.K. Varma, S. Auddy and Y. Semsedini, “Mitigation of subsynchronous resonance in a series-compensated wind farm using FACTS controllers”, *IEEE Transactions on Power Delivery*, Vol 23(3), July 2008, pp. 1645-654.

21. J. Adams, C. Carter and S.H. Huang, “ERCOT Experience with Sub-synchronous Control Interaction and Proposed Remediation”, *Transmission and Distribution Conference and Exposition (T&D), 2012 IEEE PES*, IEEE, May 2012, pp. 1-5.

22. H. Liu, X. Xie, Y. Li, H. Liu and Y. Hu, “Damping subsynchronous resonance in series-compensated wind farms by adding notch filters to DFIG controllers”. *Innovative Smart Grid Technologies-Asia (ISGT ASIA), 2015 IEEE*, November 2015, pp. 1-5.

23. S. Svensson and K. Mortensen, “Damping of Subsynchronous Oscillations By an HVDC Lins. An HVDC Simulator Study”, *IEEE Transactions on Power Apparatus and Systems*, Vol 3, March 1981, pp. 1431-1439.

24. N. Prabhu and K. R. Padiya, “Investigation of subsynchronous resonance with VSC-based HVDC transmission systems”, *IEEE Transactions on Power Delivery*, Vol *24*(1), January 2009, pp. 433-440.

25. M. Amin and M. Molinas, “Understanding the origin of oscillatory phenomena observed between wind farms and HVDC systems”, *IEEE Journal of Emerging and Selected Topics in Power Electronics*, Vol 5(1), 2017, pp. 378-392.

26. M. Bahrman, E.V. Larsen, R.J. Piwko and H.S. Patel, “Experience with HVDC turbine-generator torsional interaction at Square Butte”, *IEEE Transactions on Power Apparatus and Systems*, Vol 3, May 1980, pp. 966-975.

27. K.R. Padiyar, “Analysis of subsynchronous resonance in power systems”, *Springer Science & Business Media,* December 2012.

28. K.R. Padiyar and N. Prabhu, “Design and performance evaluation of subsynchronous damping controller with STATCOM”, *IEEE Transactions on Power Delivery*, Vol *21*(3), July 2006, pp. 1398-1405.

29. N. Prabhu, M. Janaki and R. Thirumalaivasan, “Damping of subsynchronous resonance by subsynchronous current injector with STATCOM”, *TENCON 2009-2009 IEEE Region 10 Conference*, January 2009, pp. 1-6.

30. B.K. Keshavan and N. Prabhu, “Damping of Subsynchronous Oscillations using STATCOM – a FACTS device”, *Transmission and Distribution Conference and Exposition, 2001 IEEE/PES,* Vol 1, 2001, pp. 1-7.

31. A. Salemnia, M Khederzadeh and A. Ghorbani, “Mitigation of Subsynchronous Oscillations by 48-pulse VSC STATCOM using Remote Signal”, *PowerTech, 2009 IEEE Bucharest*, June 2009, pp. 1-7.

32. A. Ghorbani, B. Mozaffari and A.M. Ranjbar, “Application of subsynchronous damping controller (SSDC) to STATCOM”, *International Journal of Electrical Power & Energy Systems*, Vol *43*(1), December 2012, pp. 418-426.

33. B.K. Keshavan and N. Prabhu, “Damping of subsynchronous oscillations using STATCOM-a FACTS controller”, *Power System Technology, 2004. PowerCon 2004. 2004 International Conference*, Vol. 1, November 2004, pp. 12-16.

34. D. Rai, G. Ramakrishna, S.O. Faried and A. Edris, "Damping subsynchronous resonance using a STATCOM operating in a phase imbalanced mode", *Power & Energy Society General Meeting, 2009. PES'09. IEEE*, July 2009, pp. 1-8.

35. H. Khalilinia and J. Ghaisari, "Improve Sub-Synchronous Resonance (SSR) damping using a STATCOM in the transformer bus" *EUROCON 2009, EUROCON'09. IEEE*, May 2009, pp. 445-450.

36. R.K. Varma, and R. Salehi, "SSR mitigation with a new control of PV Solar Farm as STATCOM (PV-STATCOM)", *IEEE Transactions on Sustainable Energy*, April 2017.

37. S.F. Torabi, D. Nazarpour and Y. Shayestehfard, "Mitigation of subsynchronous resonance by static compensator with the aid of fuzzy logic controller and adaptive neuro fuzzy inference system controller", *Electrical Power Distribution Networks (EPDC), 2012 Proceedings of 17th Conference on*, May 2012, pp. 1-5.

38. S. Golshannavaz, M. Mokhtari and D. Nazarpour, "SSR suppression via STATCOM in series compensated wind farm integrations", *Electrical Engineering (ICEE), 2011 19th Iranian Conference on,* May 2011, pp. 1-6.

39. S.T. Nagarajan and N. Kumar, "Fuzzy logic based control of STATCOM for mitigation of SSR", *Power Electronics (IICPE), 2012 IEEE 5th India International Conference on*, December 2012, pp. 1-6.

40. W. Gu, X. Li and Y. Wang, "Design of subsynchronous damping control based on improved particle swarm optimization algorithm by STATCOM", *Power and Energy Engineering Conference (APPEEC), 2010 Asia-Pacific,* March 2010, pp. 1-4.

41. M. Anju and R. Rajasekaran, "Co-ordination of SMES with STATCOM for mitigating SSR and damping power system oscillations in a series compensated wind power system", *Computer Communication and Informatics (ICCCI), 2013 International Conference on*, January 2013, pp. 1-6.

42. R.K. Varma, Y. Semsedini and S. Auddy, "Mitigation of subsynchronous oscillations in a series compensated wind farm with thyristor controlled series capacitor (TCSC)", *Power Systems Conference: Advanced Metering, Protection, Control, Communication, and Distributed Resources, 2007. PSC 2007*, March 2007, pp. 331-337.

43. S.R. Joshi, P. E. Cheriyan and A. M. Kulkarni, "Output feedback SSR damping controller design based on modular discrete-time dynamic model of TCSC", *IET Generation, Transmission & Distribution* Vol 3(6), June 2009, pp. 561-573.

44. D. Rai, S.O. Faried, G. Ramakrishna and A. Edris, "Hybrid series compensation scheme capable of damping subsynchronous resonance", *IET Generation, Transmission & Distribution*, Vol 4(3), March 2010, pp. 456-466.

45. H. Hosseini and B. Tousi, "Mitigating SSR in Hybrid System with Steam and Wind turbine by TCSC", *Electrical Power Distribution Networks (EPDC), 2012 Proceedings of 17th Conference on,* IEEE, May 2012, pp. 1-6.

46. R. Zheng, T. Joseph, S. Wang, and J. Liang, "A control strategy for TCSC to mitigate SSR with local measurements", *AC and DC Power Transmission (ACDC 2017), 13th IET International Conference on,* IET, February 2017, pp. 6-6.

47. R. Bazyar, M. R. Javadi, A. Ghasemi and A. Yusefi, "Analysis and study subsynchronous resonance (SSR) in Tabriz thermal power plant using thyristor controlled series compensator", *Thermal Power Plants (CTPP), 2011 Proceedings of the 3rd Conference on*, October 2011, pp. 1-5.

48. T. Yi and Y. Rui-qian, "Mechanism analysis of using thyristor controlled serious compensation to mitigate Subsynchronous Resonance", *IPEC, 2010 Conference Proceedings*, October 2010, pp. 1094-1099.

49. L. Wang and C.W. Huang, "Suppression of subsynchronous resonance using robust H/sup/spl infin//TCSC damping controllers", *Power Engineering Society 1999 Winter Meeting, IEEE*, Vol 1, 1999, pp. 610-615.

50. S. Svensson and K. Mortensen, "Damping of Subsynchronous Oscillations By an HVDC Lins. An HVDC Simulator Study", *IEEE Transactions on Power Apparatus and Systems*, Vol 3, 1981, pp 1431-1439.

51. H. Knudsen and S. Stgzlvring-Hallsson, "HVDC generated SSR oscillations and SSR damping controllers in HVDC", *International conference on power system transients IPST'97*. 1997.

52. L. Livermore, C. Ugalde Loo, J. Liang, J. Ekanayake and N. Jenkins, "Damping of subsynchronous resonance using a vsc-hvdc link in a three machine model", 2011.

53. L. Livermore, C.E. Ugalde-Loo, Q. Mu, J. Liang, J.B. Ekanayake and N. Jenkins, "Damping of subsynchronous resonance using a voltage source converter-based high-voltage direct-current link in a series-compensated Great Britain transmission network", *IET Generation, Transmission & Distribution*, Vol *8*(3), March 2014, pp. 542-551.

54. M. Janaki, N. Prabhu, R. Thirumalaivasan and D.P. Kothari, "Mitigation of SSR by subsynchronous current injection with VSC HVDC", *International Journal of Electrical Power & Energy Systems*, Vol *57*, May 2014, pp. 287-297.

55. L. Fan and Z. Miao, "Mitigating SSR using DFIG-based wind generation" *IEEE Transactions on Sustainable Energy*, Vol *3*(3), July 2012, pp. 349-358.

56. C. Zhu, L. Fan and M. Hu, "Control and analysis of DFIG-based wind turbines in a series compensated network for SSR damping", *Power and Energy Society General Meeting, 2010 IEEE*, July 2010, pp. 1-6.

57. S.O. Faried, I. Unal, D. Rai and J. Mahseredjian, "Utilizing DFIG-based wind farms for damping subsynchronous resonance in nearby turbine-generators", *IEEE Transactions on Power Systems*, Vol *28*(1), February 2013, pp.452-459.

58. M. Mokhtari, J. Khazaei and D. Nazarpour, "Sub-synchronous resonance damping via doubly fed induction generator", *International Journal of Electrical Power & Energy Systems*, Vol *53*, December 2013, pp. 876-883.

59. G.N. Pillai, A. Ghosh and A. Joshi, "Robust control of SSSC to improve torsional damping", *Power Engineering Society Winter Meeting, 2001. IEEE*, Vol. 3, 2001, pp. 1115-1120.

60. M. Farahani and S. Ganjefar, "Intelligent control of static synchronous series compensator via an adaptive self-tuning PID controller for suppression of torsional oscillations", *International Journal of Control, Automation and Systems*, Vol *10*(4), August 2012, pp.744-752.

61. M. Farahani, "Damping of subsynchronous oscillations in power system using static synchronous series compensator", *IET generation, transmission & distribution*, Vol *6*(6), June 2012, pp. 539-544.

62. G. Maheswaran and K.S. Naidu, "Comparison of fuzzy and PI controller based SSSC for damping of sub synchronous resonance", *Science Engineering and Management Research (ICSEMR), 2014 International Conference*, November 2014, pp. 1-5.

63. S. Panda, A.K. Baliarsingh, S. Mahapatra, and S.C. Swain, "Supplementary damping controller design for SSSC to mitigate sub-synchronous resonance", *Mechanical Systems and Signal Processing* Vol 68, February 2016, pp. 523-535.

64. R. Thirumalaivasan, M. Janaki and N. Prabhu, "Damping of SSR using subsynchronous current suppressor with SSSC", *IEEE Transactions on Power Systems*, Vol *28*(1), February 2013, pp. 64-74.

65. T. Rajaram, J.M. Reddy and Y. Xu, "Kalman Filter Based Detection and Mitigation of Subsynchronous Resonance with SSSC", *IEEE Transactions on Power Systems*, Vol 32(2), March 2017, pp. 1400-1409.

66. H. Barati, A.L. Ara, M. Ehsan, M. Fotuhi-Firuzabad and S.M.T. Bathaee, "Application of static synchronous series compensator to damp sub-synchronous resonance", *Power Electronics, Drives and Energy Systems, 2006. PEDES'06. International Conference on*, December 2006, pp. 1-6.

67. M. Bongiorno, J. Svensson and L. Angquist, "On control of static synchronous series compensator for SSR mitigation", *IEEE Transactions on Power Electronics*, Vol 23(2), March 2008, pp.735-743.

68. M. Bongiorno, L. Angquist and J. Svensson, "A novel control strategy for subsynchronous resonance mitigation using SSSC", *IEEE Transactions on Power Delivery* Vol 23(2), April 2008, pp. 1033-1041.

69. K. Rachananjali, N. Pavani, S. Suman and D.B. Chaitanya, "Damping of subsynchronous resonance using SSSC with hysteresis current control", *Green Computing Communication and Electrical Engineering (ICGCCEE), 2014 International Conference*, March 2014, pp. 1-5.

70. C.E. Prasad and S. Vadhera, "Fuzzy logic based SSSC as sub-synchronous resonance damping controller", *Energy, Power and Environment: Towards Sustainable Growth (ICEPE), 2015 International Conference*, June 2015, pp. 1-4.

71. X. Xiao, B. Gao, C. Zhao and X. Kun, "A novel SSR-damping scheme based on imbalance operation of SSSC", *Power System Technology (POWERCON), 2010 International Conference on*, October 2010, pp. 1-5.

72. D. Rai, S.O. Faried, G. Ramakrishna and A.A. Edris, "Impact of imbalanced phase operation of SSSC on damping subsynchronous resonance", *Power and Energy Society General Meeting, 2011 IEEE*, July 2011, pp. 1-7.

73. D. Rai, S.O. Faried, G. Ramakrishna and A.A. Edris, "An SSSC-based hybrid series compensation scheme capable of damping subsynchronous resonance", *IEEE Transactions on Power Delivery*, Vol *27*(2), April 2012, pp. 531-540.

74. R.M. Mathur and R.K. Varma, "Thyristor-based FACTS controllers for electrical transmission systems", *John Wiley & Sons*, February 2002.

75. Y.M. Alharbi, A.A. Siada and A.F. Abdou, "Application of UPFC on stabilizing torsional oscillations and improving transient stability", *Power Engineering Conference (AUPEC), 2013 Australasian Universities*, September 2013, pp. 1-4.

76. D.K. Raju, B.S. Umre, A.S. Junghare, M.P. Thakre, R. Motamarriand and C. Somu, "Fractional-order PI based STATCOM and UPFC controller to diminish subsynchronous resonance", *SpringerPlus*, Vol *5*(1), 2016, p.1599.

77. Z.H.U. Xinyao, J.I.N. Meng, K.O.N.G. Xiangping, Z.H.A.O. Jingbo, L.I.U. Jiankun and Z.H.O.U. Qian, "Subsynchronous resonance and its mitigation for power system with unified power flow controller", *Journal of Modern Power Systems and Clean Energy*, pp. 1-9.

78. P. Kundur, N.J. Balu and M.G. Lauby. *Power system stability and control*. Vol 7. New York: McGraw-Hill, 1994.

79. B.S. Rigby, "Analysis and Implementation of a FACTS Series Compensator based on A Single Voltage-Source Inverter", *PhD Thesis*, University of Natal, Durban, South Africa, 1997.

80. G. Tang, "Damping subsynchronous resonance oscillations using a VSC HVDC back-to-back system", *Master of Engineering Dissertation*, University of Saskatchewan, Saskatoon, Canada, 2006.

81. B.S. Rigby and R.G. Harley, "An improved control scheme for a series-capacitive reactance compensator based on a voltage-source inverter", *IEEE Transactions on Industry Applications*, Vol *34*(2), March 1998, pp. 355-363.

82. R. Pillay Carpanen and B.S. Rigby, "An improved SSSC-based power flow controller design method and its impact on torsional interaction", *International Journal of Electrical Power & Energy Systems*, Vol *43*(1), December 2012, pp.194-209.

83. J.W. Park, R.G. Harley and G.K. Venayagamoorthy, "Power system optimization and coordination of damping controls by series FACTS devices", *Power Engineering Society Inaugural Conference and Exposition in Africa, 2005 IEEE*, July 2005, pp. 293-298.

84. B.S. Rigby, N.S. Chonco and R.G. Harley, "Analysis of a power oscillation damping scheme using a voltage-source inverter", *IEEE Transactions on Industry Applications*, Vol *38*(4), July 2002, pp.1105-1113.

85. M.J. Masenkane and R. Pillay Carpanen, "Resonant characteristics of the transmission line compensated with the Static Synchronous Series Compensator", *AFRICON, 2017 IEEE 2017*, September 2017, pp. 614-619.

86. Manitoba HVDC Research Centre, "PSCAD Version 4.2.1 User's Guide", *Manitoba HVDC Research Centre Inc.*, 2006.

87. B.S. Rigby and R.G. Harley, "Resonant characteristics of inverter-based transmission line series compensators", *Power Electronics Specialists Conference, 1999. PESC 99. 30th Annual IEEE*, Vol 1, August 1999, pp. 412-417.

88. R.H. Webster, A.P. Mane and O.J. Smith, "Series capacitor switching to quench electromechanical transients in power systems", *IEEE Transactions on Power Apparatus and Systems*, Vol 2, Mar 1971, pp. 427-33.

89. S. Panda, "Multi-objective evolutionary algorithm for SSSC-based controller design", Electric Power Systems Research, Vol 79(6), June 2009. pp. 937-944.

90. M.J. Masenkane and R. Pillay Carpanen, "Damping Subsynchronous Resonance using a Static Synchronous Series Compensator based Supplimentary Damping Controller", to appear in International Journal of Engineering Research in Africa, 2019.